

## NE2001. II. USING RADIO PROPAGATION DATA TO CONSTRUCT A MODEL FOR THE GALACTIC DISTRIBUTION OF FREE ELECTRONS

J. M. CORDES

Astronomy Department and NAIC, Cornell University, Ithaca, NY 14853  
cordes@spacenet.tn.cornell.edu

T. JOSEPH W. LAZIO

Naval Research Lab, Code 7213, Washington, D.C. 20375-5351  
Joseph.Lazio@nrl.navy.mil*Draft version September 20, 2018*

## ABSTRACT

In Paper I we present a new model for the Galactic distribution of free electrons. In this paper we describe the input data and methodology for determining the structure and parameters of the model. We identify lines of sight on which discrete regions either enhance or diminish the dispersion or the scattering. Most do not coincide with known H II regions or supershells, most likely because the enhancements correspond to column densities smaller than detection thresholds for the emission measure in recombination-line surveys.

*Subject headings:* distance measurements, interstellar medium, electron density, pulsars

## 1. INTRODUCTION

In Paper I (Cordes & Lazio 2002) we present a new model for the Galactic electron density and its fluctuations. This model aims to quantify the density of thermal electrons in the Galaxy which may be used for inverting pulsar dispersion measures into pulsar distances. It also quantifies small-scale electron density fluctuations that are responsible for the scattering and scintillations of compact radio sources, ranging from Galactic pulsars and masers, and Sgr A\* to active galactic nuclei (AGN) and gamma-ray burst (GRB) afterglows in other galaxies.

In this paper, we present the data and the formalism used to construct the model. We describe the formalism that relates measureable quantities to line of sight measures that provide the basis for testing models. We also describe methods used to test the model, including a likelihood analysis, and we demonstrate the need for inclusion of various model components using the likelihood function and other measures for the goodness of fit. Finally, we describe lines of sight that provide especially important constraints on the model or that otherwise require special treatment through inclusion of clumps or voids somewhere along the propagation path.

Our model is constructed for multiple purposes. First and foremost is to allow estimation of pulsar distances and scattering. In this regard, the number of parameters of the model is unrestricted by any notions of parsimony: good estimates are the bottom line. However, a conflicting goal — determining the ionized structure of the Galaxy on a variety of length scales — does require considerations of model complexity and whether specific features are demanded by the data.

The organization of the paper is as follows. Observables and integrated measures are discussed in §2. In §3 we discuss the components of the model that are required by the data. We use straight-forward empirical distributions to argue for the existence of the various components.

§4 presents the detailed model. §5 discusses our fitting methods and figures of merit. §6 compares results of model fitting when we exclude one or more components from the model. We also compare NE2001 with TC93 and a more recent model of Gómez, Benjamin, & Cox (2001; hereafter GBC01). §7 discusses additional aspects of model performance. §8 discusses particular lines of sight that are either problematic or especially informative. §9 presents limitations of the model and §10 summarizes our results and future models that we anticipate. In Appendix A we derive estimators for the scattering measure from relevant scintillation and scattering observables. Tables in the Appendix give scattering data for the lines of sight in our database of measurements.

## 2. OBSERVABLE QUANTITIES AND INTEGRATED MEASURES

In Paper I we summarized the kinds and number of input data used for our model. They include measurements on pulsars of the dispersion measure, DM, and various scattering observables of pulsars and other compact Galactic and extragalactic sources that include the angular broadening,  $\theta_d$ , the pulse broadening time  $\tau_d$  and the scintillation bandwidth,  $\Delta\nu_d$ . In our analysis, we consider scattering observables only in the so-called strong-scattering regime (Rickett 1990; Cordes & Lazio 1991) where wavefronts from sources with a high degree of spatial coherence are perturbed by much more than 1 rad (rms) when propagating through the ionized interstellar medium (ISM). In particular, the phase *difference* between two ray paths separated by the Fresnel scale ( $\sim \sqrt{\lambda D} \approx 10^{11}$  cm), where  $\lambda$  is the electromagnetic wavelength and  $D$  is a characteristic distance through the medium, is much larger than 1 rad in order that scattering effects occur. In strong scattering, there are no unscattered components to the source's wavefield and the diffracted intensity is correlated over a frequency scale (the 'scintillation bandwidth')  $\Delta\nu_d \ll \nu$  where  $\nu = c/\lambda$ .

In Appendix A, we discuss how the scattering observables may be used to estimate the scattering measure, SM, in the strong-scattering regime.

For completeness, we point out that there are other scattering observables, but they are of less utility. The characteristic scintillation time scale  $\Delta t_d$  is not particularly useful for quantifying SM because an unknown characteristic velocity is also needed to make the relation between  $\Delta t_d$  and SM. No spectral-line Galactic or extragalactic sources whose emission line widths are narrow enough to display spectral broadening are known, though future detection of extraterrestrial transmitters may change this situation (Cordes & Lazio 1991). Finally, measurements exist for some lines of sight of scintillations in the weak-scattering regime which also can yield estimates for SM. Rickett, Coles, & Markkanen (2000) describe such measurements and how to calculate SM in that regime.

Independent distance measurements of Galactic sources, particularly pulsars but also masers, microquasars and Sgr A\*, are also crucial for calibrating the model. As described in Paper I, we cast these in the form of a distance range,  $[D_L, D_U]$ .

In Figure 1 and Table 1 of Paper I, we summarize the numbers of available measurements, which include upper bounds as well as interval constraints. In Tables 3–5 we tabulate scattering measures and relevant input data for lines of sight toward pulsars, other Galactic sources, and extragalactic sources.

### 3. BASIC STRUCTURE OF THE MODEL BASED ON EMPIRICAL DISTRIBUTIONS

The electron density model presented in Paper I contains a number of components that are suggested by the data. These are: (a) a thick disk with large Galactocentric scale height; (b) a thin, annular disk in the inner Galaxy; (c) spiral arms; (d) a Galactic center component; (e) structures in the vicinity of the Sun that we collectively refer to as the local ISM component; and (f) other over-or-underdense regions that we refer to as clumps and voids. These salient features may be identified through investigation of observable quantities plotted against Galactic coordinates and other variables, as we discuss in this section. Detailed fitting of the parameters of the components and identification of lines of sight that intersect voids and clumps are discussed in later sections.

#### 3.1. DM and Independent Distance Constraints

From DMs and independent distance constraints, we may infer the scale height of the thick disk close to the Sun, the need for a thin disk and spiral arms, and the existence of enhancements and deficits of electron density near the Sun.

##### 3.1.1. Evidence for a Thick Disk

Figure 1 shows  $DM \sin |b|$  plotted against  $|z|$  for pulsars with independent distant estimates; similar versions of this figure, though based on fewer data, have been discussed by Reynolds (1991); Nordgren, Cordes & Terzian (1992); and GBC01. Schematic, plane-parallel models for the electron density are overplotted for different mid-plane

densities and scale heights. Figure 1 demonstrates that (a) the average electron density along a given line of sight is typically in the range of  $0.01\text{--}0.1 \text{ cm}^{-3}$ , as indicated by the dashed lines; (b) the paucity of Galactic pulsars with  $DM \sin |b| \gtrsim 25 \text{ pc cm}^{-3}$  indicates that the free electron distribution is bounded in the  $z$  direction with a scale height  $\sim 1 \text{ kpc}$ ; and (c) the variations in mean density are larger than can be explained by distance errors, signifying changes in electron density on a variety of scales. For a plane parallel medium, examples of which are shown as solid lines in Figure 1, the midplane density is about  $0.02\text{--}0.04 \text{ cm}^{-3}$  with (exponential) scale height  $\sim 0.75 \pm 0.25 \text{ kpc}$ . Our model described below is considerably more complex than a plane-parallel medium so these estimates are only by way of example. These results echo the statements of Kulkarni & Heiles (1988) that simple plane parallel models are “only statistical in nature and should not be interpreted too literally.”

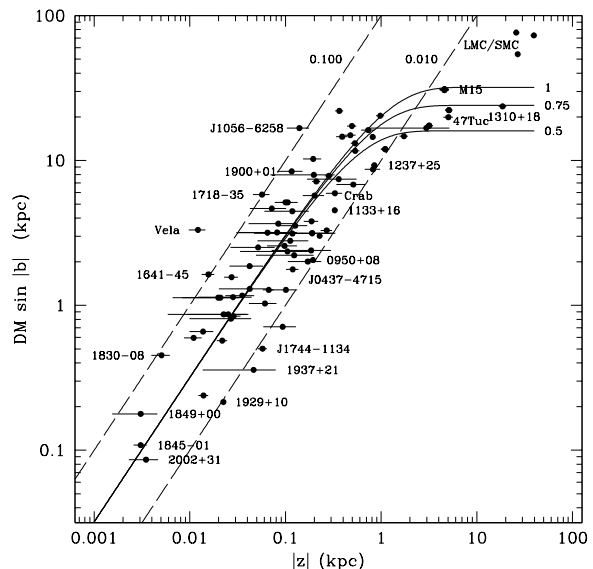


FIG. 1.— Component of DM perpendicular to the Galactic plane,  $DM \sin |b|$ , plotted against  $z$  distance for those pulsars having independent distance constraints of the form  $[D_L, D_U]$  and where the implied  $z$  range spans less than one decade. The dashed lines show curves for media with constant  $n_e = 0.01$  and  $0.1 \text{ cm}^{-3}$ . The solid lines represent plane parallel models with exponential scale heights of 0.5, 0.75 and 1 kpc (as labelled). For these models, the midplane density is held fixed at  $0.032 \text{ cm}^{-3}$ . The paucity of objects with  $DM \sin |b| \gtrsim 25 \text{ pc cm}^{-3}$ , apart from those in the LMC and SMC with resultant contamination of their DMs, is consistent with a well defined truncation of the Galaxy’s free electron layer at or near an effective scale height of 1 kpc.

#### 3.1.2. The Thin, Inner-Galaxy Disk and Spiral Arms

The thin disk and spiral arms can be inferred from the distribution of DM in Galactic longitude  $\ell$ . Figure 2 shows DM plotted against  $\ell$  for 8 ranges of  $b$ . The mean DM in each frame falls off monotonically with mean  $b$ , indicating the existence of a disk-like distribution. The structure evident in Figure 2 reflects (a) the existence of a small scale-height region in the inner Galaxy that is responsible for large DMs at low Galactic latitudes, and (b) a scale height for the inner disk component  $\sim 0.15 \text{ kpc}$ . At high latitudes, there is little systematic variation with  $\ell$ . At low latitudes, the largest values of DM are in the longitude

range  $-90^\circ \lesssim \ell \lesssim 70^\circ$ . The asymmetry of this range about  $\ell = 0^\circ$  has been noted by others (Johnston et al. 1992; TC93) and was explicitly used by TC93 to aid in the definition and fitting of spiral arms. With more than twice the number of pulsars now available, the asymmetry is even more striking and again suggests the presence of spiral structure as the most reasonable cause for the asymmetry. Selection effects are unlikely to be the cause of the asymmetry as a number of deep searches at low latitudes near  $\ell \approx 60^\circ$  have been carried out with the Arecibo Observatory, yet the number of pulsars around  $\ell \approx -60^\circ$  is clearly much higher. An alternative suggestion is that a Galactic bar (e.g., Blitz & Spergel 1991) underlies this asymmetry. However, the typical size and orientation usually attributed to the bar suggest that its effects would appear for longitudes in the range  $\sim \pm 20^\circ$ , much smaller than the range in which asymmetry is seen.

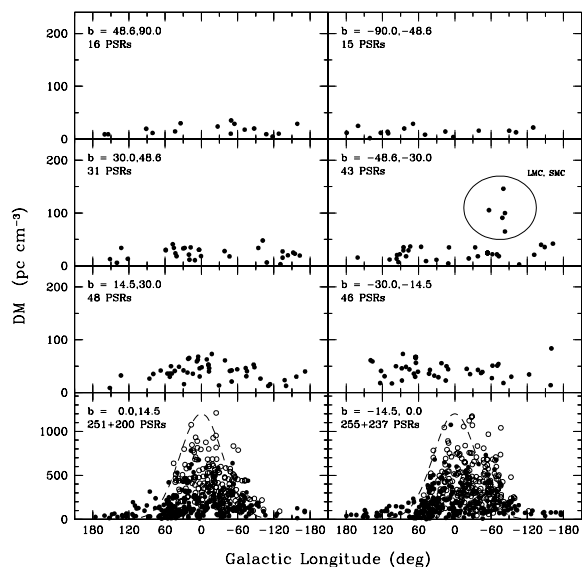


FIG. 2.— Scatter plots of DM vs. Galactic longitude for eight ranges of latitude. Filled circles: data from the Princeton pulsar catalog (Taylor, Lyne, & Manchester 1993 with updates); open circles: data from the Parkes Multibeam survey. The latter covers only low latitudes and thus contributes only to the bottom two panels. Note that the DM scale for the bottom two panels is different from the others. The circle in the right, second-from-top panel indicates pulsars whose DMs receive contributions from the LMC and SMC. The dashed lines in the bottom two panels show a Gaussian function with  $1/e$  width of  $50^\circ$  centered on  $\ell = 0^\circ$ . It helps delineate the asymmetry of the data points about  $\ell = 0^\circ$ .

Figure 3 shows the latitude dependence of DM for eight longitude ranges. Here, again, the strong longitude dependence at low latitudes is evident. The upper envelopes of DM values appear to be well described, though not perfectly, by a plane-parallel model that yields  $DM_{90} |\csc(b)|$  with  $DM_{90} \approx 24 \text{ pc cm}^{-3}$  (apart from pulsars in the LMC and SMC). As described below, this value for  $DM_{90}$  is consistent for many lines of sight with our formal model fitting, though our model is not plane-parallel in form.

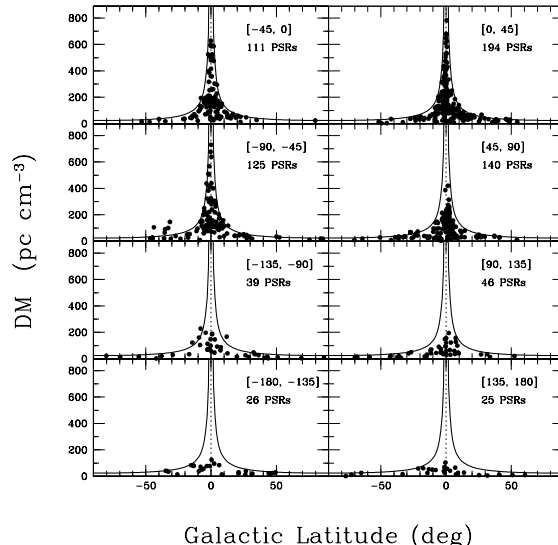


FIG. 3.— Scatter plots of DM vs. Galactic latitude for ranges of longitude. The data are from the Princeton catalog. The solid lines represent the maximum DM for a plane parallel medium with  $DM = 24 \text{ pc cm}^{-3}$  for  $|b| = 90^\circ$ .

Taken together, Figures 2–3 require the existence of an inner Galaxy region with electron density larger than and scale height smaller than those of the thick disk. Physically, this region could be made up solely of spiral arms, of an annular disk like the molecular ring, or a combination of the two, as was chosen in TC93 and which we follow here.

Figure 4 shows schematically an inner-Galaxy disk and how it is expected to be manifested for lines of sight with longitudes smaller than  $\ell_{\max} \approx \sin^{-1} r_d/R_\odot$  and latitudes smaller than  $b_{\max} \approx \sin^{-1} H_d/(R_\odot - r_d)$ , where  $r_d$  and  $H_d$  are the characteristic radius and scale height of the disk. Evaluating using  $\ell_{\max} \approx 60^\circ$  and  $b_{\max} \approx 2^\circ$ , we find that  $r_d \approx 4.3 \text{ kpc}$  and  $H_d \approx 0.15 \text{ kpc}$ . These estimates for the radius and scale height of an inner-Galaxy disk correspond to our formal model parameters,  $H_2$  and  $A_2$ .

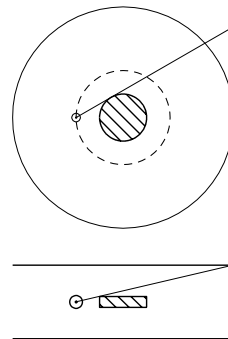


FIG. 4.— Schematic views of the Galaxy. Top: view from above the Galactic plane showing the thin, inner-Galaxy component (hatched) and thick outer Galaxy disk. A line of sight is shown emanating from the solar circle with radius  $R_\odot$  (dashed circle). Bottom: view of the Galaxy from the side.

While we have argued for the presence of spiral structure in  $n_e$  using the asymmetry of DM in Galactic longitude, a stronger argument can be made for spiral structure by investigating residual dispersion measures, as we have discussed in Paper I. Briefly, one can compare the difference between the DM integrated to infinite distance in a model and the pulsar DM. Doing so for axisymmetric models (Figure 4, Paper I) yields clearly insufficient electron column densities along lines of sight populated by other spiral arm tracers (e.g., H II regions, radio recombination lines). We take these deficiencies from an axisymmetric model to be an indication that spiral structure is a necessary component of any complete Galactic  $n_e$  model.

### 3.1.3. Evidence for Strong Fluctuations

Figure 5 shows  $\bar{n}_e \equiv \text{DM}/D$ , where  $D$  is constrained to an interval  $[D_L, D_U]$  from measurements independent of DM. It is obvious that  $\bar{n}_e$  varies significantly between lines of sight, by more than two orders of magnitude. Some DM excesses are seen on short paths, such as the line of sight to the Vela pulsar  $\sim 0.25$  kpc away, while others are significant fractions of the distance to the Galactic center (assumed to be 8.5 kpc). The estimates of  $\bar{n}_e$  therefore show evidence for strong departures from a local electron density that varies only smoothly with location. Such results are not surprising given the known complexity of the phase structure of the ISM, but they imply that a model for the electron density must contain small scale structure combined with large-scale structure.

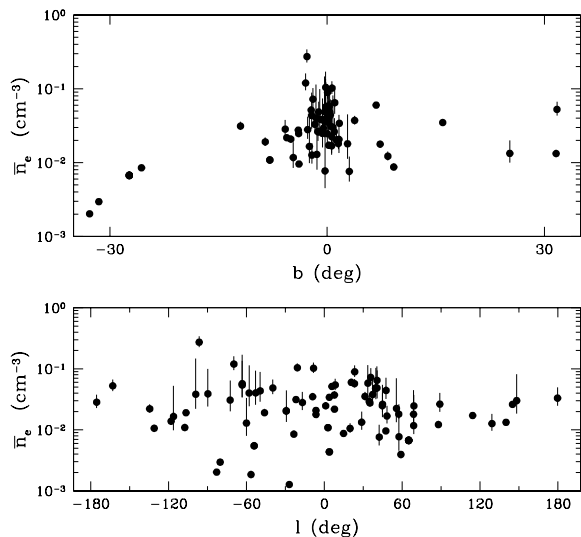


FIG. 5.— Plot of  $\bar{n}_e$  against Galactic latitude and longitude for pulsars with independent distance constraints,  $[D_L, D_U]$ . The points designate DM divided by the mean distance while the plotted bars, some of which are too small to be visible, designate the range of allowed  $\bar{n}_e$ . The smallest values are for pulsars in the Magellanic clouds and in globular clusters, the lines of sight to which largely intersect regions outside the Galactic disk with low electron density.

### 3.2. Constraints from Scattering Measurements

The same electrons responsible for causing the dispersion of pulsar signals also appear to be responsible for the observed scattering (Cordes et al. 1991). While scattering measurements are fewer in number than the sample of DMs, they provide additional lines of sight to help constrain the model and cover the sky sufficiently well that the scattering properties of the ISM can be modelled also.

Figure 6 shows that the scattering measure has a distribution in  $b$  that is only approximately described by a cosecant law. The solid line is a cosecant law  $\text{SM}(b) = \text{SM}_{90} |\csc b|$  for an exponential  $z$  falloff, where we relate SM to DM using the formalism of Paper I (equations [11]–[13]):

$$\text{SM}_{90} = C_{\text{SM}} F \text{DM}_{90}^2 / 2H \approx 10^{-6.04} F \text{DM}_{90}^2 / H, \quad (1)$$

where the second equality holds for DM and SM in standard units. Using  $\text{DM}_{90} \approx 24 \text{ pc cm}^{-3}$ , a scale height of 0.95 kpc and a fluctuation parameter  $F = 0.1$  we obtain  $\text{SM}_{90} \approx 10^{-4.25} \text{ kpc m}^{-20/3}$  at  $|b| = 90^\circ$ . This asymptotic value for  $\text{SM}_{90}$  is about right, but there are strong departures from this model both at low and high latitudes. Evidently the ISM is patchy everywhere. At low latitudes, values of SM are much larger than the model, indicating the clear need for a thin-disk component for scattering material, in accord with previous studies indicating that the most intense scattering is associated with extreme Population I activity in the Galaxy (e.g., Cordes, Weisberg, & Boriakoff 1985). At high latitudes,  $|b| > 15^\circ$ , SM shows little systematic variation with latitude, suggesting the presence of a thick disk component of scattering material.

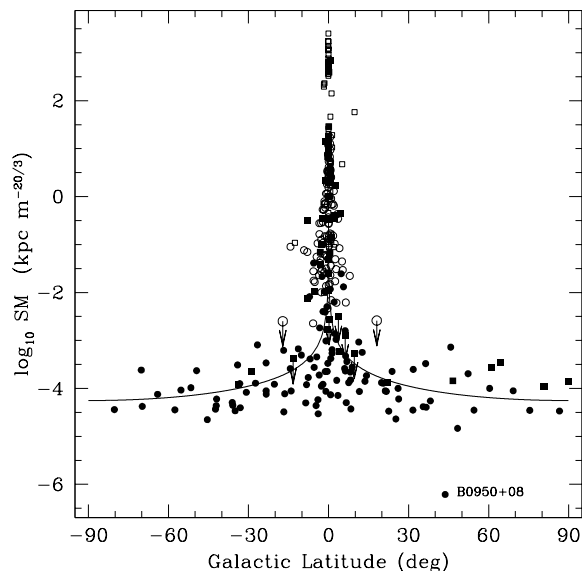


FIG. 6.— Scatter plot of  $\log \text{SM}$  vs. Galactic latitude. Values for SM depend in some cases on a distance estimate which is obtained from the model presented in this paper. Open circles: pulse broadening times ( $\tau_d$ ); Filled circles: scintillation bandwidths ( $\Delta\nu_d$ ); Open squares: Scattering diameters ( $\theta_d$ ) of Galactic sources; Filled squares: Scattering diameters of extragalactic sources. The solid line is a cosecant model for a plane parallel medium with the same  $\text{DM}_{90} = 24 \text{ pc cm}^{-3}$  as in Figure 2, a scale height of 0.95 kpc (for  $n_e$ ), and a fluctuation parameter  $F = 0.1$ , combined according to Eq. 1. This plot shows measured values and only a few upper bounds; nonconstraining upper bounds are excluded for clarity.

One might question whether the high latitude measurements signify the existence of a very large Galactic halo of scattering material or intergalactic scattering. The answer is that high latitude scattering is dominated by a thick ( $\sim 1$  kpc) disk because the scattering measures of pulsars above the disk component are nearly identical to the values of SM for extragalactic sources. This conclusion is consistent with the argument we gave in the discussion of Figure 1.

Investigation of pulse broadening as a function of DM yields nearly direct evidence for strong Galactic structure in the scattering medium. Pulse broadening is, of course, correlated with DM, but not perfectly. Figure 7 shows  $\tau_d$  plotted against DM. We have scaled all available measurements to 1 GHz using a frequency dependence  $\tau_d \propto \nu^{-4.4}$ , the scaling law for a Kolmogorov medium with negligible inner scale (see Appendix). Also shown is a parabolic fit (solid line) and  $\pm 1.5\sigma$  lines (dashed). The fit is with  $\log DM$  as the independent variable:

$$\log \tau_d (\mu s) = -3.59 + 0.129 \log DM + 1.02 (\log DM)^2 - 4.4 \log \nu_{\text{GHz}}. \quad (2)$$

The scattering time for individual pulsars can deviate considerably from the fit, with  $\sigma_{\log \tau} = 0.65$ .

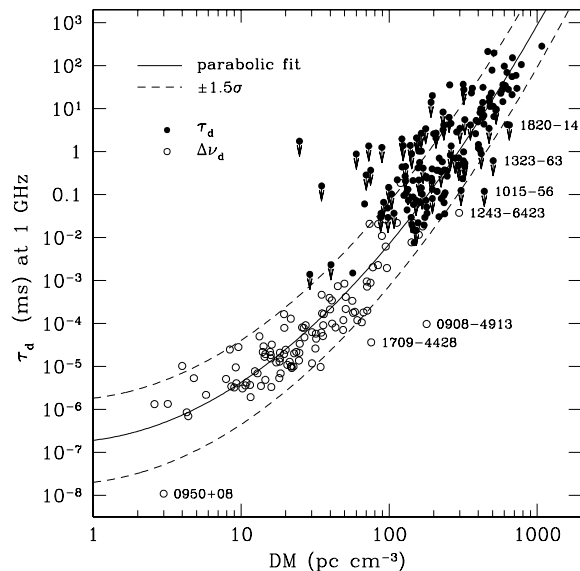


FIG. 7.— Pulse broadening time at 1 GHz plotted against dispersion measure. Filled circles indicate direct measurement of the scattering time; open circles represent scattering times estimated from scintillation bandwidth measurements. All measurements are scaled to 1 GHz using  $\tau_d \propto \nu^{-4.4}$ . The solid line is the parabolic fit given in Eq. 2; dashed lines are at  $\pm 1.5\sigma$ .

Figure 8 shows that the derived values of scattering measure, when plotted against DM, generally mimic the trend of pulse broadening time against DM though with significant differences owing to the scatter of distance values for identical values of DM. The rough trend in Figure 8 for  $DM \lesssim 20 \text{ pc cm}^{-3}$  is in accord with what is expected for a homogeneous medium (e.g. Kuzmin 2001). However, for  $DM \gtrsim 20 \text{ pc cm}^{-3}$ ,  $SM \propto DM^3$ , a variation much stronger than the linear trend expected for a (statistically) homogeneous medium in which DM is strictly proportional to distance and  $dSM \propto dDM$  (e.g. Shitov 1994). Though remarked upon by many

as being anomalous and perhaps difficult to explain the variation can be accounted for quite easily by relaxing one or more assumptions that underly the calculation of SM and its interpretation. In particular, an inhomogeneous medium comprising clumps of enhanced scattering with a power-law distribution of column densities, can account for the variations (e.g. Cordes, Weisberg & Boriakoff 1985).

Following Cordes et al. (1991) and using Equations 11–12 of Paper I, we write

$$\frac{dSM}{dDM} = C_{\text{SM}} F n_e, \quad (3)$$

where  $n_e$  is the local electron density. The derivative is constant for a statistically homogeneous medium. Recall that  $C_{\text{SM}}$  is a numerical constant that depends on the slope of the wavenumber spectrum (Paper I) while the fluctuation parameter  $F$  depends on the outer scale, filling factor, and the local ratio,  $\delta n_e/n_e$ . A non-Kolmogorov wavenumber spectrum, combined with use of a Kolmogorov spectrum in calculating SM, could cause seemingly anomalous values of  $dSM/dDM$  (Cordes, Weisberg & Boriakoff 1985). Though evidence exists for non-Kolmogorov wavenumber spectra along specific lines of sight, our assessment is that the number of departures from such spectra is not sufficient to produce the large variations and steep trend of SM with DM.

Systematic variations of the product  $F n_e$  with location in the Galaxy can easily account for the distribution of points in Figure 8. However, large scale variations in the local mean electron density alone are not sufficient. In the large-scale components of NE2001 (i.e., excluding clumps and voids), the local mean density changes by only a factor of 10. Evidently, systematic changes in  $F$  are also needed. Evidence exists that the outer scale varies, being smaller in directions of intense scattering, such as the lines of sight toward Sgr A\* (Lazio & Cordes 1998a, 1998b), NGC6334B (Moran et al. 1990), and Cyg X-3 (Wilkinson, Narayan, & Spencer 1994) and potentially larger in regions of less intense scattering. One also expects differences in filling factor and perhaps  $\delta n_e/n_e$  between the inner Galaxy and the solar vicinity. Therefore, the steep trend of SM with DM and the large fluctuations of SM reflect a combination of smooth changes in electron density and fluctuation parameter, and clumpiness of the ionized medium.

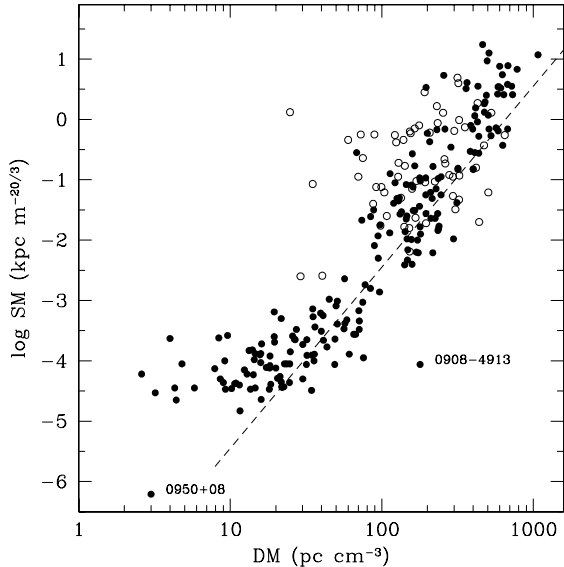


FIG. 8.— SM plotted against DM for 269 pulsars. Filled circles show measurements while open circles are upper limits. The dashed line has slope 3 and is placed by eye to indicate the general trend of points for large values of DM. The point near  $DM \approx 179 \text{ pc cm}^{-3}$  and  $\log SM \approx -4$  is from a scintillation bandwidth measurement (Johnston, Nicastro & Koribalski 1998) of PSR J0908-4913, whose line of sight passes near or through the Gum Nebula and Vela supernova remnant. The low value of SM is not caused by an overestimated distance but, rather, by the low, effective value of the pulse broadening time, as labelled in Figure 7. The same holds for pulsar B0950+08.

#### 4. GALACTIC MODEL FOR ELECTRON DENSITY

As in TC93, we use a right-handed coordinate system  $\mathbf{x} = (x, y, z)$  with origin at the Galactic center,  $x$  axis directed parallel to  $l = 90^\circ$ , and  $y$  axis pointed toward  $l = 180^\circ$ . The Galactocentric distance projected onto the plane is  $r = (x^2 + y^2)^{1/2}$ .

The structure of the model is described in Table 2 of Paper I and associated text and includes thin-and-thick disk (axisymmetric) components; a local ISM component; a Galactic center component; spiral arms; clumps of enhanced electron density or fluctuation parameter; and voids with small electron density and fluctuation parameter.

##### 4.1. Modeling Issues

Our ultimate goal is to estimate local values of mean electron density and  $C_n^2$  from line-of-sight measurements. As with many inversion problems with insufficient sampling, significant background information must be used to provide structure for the model and, regardless, the result will not be unique. This is especially true for modeling the warm ionized medium (WIM) in the Galaxy because structure is known to exist on a wide range of scales that is grossly undersampled by the available lines of sight. Our goal may be stated more realistically as aiming to model the measurements (as integrated measures) for the available lines of sight and to extrapolate to other lines of sight for predictive purposes. As byproducts, we hope to identify and model Galactic structure in the WIM.

1

The meaning of  $F_c$  is likely different for a single clump than for a distributed medium as we originally define  $F$  in Eq. 13 of Paper I,  $F = \zeta c^2 \eta^{-1} \ell_0^{-2/3}$ . In the latter case,  $F$  includes factors involving the filling factor ( $\eta$ ), the internal fractional variation of electron density,  $\epsilon = \text{rms} n_e / n_e$ , cloud to cloud variance ( $\zeta$ ) of clouds, and the outer scale,  $\ell_0$ . For a single cloud, one may consider  $\eta \rightarrow 1$  and  $\zeta \rightarrow 1$ .

To illustrate issues of nonuniqueness, consider a single pulsar line of sight on which we have measurements of DM and pulse broadening,  $\tau_d$ , and perhaps constraints on the range of possible distances,  $[D_L, D_U]$ . Suppose that we model the line of sight with the simplest possible medium, namely, a single H II region or “clump.” The clump would be characterized by  $DM_c$  and  $SM_c$  related to the physical quantities  $n_{e_c}$ ,  $F_c$ ,  $\Delta s$ , and  $d_c$  (electron density inside the clump, fluctuation parameter,<sup>1</sup> path length through clump, and distance from Earth),

$$DM_c = n_{e_c} \Delta s \quad (4)$$

$$SM_c = C_{SM} F_c n_{e_c}^2 \Delta s. \quad (5)$$

The pulse broadening yields a weighted  $SM \propto (d_c/D)(1 - d_c/D)SM_c$  (cf. Eq. 7 of Paper I). At best we have three measurements ( $DM$ ,  $\tau_d$  and  $D \in [D_L, D_U]$ ) and four unknowns,  $DM_c$ ,  $SM_c$ ,  $D$  and  $d_c$ . Physically,  $DM_c$  and  $SM_c$  map into three unknowns, so there are really five total unknowns ( $n_{e_c}$ ,  $\Delta s$ ,  $F_c$ ,  $d_c$  and  $D$ ) and at most three measurements. If the same region is probed by multiple ( $N_p$ ) pulsars and if the region has simple, known geometry (so that  $\Delta s$  can be calculated for each LOS), then the number of unknowns is  $N_p + 4$  ( $N_p$  distances and four clump parameters) and there are  $3N_p$  measurements if pulsar distances are known. A unique solution exists for  $N_p \geq 2$  pulsars if observables are known perfectly. (With finite measurement errors, the solution is unique in the mean.) However, if distances are not known, a unique solution requires  $N_p \geq 4$  pulsars. If  $N_c$  clumps contribute to the observations of  $N_p$  pulsars, the number of pulsars needed is  $2N_c$  and  $4N_c$ , respectively, with and without distance constraints on the pulsars.

In practice, sampling of the same structure by multiple pulsars is relevant for large-scale features in the Galaxy (e.g., disk and spiral-arm components) but not, generally, for individual H II regions. The typical spacing between lines of sight is simply too large with the available sample to model small scale features such as H II regions uniquely. Underdense regions such as supershells tend to be larger than standard H II regions, so there is hope to probe them. To the extent that large-scale structures dominate observables, it is plausible that a model can be fitted accurately. However, any imperfections of the adopted structure will be manifest as systematic errors and, of course, small scale structures will be poorly modeled. An exception to this statement is the local ISM which, because of its proximity, is sampled by many lines of sight.

##### 4.2. Alternative Approaches

Different approaches for modeling  $n_e$  are possible. The approach of this paper is to adopt smoothly varying, large-scale components that are perturbed by small-scale regions that are under-or-over dense. By contrast, one could adopt a model made up solely of clumps that would correspond to structures containing the WIM phase component. One could thus *synthesize* the large-scale structure out of those clumps required for modeling DM

and SM. While this approach is attractive in that it would rely only on DM and SM data to define Galactic structure, there are insufficient lines of sight available at present to allow discrimination between large and small scale components. Future pulsar surveys that cover the Galaxy to the same or greater depth than the Parkes Multibeam survey (Manchester et al. 2001) may yield sufficient measurements, especially when combined with scattering measurements of a large sample of extragalactic objects. A variation on this theme is to recognize that the fundamental structures comprising the WIM are filled H II regions and shells, particularly supershells, having underdense interiors and overdense walls. With sufficient lines of sight and using prior information regarding locations of known shells and H II regions, one could synthesize a large scale model out of such structures.

With sufficient lines of sight through the Galaxy, the best approach for fitting the Galactic density is a function of the WIM itself, in particular whether a smooth distribution or a distribution based on discrete regions is the best starting model. The statistics of observables will be determined by the filling factor of overdense regions and the mean free path for intersecting them. These factors, in turn, are related to the overall porosity of the WIM which is affected by percolation of regions of hot phase (shells and supershells). If the WIM is largely smooth with occasional over and underdense regions, a fitting approach that begins with smooth components and then identifies outliers is warranted. However, if the medium is essentially a complex of over and underdense regions, given adequate sampling (numbers of lines of sight), explicit modeling of individual regions would be best. We take this first approach because small scale structures are undersampled by the available lines of sight; also, a smooth model appears to fit many objects quite well, though it does require significant augmentation by clumps and voids.

### 4.3. Smooth, Large-Scale Components

#### 4.3.1. Outer, Thick Disk Component

The outer, thick disk component is responsible for the DMs of globular cluster pulsars and the low-frequency diameters of high-latitude extragalactic sources (e.g., as inferred from interplanetary scintillation measurements and low-frequency VLBI). In TC93 this component was determined to have a scale height of roughly 1 kpc with a Galactocentric radial scale length of roughly 20 kpc. However, the data available for TC93 did not allow a firm constraint on the Galactocentric scale length; scale lengths as large as 50 kpc were also allowed by the data.

Lazio & Cordes (1998a) measured the angular diameters of eleven extragalactic sources toward the anticenter, and Lazio & Cordes (1998b) augmented these observations with those used by TC93 and other measurements in the literature to improve the constraints on the Galactocentric scale length. A likelihood method was used to constrain not only the scale length, but also to search for any signature of a warp. Their analysis favors an unwarped, non-flaring disk with a scale height of 1 kpc (though this may reflect the non-uniform and coarse coverage of the anticenter provided by the available data).

The likelihood is maximized for a radial scale length of 15–20 kpc, but the data cannot distinguish between a

gradual decrease in the electron density and a truncated distribution. Lazio & Cordes (1998b) favored a truncated one, in which the scattering is associated with massive star formation, which is also truncated near 20 kpc. A radial extent of 20 kpc is also comparable to the radial extent of H $\alpha$  emission observed for nearby spiral galaxies.

The functional expression for the electron density outside the solar circle is  $n_{e1}(r) = n_{e1}g_1(r)$ , where

$$g_1(r) = \begin{cases} \cos(\pi r/2A_1)/\cos(\pi R_\odot/2A_1), & r \leq A_1; \\ 0, & r > A_1. \end{cases} \quad (6)$$

In this functional form chosen by Lazio & Cordes (1998b) for the electron density in the outer disk, there is no additional scattering at  $r > A_1$  because  $n_e = 0 \text{ cm}^{-3}$  for  $r > A_1$ . An equivalent model is one in which there is ionized gas beyond  $A_1$  but fluctuations are turned off:  $F_1 = 0$  for  $r > A_1$ . Such truncation could occur if the distribution of scattering agents decreased more rapidly with  $r$  than does  $n_e$ . Given the current paucity of both pulsars and scattering measurements toward the anticenter, we do not regard this distinction as important. Additional data, particularly if one could compare the DMs of distant, anticenter pulsars with the scattering measures of extragalactic sources, might allow this distinction to be resolved.

#### 4.3.2. Inner, Thin Disk Component

An inner Galaxy component ( $n_2$ ) consisted of a Gaussian annulus in TC93. Data available to TC93 could not distinguish a filled Gaussian form in Galactocentric radius from an annular form, but the latter was chosen for consistency with the molecular ring seen in CO (e.g., Dame et al. 1987). Here, we consider two alternatives. First is the annular form of TC93. Second is a model based on a 99 GHz CS ( $2 \rightarrow 1$ ) survey for ultra-compact H II regions (which is assumed to trace the OB star distribution) by Bronfman et al. (2000).

Bronfman et al. (2000) report the surface density and scale height of ultra-compact H II (UCHII) regions, assuming an axisymmetric distribution. We have fit functional forms described below to these quantities and determined the best-fitting parameter values using a chi-square test.

The radial distribution of ultra-compact H II regions peaks near  $0.7R_\odot$ , with an approximately gaussian increase interior to  $0.7R_\odot$  and an approximately exponential decrease exterior to  $0.7R_\odot$ . The scale length for the gaussian increase is 0.22 kpc while the scale length for the exponential increase is 0.27 kpc. The  $z$  distribution of ultra-compact H II regions has a half-width that is approximately constant at 30 pc interior to a Galactocentric radius of  $0.5R_\odot$ , increasing through 100 pc by  $R_\odot$ , and exceeding 200 pc by  $1.5R_\odot$ . The  $z$  distribution was modelled as a gaussian with a scale height of 1 kpc. In comparing the two models, we find that the second is not an adequate replacement for an annular disk. Our assessment is that the UCHII population most likely resides in a spiral arm distribution and may reflect a low-scale height component of the spiral arms (see below). At the present time, we find that the annular component combined with our spiral arm components provides the best fit. In the future, the UCHII distribution may be

required when sufficient lines of sight are probed that one or more is likely to pierce an UCHII.

#### 4.3.3. *Spiral Arms*

The spiral arm components in TC93 were modeled by specifying the locations of the spiral arm centroids in the  $(x, y)$  plane and then fitting for the density, thickness and scale height of each arm. Arm centroids were defined using the locations of H II regions augmented by use of directions where radio continuum and neutral hydrogen (21 cm H I) emission are enhanced along spiral arm tangents. We have reconsidered these definitions because (a) recently discovered pulsars appear to require thicker arms because the TC93 model provides too few electrons in some directions to account for measured DMs and it either over-or-under predicts the scattering;<sup>2</sup> (b) there is evidence for the influence of a local (‘Orion-Cygnus’) arm on the scattering of some pulsars (Gupta et al. 1994); (c) the spiral arms in TC93 were truncated arbitrarily in their arc lengths and there is evidence suggesting that they need to be extrapolated further; (d) on general principles, it is worthwhile to consider alternative, mathematically defined forms for the spiral arms, such as the logarithmic spiral forms considered in discussions of magnetic fields in the Galaxy and in other galaxies (e.g., Vallée 2002; Beck et al. 1996; Wainscoat et al. 1992).

The functional form of the spiral arm density is

$$n_{\text{arms}} = n_a G_a(\mathbf{x}), \quad (7)$$

$$G_a(x, y, z) = \sum_{j=1}^{N_{\text{arms}}} f_j g_{a_j}(r, s_j/w_j) h(z/h_j h_a), \quad (8)$$

where the summation ranges over  $N_{\text{arms}} = 5$  spiral arms. Factors of order unity,  $f_j$ ,  $w_j$  and  $h_j$ , allow control of the electron density, width and scale height of each spiral arm, respectively. Each arm also has a separate  $F$  parameter,  $F_{a_j}$ ,  $j = 1, 5$ .

Figure 9 shows the locations of spiral arms as defined in TC93 and as modified by us. For the most part, the spiral arm definitions in TC93 are satisfactory to account for the overall shape of the distribution of DM vs.  $\ell$ . The fast rolloff of DM for negative longitudes at  $\ell \sim -75^\circ \pm 15^\circ$  is associated with the ‘Carina’ side of the Carina-Sagittarius arm while the corresponding ‘Sagittarius’ rolloff is at positive longitudes at  $\ell \sim 45^\circ \pm 5^\circ$ . Analogous features from arms interior to the Carina-Sagittarius arm are not obvious in the figure owing to crowding of objects. However, the local ‘Cygnus-Orion’ arm and possibly the exterior ‘Perseus’ arm are more evident at positive than negative longitudes because they are nearer the Galactic center at positive longitudes and appear to have greater densities as a consequence. This asymmetry is manifested in Figure 2 by the slower rolloff of DM for  $60^\circ \lesssim \ell \lesssim 180^\circ$  than in the corresponding range of negative longitudes.

The spiral arm centroids are defined as perturbed logarithmic spirals. To begin, we define the centroid of the  $j^{\text{th}}$  arm according to

$$\theta_j(r) = a_j \ln(r/r_{\text{min},j}) + \theta_{\text{min},j}, \quad (9)$$

where  $\theta_j$  is measured anticlockwise from the  $y$  axis (with the Galactic center at the origin increasing positively

toward the Sun) and  $r$  is Galactocentric radius. Values for  $a_j$ ,  $\theta_{\text{min},j}$  and  $r_{\text{min},j}$  are taken from Wainscoat et al. (1992). The spiral structure is similar to that proposed by Ghosh & Rao (1992) and also described by Vallée (1992). We use a Sun-Galactic Center distance of 8.5 kpc, the IAU recommended value (but see §9). We perturb the shapes of the arms in the vicinity of the Sun to match the shapes defined in TC93. These perturbations are guided by the detailed distributions of DM in Galactic longitude and by the locations of spiral arm tangents in a number of tracers. In practice, we tested three spiral arm models against the data: (1) the TC93 spiral arms; (2) pure logarithmic spirals as described in Wainscoat et al. (1992); and (3) logarithmic spiral arms perturbed to match arm shapes near the Sun as described in TC93. The likelihood analysis disfavors the first case and slightly prefers model (3) over model (2).

*Caveat:* The spiral arm components in our model, like those in TC93, are modeled as overdense regions. Astrophysically, however, the enhanced star formation in spiral arms will produce underdensities as well as overdensities, as has been demonstrated by the identification of supershells. Though we have adopted spiral arms as overdense regions, to account for DM and SM we have had to introduce ellipsoidal underdense perturbations (‘voids’) in particular directions, as discussed below.

#### 4.4. *Local ISM (LISM)*

The local ISM displays density enhancements and deficits associated with the particular star-formation history, including supernovae, in the region and with existing stars that ionize local gas. As such, the LISM is not at all unique in the Galaxy. However, we must model it carefully because we view the rest of the Galaxy — and the entire Universe — through it.

We model the local ISM in accord with DM and SM measurements of nearby pulsars combined with parallax measurements and guided by H $\alpha$  observations that provide estimates of EM. Observations and analysis by Heiles (1998) and Toscano et al. (1999 and references therein) suggest the presence of four regions of low density near the Sun: (1) a local hot bubble (LHB) centered on the Sun’s location that is long known because of its prominence in H I and X-ray observations; (2) the Loop I component (North Polar Spur) that is long known because of its prominence in nonthermal continuum maps; (3) a local superbubble (LSB) in the third quadrant; and (4) a low density region (LDR) in the first quadrant. Additional features have been identified by Heiles (1998) but the available lines of sight to pulsars appear to not require their inclusion in our model. Bhat et al. (1999) explicitly fitted for parameters of the LHB using pulsar measurements and a model having a low-density structure surrounded by a shell of material that produces excess scattering. Some of the parallax distances used by Toscano et al. (1999) have been revised (Briskin et al. 2000; Briskin 2001; Briskin et al. 2002), in some cases substantially,

<sup>2</sup> A thicker or more dense spiral arm can either increase or decrease the scattering through the competing effects of increasing the angular scattering while bringing the pulsar nearer to the observer and also changing lever-arm effects that influence scattering observables.

implying lower densities in the third quadrant than they inferred.

We have used the work of Heiles (1998), Bhat et al. (1999), and Toscano et al. (1999), along with comprehensive work by Frisch (1996, 1998) as guides for defining structures in the local ISM but we have made new fits to the locations, sizes, shapes and densities in order to estimate both the distances and the scattering of nearby pulsars to within the measurement errors. We include the four structures as follows. For the LSB and LDR, we use a gaussian ellipsoid with uniform electron density and  $F$  parameter inside the  $1/e$  contour. For the Loop I structure, we use a spherical volume of low density surrounded by a shell of higher density and fluctuation parameter. The LHB has a more complex structure as delineated by X-ray observations (Snowden et al. 1998) and Na I absorption (Maíz-Apellániz 2001 and references therein). Based on contours shown in Sfeir et al. (1999), we model the LHB as a cylinder with ellipsoidal cross section having constant area for  $z \geq 0$  and decreasing area for  $z < 0$ . The cylinder is vertical in the  $x$ - $z$  plane and slanted in the  $y$ - $z$  plane such that the cylinder axis has  $dy/dz > 0$ . As suggested by Sfeir et al. (1999) and by the results of our fitting, the LHB has a “blow out” structure for positive  $z$ , but is pinched off at negative  $z$ . Appendix A describes the mathematical models used for the four regions. Table 4 of Paper I lists the parameters of the local ISM model and gives values based on the fitting we describe below.

Because  $n_e$  is smaller inside each of these regions than outside, we define a weight factor  $w_{\text{lism}}$  that is unity for a location inside any of the four regions and is zero outside. As seen in Table 1 of Paper I, the electron density is set to either the LISM value or the ambient value by using  $w_{\text{lism}}$  as a switch. Similarly, because the LHB has lower density and  $F$  parameter than the LDR and LSB, we assign a weight to the LHB component,  $w_{\text{lhb}}$ , that is unity inside its  $1/e$  contour and which allows the LHB component to determine  $n_e$  and turns off any contribution from the LSB and LDR components. We also use the weight for the LSB component to override the LDR component. The LISM model therefore is of the form

$$n_{\text{lism}}(\mathbf{x}) = (1 - w_{\text{lhb}})\{(1 - w_{\text{loopI}}) \times [(1 - w_{\text{lsb}})n_{\text{ldr}}(\mathbf{x}) + w_{\text{lsb}}n_{\text{lsb}}(\mathbf{x})] + w_{\text{loopI}}n_{\text{loopI}}(\mathbf{x})\} + w_{\text{lhb}}n_{\text{lhb}}(\mathbf{x}) \quad (10)$$

$$F_{\text{lism}}(\mathbf{x}) = (1 - w_{\text{lhb}})\{(1 - w_{\text{loopI}}) \times [(1 - w_{\text{lsb}})F_{\text{ldr}}(\mathbf{x}) + w_{\text{lsb}}F_{\text{lsb}}(\mathbf{x})] + w_{\text{loopI}}F_{\text{loopI}}(\mathbf{x})\} + w_{\text{lhb}}F_{\text{lhb}}(\mathbf{x}) \quad (11)$$

$$w_{\text{lism}}(\mathbf{x}) = \max(w_{\text{ldr}}, w_{\text{lhb}}, w_{\text{lsb}}, w_{\text{loopI}}). \quad (12)$$

#### 4.5. Gum Nebula and Vela Supernova Remnant

Features in or near the nearby Gum Nebula have discernible influence on the dispersion measures and scattering measures of several pulsars. In TC93 a large region was included which perturbed the dispersion measures of pulsars viewed through the Gum Nebula but did not influence the scattering. This choice was made because, at the time, there were insufficient lines of sight with pulse broadening measurements to model scattering of the Gum Nebula. Since the writing of TC93,

investigations of the Vela pulsar and other pulsars indicate that scattering is large within a region of at least 16 degrees diameter centered roughly on the direction of the Vela pulsar (Mitra & Ramachandran 2001). We have modeled the Gum/Vela region based on the scattering measurements and also on the fact that an enhanced, local mean electron density is required to account for the dispersion measures of five objects,

We model the region with an overlapping pair of spherical regions, one describing the Gum Nebula, the other the immediate vicinity of the Vela pulsar.

The pulsars with high DMs and overestimated distances are B0736–40, J0831–4406, B0808–47, B0833–45 (Vela), B0743–53, J0855–4658, and B0950–38. For all objects except Vela, the model DM without the Gum/Vela components is smaller than the measured DM even when integrated to 30 kpc. For Vela the estimated distance is 2.8 kpc without these components, compared to recent distance estimates,  $0.25 \pm 0.03$  kpc (Cha et al. 1999) and  $0.29^{+0.076}_{-0.05}$  kpc (Caraveo et al. 2001).

#### 4.6. Galactic Center (GC) Component

The scattering diameters of Sgr A\* and several nearby OH masers indicate that a region of enhanced scattering is along the line of sight to the Galactic center (van Langevelde et al. 1992; Rogers et al. 1994; Frail et al. 1994). Typical diameters, scaled to 1 GHz, are approximately  $1''$ , roughly 10 times greater than that predicted by TC93, even with the general enhancement of scattering toward the inner Galaxy in that model.

Scattering measurements of GC sources alone do not constrain the *radial* location of the scattering region for the following reason: for such sources, a region of moderate scattering located far from the Galactic center can produce angular broadening equivalent to that from a region of intense scattering located close to the Galactic center. Indeed, previous estimates for the location of the scattering region ranged from 10 pc to 3 kpc from the GC.

The degeneracy between the scattering strength and radial location can be broken by observing distant sources through the scattering region. Lazio & Cordes (1998c) conducted a survey for extragalactic sources observed through the Galactic center. They found a paucity of sources, suggestive of a hyperstrong scattering region located in or near the Galactic center. Lazio & Cordes (1998d) combined the results of this survey with the extant radio-wave scattering data and free-free emission and absorption measurements in a likelihood analysis that constrained the GC-scattering region separation,  $\Delta_{\text{GC}}$ , and the angular extent of the region,  $\psi_\ell$ . The maximum likelihood estimates of these parameters were  $\Delta_{\text{GC}} = 133^{+200}_{-80}$  pc,  $0.5^\circ \leq \psi_\ell \lesssim 1^\circ$ . Lazio & Cordes (1998d) argued that the close correspondence between  $\Delta_{\text{GC}}$  and  $\psi_\ell D_{\text{GC}}$  indicates that the scattering region encloses the GC.

Lazio & Cordes (1998d) suggested an axisymmetric Gaussian form for the GC region with radial scale  $R_{\text{GC}} = 0.15$  kpc and scale height  $H_{\text{GC}} = 0.075$  kpc with a nominal central density  $n_{\text{GC}} = 10 \text{ cm}^{-3}$ , which they estimated using free-free absorption measurements incorporated into their likelihood analysis. We have altered this model in order to match the scattering diameters of nearby

sources. In particular, the data require a smaller scale height  $H_{\text{GC}} \approx 0.026$  kpc and slightly smaller radial scale,  $R_{\text{GC}} \approx 0.145$  kpc. In addition we have offset the center of the distribution by  $(x_{\text{GC}}, z_{\text{GC}}, z_{\text{GC}}) = (-0.01, 0, -0.02)$  kpc. The model for the electron density in the GC is

$$n_e(\mathbf{x}) = \exp \left[ - \left( \frac{\delta r_{\perp}^2}{R_{\text{GC}}^2} + \frac{(z - z_{\text{GC}})^2}{H_{\text{GC}}^2} \right) \right] \quad (13)$$

$$\delta r_{\perp}^2 = (x - x_{\text{GC}})^2 + (y - y_{\text{GC}})^2,$$

which is truncated to zero for arguments of the exponential smaller than  $-1$ . The truncation allows the GC component to leave unaffected lines of sight to nearby OH masers that show much less scattering than those seen through the GC component. A value  $F_{\text{GC}} \sim 6 \times 10^4$  produces SM values needed to account for the scattering diameters of Sgr A\* and the OH masers.

#### 4.7. Regions of Intense Scattering (“Clumps”)

In addition to regions that perturb the scattering of the Vela pulsar and other pulsars near it and the Galactic center, other regions of intense scattering must exist to account for the large angular diameters and/or pulse broadening seen toward a number of Galactic and extragalactic sources.

We define “clumps” as regions of enhanced  $n_e$  or  $F$ , or both, and identify them by iterating with preliminary fits to the smooth components of the electron-density model (e.g., the thin and thick disk components and the spiral arms).

We model clumps with thickness  $\Delta s \ll D$  and we use parameters  $n_{e,c}$ ,  $F_c$  and  $d_c$  (electron density inside the clump, fluctuation parameter, and distance from Earth). The implied increments in DM and SM are

$$\begin{aligned} \text{DM}_c &= n_{e,c} \Delta s \\ \text{SM}_c &= C_{\text{SM}} F_c n_{e,c}^2 \Delta s \\ &= 10^{-5.55} \text{DM}_c^2 F_c / \Delta s_{\text{kpc}}, \end{aligned} \quad (14)$$

where the last equality holds for DM and SM in standard units. Eq. 14 implies that relatively modest contributions to DM can produce large changes in SM if the clump is small and fluctuation parameter large. For example,  $\text{DM}_c = 10$  pc cm<sup>-3</sup>,  $F_c = 1$  and  $\Delta s = 0.02$  kpc yield  $\text{SM}_c = 0.014$  kpc m<sup>-20/3</sup>. For a pulsar 1 kpc away, the clump would perturb DM and the resultant distance estimate by perhaps 30% while SM would increase by about a factor of 100. Thus pulsars which have anomalous scattering relative to the smooth model can, in many cases, be well modeled with small perturbations to the DM predictions of the model. This also means that the model is expected to be much better for distance and DM estimation than for scattering predictions.

In some cases the pulsar’s distance is much smaller than implied by DM and the smooth parts of the model. If the pulsar’s distance is well constrained, then we require  $d_c < D_L$  and  $\text{DM}_c$  is bounded by the requirement that the new distance estimate (including the clump) must match the measured distance to within the errors.

#### 4.8. Regions of Low Density (“Voids”)

We also found that some pulsar distance constraints could not be satisfied using the previously defined

structures without recourse to placement of a low-density region along the line of sight. We call these regions “voids” although they simply represent, typically, lower-than-ambient density regions. By necessity, they take precedence over all other components (except clumps), which we effect by usage of a void weight parameter,  $w_{\text{voids}} = 0, 1$ , that operates similarly to  $w_{\text{lism}}$ . The mathematical form is given in Table 2 of Paper I. We use elliptical gaussian functions with semi-major and semi-minor axes  $a, b, c$  and rotation angles  $\theta_y, \theta_z$  about the  $x$  and  $z$  axes.

#### 4.9. Components Not Included

We tested inclusion of a Galactic bar component using a shape guided by the work of Blitz & Spergel (1991) and others, but varied the size, orientation and density. We found that the likelihood function was not increased sufficiently by inclusion of the bar to warrant inclusion in the final model. This insensitivity to a bar component may arise from an insufficient number of pulsars that probe it and also because of degeneracy with the inner ring and inner spiral-arm components.

### 5. METHODOLOGY OF PARAMETER ESTIMATION

The electron density model is a combination of large and small scale structures. Some components are sufficiently disjoint from others that their parameters can be estimated without a global analysis. The Galactic center component is the best example of such independence, and we have used the model described in Lazio & Cordes (1998d), with the modifications described in §4.6. The local ISM structures are independent of many, but not all, of the large-scale components. However, other components are highly coupled. Given that the nonlinear model contains too many parameters to allow a straightforward optimization, we have taken an iterative, ad hoc approach that yields an acceptable solution. However, we emphasize that the model is not unique, and it is probable that we have not found the best, global solution for the assumed structure of the model. Additionally, we have included only those structures required by the dispersion and scattering data. Alternatively, we could have also included known H II regions whose sizes and densities are well estimated. At present, most known pulsars are unaffected by known H II regions. In the future, when more pulsars are known, inclusion of H II regions will become warranted.

#### 5.1. The Role of the Galactic Pulsar Distribution

The optimal procedure would consist of simultaneous modeling of the Galactic distributions of pulsars and the electron density (for the case where the distances of most pulsars are not known independently). Such a procedure requires accurate knowledge of the pulsar luminosity function which, owing to beaming of the pulsar radiation, is not yet known (but see Arzoumanian, Chernoff, & Cordes 2002). For our present effort, we assume that there is considerable spatial overlap of Galactic pulsars and electrons. In fact, we assume that the overlap is such that the vast majority of pulsar distances are *determinable* from their dispersion measures. Counterexamples exist,

of course, in the pulsars within globular clusters that are well outside the Galactic plane whose DM-determined distances have large errors. Objects in the LMC and SMC also have distances indeterminable from the measured DM. For most other objects in the known pulsar sample, however we assume that they are near enough so that  $DM < DM_\infty$ . Thus, we impose on our model the requirement that  $N_{\text{over}} = 0$  for objects not in globular clusters or the Magellanic clouds (see below). This requirement may bias the model in some directions because high-velocity objects are expected that, over a typical pulsar lifetime  $\sim 10$  Myr, can move well outside the regions of significant free electron density.

### 5.2. Component Inclusion and Figures of Merit

Our overall fitting philosophy follows Occam's Razor in that we attempt to account for the dispersion and scattering of as many lines of sight as possible using large scale structures. Only when required do we include, ad hoc, an additional small-scale perturbing cloud or clump along a particular line of sight. As diagnostics and figures of merit for the model, we used:

1. The likelihood function for pulsar distances and DMs,  $\mathcal{L}_d$ , is maximized as one measure of best fit to the available measurements.
2.  $N_{\text{hits}}$ , the number of pulsars having independent distance measurements, expressed as a range  $[D_L, D_U]$ , and for which the model yields  $\hat{D} \in [D_L, D_U]$ . We maximize  $N_{\text{hits}}$ . Maximizing  $N_{\text{hits}}$  is identical to maximizing the likelihood function for distance and DM data,  $\mathcal{L}_d$ , defined below. However, in practice, we tended to use  $N_{\text{hits}}$  for constraining the local ISM and  $\mathcal{L}_d$  for the larger scale medium.
3.  $N_{\text{over}}$ , the number of pulsars with  $DM > DM_\infty(\ell, b)$ , the maximum DM allowed by the model when integrating to infinite distance. We minimize  $N_{\text{over}}$ . When fitting large-scale components to account for pulsar DMs, we calculated a DM-residual plot for those pulsars in a given iteration that had DMs larger than the model could account for. By plotting  $\Delta DM = DM - DM_\infty$  against Galactic coordinates  $\ell, b$ , we identified which model components needed adjustment. For the TC93 model, a plot of such residuals is shown in Figure 4 of Paper I.
4.  $N_{\text{lum}}$ , the number of pulsars with discrepant luminosities, where "luminosity" is defined as the pseudo-luminosity,  $L_p = S\hat{D}^2$ , where  $S$  is the period-averaged flux density (typically at either 0.4 or 1.4 GHz). The goal is to minimize  $N_{\text{lum}}$ . In practice, utilizing  $N_{\text{lum}}$  is subjective for individual objects because pulsar surveys are subject to Malmquist-type bias that is complicated by the fact that both the detection limits and the pseudo-luminosities are period and DM dependent.

Nonetheless, one expects that the upper envelope on  $L_p$  should be constant as a function of DM if there is a cutoff in the luminosity function and once sufficient volume has been searched to find the most luminous objects. For the present work, we have only made cursory use of this figure of merit because use of  $N_{\text{over}}$  accomplished essentially the same thing.

5. Likelihood functions for scattering observables as defined below:  $\mathcal{L}_{\text{psr},s}$ ,  $\mathcal{L}_{\text{gal},s}$  and  $\mathcal{L}_{\text{xgal},s}$  for the separate subsamples of pulsars, other Galactic sources, and extragalactic sources. As usual, we maximize these likelihoods.

### 5.3. Definitions of Likelihood Functions

We calculate the likelihood function using model predictions and PDFs for the errors in the observables. The likelihood function is factorable according to the statistical independence of four kinds of measurements: (1) pulsars with independent distance constraints; (2) scattering measurements of pulsars (pulse broadening or scintillation bandwidth); (3) scattering measurements of other Galactic sources; and (4) scattering measurements of extragalactic sources. We factor the total likelihood,  $\mathcal{L}$ , into a factor for pulsar distances and a factor for all scattering measurements:

$$\mathcal{L} = \mathcal{L}_d \mathcal{L}_s \quad (15)$$

$$\mathcal{L}_s = \mathcal{L}_{\text{psr},s} \mathcal{L}_{\text{gal},s} \mathcal{L}_{\text{xgal},s}. \quad (16)$$

For the distance factor, we use the fact that some pulsars are attributed distances in an interval  $[D_L, D_U]$  with essentially no preference for any distance within the interval. We therefore adopt a flat distribution inside the interval and exponential decays for model distances outside the interval. The e-folding scales are proportional to  $D_L$  and  $D_U$ . Thus the distance PDF is

$$f_D(D; D_L, D_U) = \mathcal{N} \times \begin{cases} 1 & D_L \leq D \leq D_U \\ e^{-(D_L - D)/\epsilon D_L} & D < D_L \\ e^{-(D - D_U)/\epsilon D_U} & D > D_U, \end{cases} \quad (17)$$

where

$$\mathcal{N} = \left[ D_U - D_L + \epsilon(D_L + D_U - D_L e^{-1/\epsilon}) \right]^{-1}. \quad (18)$$

We choose  $\epsilon = 0.05$  because distance constraints are typically hard bounds for H I absorption, as opposed to describing Gaussian error bounds. The likelihood factor for distances becomes

$$\mathcal{L}_d = \prod_{j=1}^{N_{\text{psr},d}} f_D(\hat{D}_j; D_L, D_U), \quad (19)$$

where  $\hat{D}_j$  is the model prediction for a given set of model parameters.<sup>3</sup>

For scattering measurements we assume that logarithms of observables  $X = (\Delta\nu_d, \tau_d, \theta_d)$  are normally distributed with standard deviation  $\sigma \approx \sigma_X/X \ll 1$ . There are also upper limits, particularly on  $\tau_d$ , for which we

<sup>3</sup>

Alternatively, we could use DM as the observable and then use the empirical distance constraint ( $D \in [D_L, D_U]$ ) to calculate a set of predicted values of DM. The two approaches are equivalent and we choose to use distance as a quasi-observable quantity.

use the cumulative distribution function of  $\log X$  to evaluate likelihood factors. The likelihood factors involving scattering observables are

$$\mathcal{L}_{y,s} = \prod_{j=1}^{N_y} \mathcal{L}_j, \quad (20)$$

where  $y=(\text{psr}, \text{gal}, \text{xgal})$  and  $N_y$  is the number of measurements of each kind and  $j$  labels the relevant line of sight. Model predictions are compared with the scattering observables,  $\theta_d$ ,  $\tau_d$  and  $\Delta\nu_d$ , through the ratio  $r_{\text{scatt}} = \widehat{\theta}_d/\theta_d$ ,  $r_{\text{scatt}} = \widehat{\tau}_d/\tau_d$ , or  $r_{\text{scatt}} = (\widehat{\Delta\nu}_d/\Delta\nu_d)^{-1}$ , such that  $r < 1$  signifies that the model *underestimates* the scattering strength along the particular line of sight. The likelihood factor for the  $j^{\text{th}}$  line of sight is

$$\mathcal{L}_j = \begin{cases} (2\pi\sigma^2)^{-1/2} e^{-(\log r_{\text{scatt}})^2/2\sigma^2} & \text{measurements} \\ \frac{1}{2} \{1 + \text{erf}(\log r_{\text{scatt}}/\sqrt{2}\sigma)\} & \text{upper limits.} \end{cases} \quad (21)$$

#### 5.4. Procedure

We took the following, general approach to fitting for model parameters:

1. Adopt preliminary values of parameters based on TC93 and on empirical distributions such as those shown in Figures 1–6.
2. Fit for parameters of the large-scale components of  $n_{\text{gal}}$  both before and after identifying and excluding outlier points that are associated with peculiarities of specific lines of sight. This fit is made by maximizing the likelihood functions defined below.
3. Fit for local ISM parameters by freezing the parameters of large scale structure and using only pulsars with  $\text{DM} \leq 40 \text{ pc cm}^{-3}$  and for which parallax distance constraints exist. Initially, only distance and DM data are used; then scattering measurements are used as well.
4. Re-fit parameters of the large scale distribution by identifying the best, compromise model that nearly minimizes  $N_{\text{over}}$  and nearly maximizes  $N_{\text{hits}}$  while achieving near-maximum likelihoods.
5. Re-fit the local ISM parameters again while holding fixed other parameters and maximizing  $N_{\text{hits}}$ .
6. Re-fit all large-scale parameters again while holding fixed the local ISM parameters.

Steps 2–6 were taken first by fitting for those parameters that determine DM while ignoring scattering. Thus, in a first pass, we optimized those parameters that determine the local mean  $n_e$ . The same steps were repeated in a second pass to optimize the parameters that determine the local mean  $C_n^2$ . For this pass, we maximized the likelihood function for scattering observables (defined below) and we maximized the number of nearby objects with parallax distances for which the scattering observable was within an acceptable range about the measured values. Once the best, smooth model was obtained in this way, we

identified “outlier” lines of sight which required “clumps” of excess  $n_e$  and/or  $C_n^2$ . We modeled these clumps to bring the outliers into conformance with measured quantities. Finally, we repeated the whole procedure once the individual clumps were included to determine the best parameters of the smooth components of the model.

#### 5.5. Identification of Regions of Enhanced Electron Density

Once solutions for the large-scale components are chosen, clumps are included in the model and a new fit is done for parameters of smooth components in the model. The clump identification process is also iterated. Our final solution results after two such iterations. Lines of sight with required clumps are given in Tables 5–7 of Paper I.

We identify clumps empirically using the following method. Starting with an initial smooth model for the Galactic  $n_e$ , which consists of  $n_{\text{gal}}$ ,  $n_{\text{lism}}$ , and the Galactic center component,  $n_{\text{gc}}$ , we investigate the line of sight for each object for which we have a scattering measurement. First consider a pulsar. If the model fits the distance constraints (if any) and the measured scattering observable to within a factor of two, no additional electrons are needed along that line of sight. If the scattering is outside a factor of two and/or  $\hat{D} > D_{\text{L}}$  then a trial clump is placed along the line of sight to bring relevant estimates into agreement with the observables. For specificity, we adopt a clump with a Gaussian density profile with radius  $r_c$  whose centroid sits on the line of sight. We choose  $r_c = 10 \text{ pc}$  in most cases as an arbitrary but not unreasonable clump radius given that some H II regions are of order this size. The clump distance (from the Sun) is chosen as being either half the lower pulsar distance limit if meaningful distance constraints exist,  $d_c = D_{\text{L}}/2$ , for nearby pulsars or it is set to the midpoint of the spiral arm which contributes the longest path length to the line of sight. This latter choice is clearly not unique for cases where the line of sight traverses multiple spiral arms, but without further information, this seems the most probable course to take. Once  $d_c$  is chosen, we step through a grid of values of electron density,  $n_{e,c}$ , and fluctuation parameter,  $F_c$ , and find pairs of values that bring the overall model values into conformance with the data.

As discussed below, this procedure generally finds multiple solutions. We select the one solution that has the minimum values for  $n_{e,c}$  and  $F_c$  while allowing a good fit.

Using a preliminary model, we calculate the ratio  $r_{\text{scatt}}$  (defined above) and identify lines of sight with significant departures from unity. Next we identify, where possible, clump parameters that bring prediction and reality into agreement, i.e.,  $0.5 \leq r_{\text{scatt}} \leq 2$ .

In assigning clumps, we analyzed each line of sight separately. We attempted to find multiple LOS affected by larger-scale clumps. Though individual OH masers (e.g., those in W49) can be treated in this way, we find that the density of known, scattered sources in the sky is too low to generally find objects that are affected by the same clump or region of enhanced scattering. We find  $F_c = 0$  in some cases which causes the distance to lessen and thus the scattering to change.

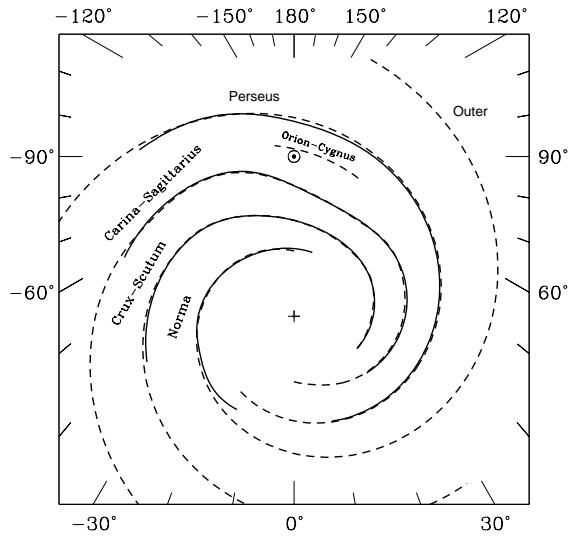


FIG. 9.— Solid lines: spiral model of the Galaxy used in TC93, defined according to work by Georgelin and Georgelin (1976), modified as in TC93. Dashed lines: a four-arm logarithmic spiral model combined with a local (to the Sun) arm using parameters from Table 1 of Wainscoat et al. (1992), but modified so that the arms match some of the features of the arms defined in TC93. The names of the spiral arms, as in the astronomical literature, are given. A + sign marks the Galactic center and the Sun is denoted by  $\odot$ .

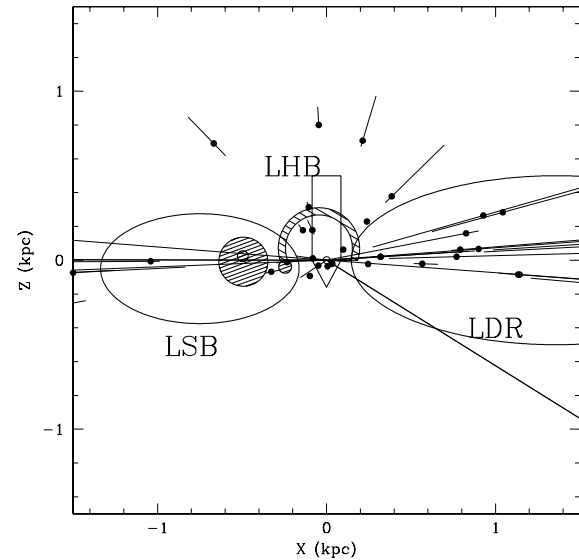


FIG. 11.— Projection onto the  $x$ - $z$  plane of the four local ISM components, LHB, LSB, LDR and Loop I. The plotted lines that point toward the Sun represent the allowed distance ranges from parallax measurements. The points show the predicted locations (using DM) of those pulsars with parallax measurements.

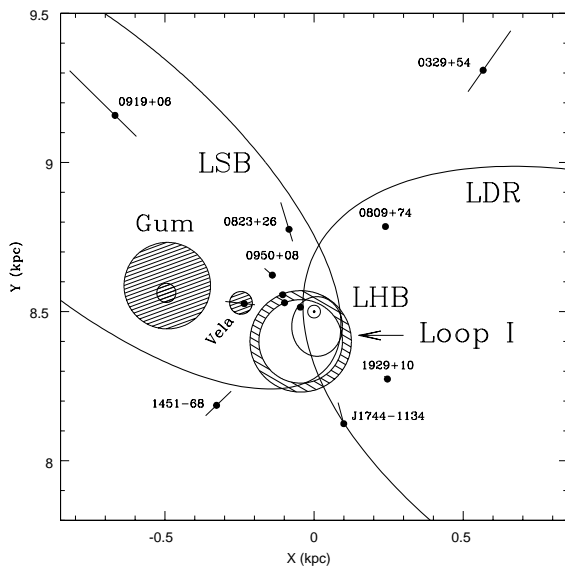


FIG. 10.— Projection onto the Galactic  $x$ - $y$  plane of the four local ISM components, LHB, LSB, LDR and Loop I. The filled circles show the DM-predicted locations of those pulsars having parallax measurements along with the range allowed from the parallax measurements. The plotted lines that point toward the Sun represent the allowed distance ranges from parallax measurements. For a few cases, these lines are too short to be visible.

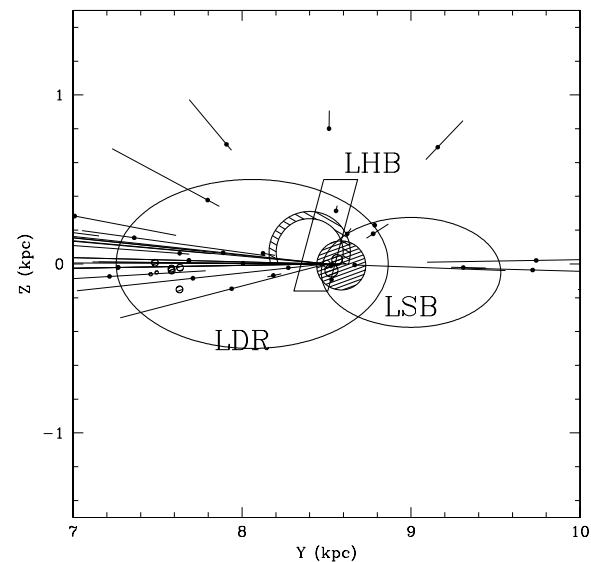


FIG. 12.— Projection onto the  $y$ - $z$  plane of the four local ISM components, LHB, LSB, LDR and Loop I. The plotted lines that point toward the Sun represent the allowed distance ranges from parallax measurements. The points show the predicted locations (using DM) of those pulsars with parallax measurements.

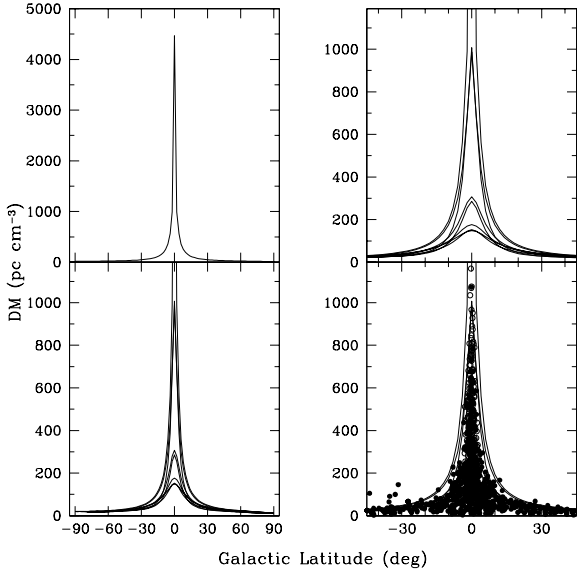


FIG. 13.— DM plotted against Galactic Latitude for model and data. Top left: For Galactic longitude  $\ell = 0^\circ$  and showing the full range of DM. Bottom left: For eight longitudes,  $\ell = 0^\circ, \pm 45^\circ, \pm 90^\circ, \pm 135^\circ,$  and  $180^\circ$  for  $DM \leq 1200 \text{ pc cm}^{-3}$ . Top right: The same eight longitudes for a partial Galactic latitude range. Bottom right: same as top right but with data points included. The points about the curves for  $b \lesssim -35^\circ$  are pulsars in the LMC and SMC, whose DMs receive contributions from their host galaxies.

## 6. MODEL COMPARISONS

The final model is considerably more complex than all previously published electron density models for the Galaxy. To demonstrate the contributions of the various model components to the end result and thus elucidate the need for such components, we compare the figures of merit discussed in §5.2 for different models that exclude one or more components of our final model. Results in Table 1 include log likelihoods and values for  $N_{\text{hits}}$ , the number of LOS for which the model yields a distance within the empirical distance range,  $[D_L, D_U]$ , and  $N_{\text{over}}$ , the number of objects for which the model provides insufficient electrons to account for DM. For each model in the table, we maximized  $\Lambda_d \equiv \log \mathcal{L}_d$  by varying relevant parameters. The reported value of  $\Lambda_d$  was the maximum value unless a slightly submaximal  $\Lambda_d$  yielded a larger value of  $N_{\text{hits}}$  or  $\Lambda_s \equiv \log \mathcal{L}_{\text{psr},s}$ . With the model parameters selected in this way, we then calculated  $N_{\text{over}}$ .

The models are listed in Table 1 in order of increasing goodness of fit, taken as a subjective combination of  $\Lambda_d, \Lambda_s, N_{\text{hits}}$  and  $N_{\text{over}}$ . As discussed in §5.1, we consider minimization of  $N_{\text{over}}$  to be a necessary requirement of a good model. The last column of Table 1 shows a decline from 77 for the simplest model (a thick, symmetric disk combined with the GC component) to 6 for the final model. The 6 objects include 5 in the LMC and SMC, which receive significant contributions from their host galaxies. The lone Galactic object (PSR J1549+2110,  $DM = 30 \text{ pc cm}^{-3}$ ) in this group of 6 has only a marginal excess over the model,  $\Delta DM = 1.3 \text{ pc cm}^{-3}$ . There is a steady increase in  $N_{\text{hits}}$  and decrease in  $\Lambda_s$  going down the table. Perusal of Table 1 also indicates the following. First, the need for clumps and voids is indicated by the sharp drops in  $\Lambda_d$  and  $\Lambda_s$  in going from models without these components (Fits 1–3) to those that do (Fits 4–6). Inclusion of the

LISM components leads to a significant increase in  $N_{\text{hits}}$  (by design) as do clumps and voids, spiral arms, and the thin disk. Spiral arms and the thin disk together reduce significantly the scattering likelihood. Spiral arms produce a large drop in  $N_{\text{over}}$ . There is considerable covariance between the spiral arms and the thin disk, which are colocated in the inner Galaxy. In this regard, the need for a thin disk and the spiral arms is best demonstrated from  $\Lambda_s$  and  $N_{\text{over}}$ , rather than from  $\Lambda_d$  and  $N_{\text{hits}}$ .

For comparison, we also show results for TC93 and for the recent model of GBC01. For these models, we have fixed their parameters to the published values. TC93 performs much less well than NE2001 in all figures of merit. GBC01 is an axisymmetric model constructed using only those pulsars having independent distance constraints and providing only the local mean electron density. Therefore no estimates of scattering may be made with GBC01. For the three relevant figures of merit, GBC01 performs less well than either TC93 or NE2001.

## 7. GOODNESS OF FIT

Figures 10–12 show nearby pulsars with empirical distance ranges (from parallax measurements) plotted as lines whose extrapolations intersect the Sun’s location. The filled circles indicate the distance estimated with NE2001. As can be seen, all objects have model-predicted distances that fall within the allowed parallax distance ranges. Paper I also discusses model performance. Figure 8 of Paper I shows distance estimates and empirical constraints (mostly from HI absorption) for objects at large distances. The model was constructed in part by attempting to get these distances correct, so the figure essentially demonstrates self-consistency of our procedure. The same can be said for Figure 9 of Paper I, which shows a scatter plot of estimated distance and empirical distance range,  $[D_L, D_U]$ .

## 8. INDIVIDUAL LINES OF SIGHT

In this section we discuss various lines of sight. We shall elaborate on the need for a clump or void on some lines of sight, while other lines of sight provide constraints on the parameters of the clumps or voids.

We have searched for H II regions, supernova remnants, and O stars within  $30'$  of the line of sight to any pulsar requiring a clump. Although many H II regions have angular sizes less than  $30'$ , they may have extended envelopes that would contribute to a pulsar’s DM (Anantharamaiah 1985) and models of H II regions surrounding O stars suggest that they could be larger than  $1^\circ$  (Miller & Cox 1993). Moreover, the size of at least one clump can be constrained to be at least  $15'$  in size (see the discussion of PSR B1849+00 below). Thus, we view  $30'$  as a reasonable estimate for the size of a clump.

Of course, it is possible that what we have modeled as a single clump is in fact the combined contribution of many H II regions or supernova remnants. Indeed, many of the pulsars have multiple objects close to their lines of sight. Thus, the discussion below should lend plausibility to our choice to insert clumps along the line of sight to many pulsars or other sources, though we in many cases cannot associate a given clump with any particular H II region or

supernova remnant. Conversely, in some cases, we believe the case for a clump is nearly self-evident, e.g., masers associated with an H II region, and we shall not discuss those lines of sight.

We also have searched for H I shells along the lines of sights where we have identified voids. Using 100 pc as a characteristic size and 3 kpc as a characteristic distance (Heiles 1979), we find that the typical shell may be able to affect lines of sight within  $1-3^\circ$ .

**NGC 6334N and NGC 6334B** The highly scattered masers in NGC 6334N are probably associated with the H II region NGC 6334 while the extragalactic source NGC 6334B is seen through it.

**OH 353.298–1.537** This line of sight does not pass through our Galactic center component. We have been able to find only one possible source of scattering toward the maser, the O star LS 4227, which is at an estimated distance of 2 kpc (Kilkenny 1993).

**OH 359.14+1.14** This line of sight does not pass through our Galactic center component, though the maser itself is thought to be more distant than the Galactic center (van Langevelde et al. 1992). We have been able to find only one possible source of scattering toward the maser, the O star system CCDM J17381–2907AB, which is at an indeterminate distance.

**OH 20.1–0.1 OH 40.6–0.2, OH 43.80–0.13** These OH masers are associated with H II regions (Hansen et al. 1993).

**PSR B0138+59** The distance constraints from H I absorption,  $1.9 \leq D \leq 3.6$  kpc (Graham et al. 1974), imply  $n_e \approx 0.01-0.018$  cm<sup>-3</sup>, substantially smaller than expected if the pulsar in fact resides within the Perseus spiral arm. To allow this distance and match the scattering, an ad hoc void is needed with substantial underdensity and smaller  $F$  parameter than is typical of the spiral arms. We suspect that the pulsar is nearer than the alleged lower distance estimate of 1.9 kpc. This low-DM pulsar ( $DM = 35$  pc cm<sup>-3</sup>) has a model distance of 2.2 kpc. Within  $3^\circ$  is the H I shell GSH 130+00+15 at an estimated distance of 0.5 kpc (Heiles 1979).

**PSR B0531+21 (= Crab pulsar)** The Crab pulsar is well-known to be associated with the Crab Nebula.

**B0809+54** ( $\ell = 140.0^\circ, b = 31.6^\circ$ ) The DM to this pulsar implies a LOS average density of 0.013 cm<sup>-3</sup> over a (parallax) distance  $0.433 \pm 0.008$  kpc. The scattering is quite low. To match the distance and DM, the model requires a significant path length through the LDR in our LISM model. Rickett, Coles & Markkanen (2000) used weak scintillation measurements to constrain the scattering medium along the LOS, finding consistency either with a uniform, but weak, Kolmogorov medium or a nonuniform one with a discrete scattering screen

$\sim 0.2$  kpc from the Sun, assuming a distance (based on TC93) of 0.31 kpc. The new distance (Briskin 2001; Briskin et al. 2002) implies a proportionately larger screen distance and an even weaker scattering medium ( $\log SM = \text{kpc m}^{-20/3}$ ). The low  $F$  parameter and low density of the LDR accommodate these measurements.

**B0950+08** This LOS has the smallest known scattering measure, owing to the path length being predominantly through the LHB and LSB, which have small electron densities and small fluctuation parameters.

**PSR 1019–5749** The line of sight to this high-DM pulsar ( $DM > 1000$  pc cm<sup>-3</sup>) passes close to a number of H II regions, which could individually or in combination account for the need for a clump along this line of sight. The H II region NGC 3199 is approximately  $10'$  from the line of sight to this pulsar. Situated in the Carina arm, Deharveng & Maucherat (1974) cite a distance of 3.8 kpc. Caswell & Haynes (1987) also find the H II region G283.978–0.920 to have a kinematic distance of approximately 5 kpc. (This is probably the same H II region that Wilson et al. [1970] name G284.0–0.9, for which they find a similar distance.)

**PSR J1022–5813** The H II regions Gum 29, G284.0–00.9, and G284.650–0.484 are within  $0^\circ 5'$  and at distances of 4–6 kpc (Wilson et al. 1970; Caswell & Haynes 1987). Also close to the line of sight is the supernova remnant SNR 284.3–01.8, which Ruiz & May (1986) argue is between 1 and 4 kpc distant and probably more likely to be at the far end of this distance range.

**PSR B1054–62** This moderate DM pulsar ( $DM = 323$  pc cm<sup>-3</sup>) has a model distance of approximately 3 kpc. At approximately the same distance is the exciting star of the H II region RCW 55 (Humphreys 1976) and for the H II region itself (Brand & Blitz 1993) Although there is some possibility for the pulsar to be in front of the H II region, the possible biases of the some of the distance estimates suggest otherwise. If we do not insert a clump in front of this pulsar, its distance would be larger than otherwise predicted by our model. The photometric distance estimate to the exciting star, if not corrected properly for dust obscuration, will tend to underestimate the distance to the H II region. Also close to the line of sight is the UCHII IRAS 10555–6242, at a comparable distance as RCW 55 (Walsh et al. 1997). The typically small angular size of UCHIIIs, however, makes it unclear whether this particular one could affect the line of sight to the pulsar.

**PSR B112–60** The line of sight to this pulsar ( $DM = 677$  pc cm<sup>-3</sup>) passes close to a number of H II regions. Our model distance for this pulsar is 15 kpc, and without the addition of a clump, its model distance would be well outside the Galaxy.

There is a cluster of H II regions (G291.205–0.267, G291.466–0.128, and NGC 3603) at approximately 8.5 kpc (Caswell & Haynes 1987). A second probable cluster of H II around 3.5 kpc, related to the Carina arm, also exists that includes NGC 3576 (Wilson et al. 1970) and the UCHII IRAS 11097–6102 (Walsh et al. 1997).

**PSR J1119–6127** Crawford et al. (2001) argue that this pulsar is associated with the supernova remnant SNR 292.2–00.5. In addition the H II region G291.9–0.7 (Wilson et al. 1970; Caswell & Haynes 1987) lies close to the line of sight. Crawford et al. (2001) adopt a distance of 5 kpc to the pulsar-SNR association, though they acknowledge that it is highly uncertain. The H II region is at approximately 10 kpc, and our model estimates a distance of 16.7 kpc from the DM of the pulsar. One resolution of these various distances would be to place multiple clumps in front of the pulsar, from both the SNR and the H II region, and locate all of the objects in the far portion of the Carina spiral arm at a distance of 8–10 kpc.

**PSR J1128–6219** Our estimated distance to this pulsar ( $DM = 675 \text{ pc cm}^{-3}$ ) is 15.4 kpc. The following H II regions are close to the line of sight and have estimated distances that place them in front of the pulsar: RCW 60 at 2.4–4 kpc (Humphreys 1974; Caswell & Haynes 1987) and G293.027–1.031 at 14.5 kpc. Also close to the line of sight are the UCHIIs IRAS 11298–6155 at 10.1 kpc and IRAS 11304–6206 at 11.1 kpc (Walsh et al. 1997). Finally, the O stars HD 99897 (in the H II region Gum 39) and HD 308570 lie close to the line of sight, but at indeterminate distances.

**PSR B1131–62** Our estimated distance to this pulsar ( $DM = 568 \text{ pc cm}^{-3}$ ) is 11.8 kpc. The following UCHIIs are close to the line of sight and have estimated distances that place them in front of the pulsar: IRAS 11304–6206 at 11.1 kpc and IRAS 11332–6258 at 1 or 7.1 kpc (Walsh et al. 1997). Also close to the line of sight, but at an indeterminate distance is the H II region G294.34–1.33.

**PSR J1201–6306** Our estimated distance to this pulsar ( $DM = 683 \text{ pc cm}^{-3}$ ) is 12.7 kpc. The H II regions G297.506–0.765 at 11.4 kpc and G297.655–0.977 at 11.7 kpc (Caswell & Haynes 1987) may lie in front of this pulsar.

**PSR J1216–6223** Our estimated distance to this pulsar ( $DM = 787 \text{ pc cm}^{-3}$ ) is 17 kpc, and its estimated distance would locate it outside the Galaxy if we did not place a clump along the line of sight to it. Lying close to the line of sight to the pulsar are the H II regions G299.016+0.148 at an estimated distance of 11.8 kpc and G298.559–0.114 at 11.7 kpc (Caswell & Haynes 1987) and the UCHII IRAS 12146–6212 at 10.6 kpc (Walsh et

al. 1997). In addition, three supernova remnants at indeterminate distances also lie close to this line of sight, SNR 298.6–0.0, SNR 299.0+0.2, and SNR 298.6+0.0.

**PSR J1305–6256** Our estimated distance to this pulsar ( $DM = 967 \text{ pc cm}^{-3}$ ) is 11.9 kpc. The SNR 304.6+0.1 has an H I absorption constraint on its distance of 9.7 kpc (Caswell et al. 1975), potentially placing it in front of the pulsar. Two O stars, at indeterminate distances, also lie close to the line of sight, HD 113754 and HD 114122.

### **B1310+18 (in NGC 5024 = M53)**

**PSR B1316–60** At an indeterminate distance, the O star SAO 252232 lies close to the line of sight to this pulsar.

**PSR J1324–6146** Close to the line of sight, at an indeterminate distance, are the H II region G307.1+1.2 and the O star GSC 08995-01924.

**PSR 1323–62** Our estimated distance to this pulsar ( $DM = 318.4 \text{ pc cm}^{-3}$ ) is 5.5 kpc. Near the line of sight is the O star LSS 3052, which, on the basis of its  $E_{B-V}$ , is approximately 3.9 kpc distant (Turner 1985). Also close to the line of sight, but at indeterminate distances, are the O stars GSC 08995-01924 and SS 246.

**PSR B1334–61** Our estimated distance to this pulsar ( $DM = 638 \text{ pc cm}^{-3}$ ) is 9.5 kpc. The following H II regions are close to the line of sight and have estimated distances that place them in front of the pulsar: G308.647+0.579 at 4.4 kpc (or a less likely distance of 8.1 kpc, Caswell & Haynes 1987), G308.6+0.6 at 4.7 or 7.8 kpc, and G308.7+0.6 at 3.9 or 8.6 kpc (Wilson et al. 1970). The supernova remnant SNR 308.7+0.0 may also be close enough to the line of sight to affect the DM; Caswell et al. (1992) adopt a distance of 6.9 kpc to it. Finally, close to the line of sight, but at indeterminate distances are the O star GSC 08995-00021 and the H II regions Gum 48c and BBW 27600.

**PSR B1338–62** Kaspi et al. (1992) argue that this pulsar ( $DM = 730 \text{ pc cm}^{-3}$ ) is associated with the supernova remnant SNR 308.8–0.1, of which SNR 308.7+0.0 forms a portion (Caswell et al. 1992). The distance, albeit highly uncertain, that they adopt for the remnant is 6.9 kpc. Our estimated distance for the pulsar is 11 kpc. Additional dispersion may be contributed by the H II region G309.057+0.186, which is at a distance of 3.9 kpc (or a less likely distance of 8.7 kpc, Caswell & Haynes 1987). Further, the O star GSC 08995-00021 lies close to the line of sight, though at an indeterminate distance.

**J1430–6623 & J1453–6413** The lower bound  $D_L = 2.0$  kpc from H I absorption for J1453–6413 (Koribalski et al. 1995) requires a void along the LOS at the Carina-Sagittarius arm. The scattering

is overestimated by a factor of  $\sim 12$ . The nearby object J1430–6623 requires a clump to bring its distance smaller so as to account for the scattering (there is no distance constraint on this object).

**PSR B1508–57** Our estimated distance to this pulsar ( $DM = 628.7 \text{ pc cm}^{-3}$  is 7.3 kpc. There are a number of H II regions close to this line of sight, but kinematic distance ambiguities make it difficult to assign reliable distances to them. Nominally in front of the pulsar are the H II regions G321.038–0.519 (Caswell & Haynes 1987) and G321.0–0.5 (Wilson et al. 1970), both at 4.4; however, both H II regions could also be approximately 11 kpc distant. Similarly, nominally behind the pulsar are the H II regions G320.379+0.139, G320.706+0.197, and G320.317–0.208 whose estimated distances are approximately 15 kpc (Caswell & Haynes 1987). Though regarded as less likely, distances between 0.2 and 0.7 kpc are also acceptable for these three H II regions. Finally, the H II region G320.3–0.2 and the O star GSC 08702-00089 are also close to the line of sight, though at indeterminate distances.

**PSR B1518–58** Close to the line of sight to this pulsar are the supernova remnant MSC 321.9–1.1 and the O star [L64] 240.

**B1534+12** The distance to this pulsar is constrained from the 6-month parallax term in pulse arrival times ( $D > 0.6$  kpc) and from correction for the Shklovsky effect on the orbital period derivative of the pulsar (Stairs et al. 1998), which implies  $D = 1.1 \pm 0.2$  kpc. The lower distance limit  $D_L = 0.9$  kpc and measured scintillation bandwidth are difficult to reconcile. With the large scale model, a distance of 0.54 kpc is obtained. A low density void is needed to reach  $D_L$ . But even with  $F = 0$  in the void, the strength of scattering is overestimated by a factor of 5. A distance near 0.6 kpc would reconcile this discrepancy but would then be inconsistent with timing analyses of the orbit. We conclude that the line of sight to this pulsar is likely dominated by conditions interior to a “blowout” region.

**PSR J1544–5308** Close to the line of sight to this pulsar are the supernova remnant MSC 327.4+1.0 and the O star [L64] 282.

**J1559–4438 & J1600–5044** The minimum H I absorption distances to these pulsars are 1.5 kpc and 5.9 kpc, respectively. The latter requires a void along the line of sight that, if larger than 200 pc in transverse extent, also influences J1559–4438. However, the large implied distance for J1559–4438 is inconsistent with the scintillation bandwidth for electron density components currently in the model; the scattering is overestimated by a factor  $\sim 6$ .

**J1602–5100** The H I absorption spectrum to this object shows a questionable feature at  $-110 \text{ km s}^{-1}$  that,

if real, indicates  $D_L \approx 7.4 \pm 0.5$  kpc. If not real, then  $D_L \approx 5.5 \pm 0.5$  kpc, a distance consistent with the present model.

**PSR J1605–5257** Our estimated distance to this pulsar ( $DM = 32 \text{ pc cm}^{-3}$ ) is 1.5 kpc. There is an UCHII along the line of sight, IRAS 15596–5301, but the estimated distance to the UCHII is either 4.8 or 12.9 kpc, placing it behind the pulsar. No other objects appear to be in front of the pulsar that could account for the need for a clump.

**PSR B1627–47** Close to the line of sight to this pulsar is the supernova remnant SNR 336.7+00.5.

**PSR B1641–45** Our estimated distance to this pulsar ( $DM = 480 \text{ pc cm}^{-3}$ ) is 5 kpc. There are a number of H II regions close to the line of sight of this pulsar that might affect its DM. Because of distance ambiguities, it is not clear that all of these H II regions can affect the pulsar’s DM, though. The following H II regions have distances compatible with being in front of the pulsar: G339.286+0.163 at 5.8 kpc, though 13 kpc is also possible; G339.128–0.408 at 3.3 kpc, though 15.4 kpc is also possible if less likely; G338.921–0.089 at 3.6 kpc, though 15.1 kpc is also possible if less likely (Caswell & Haynes 1987); and G338.9–0.1 at 3.6 kpc, though 15.1 kpc is also possible (Wilson et al. 1970). The UCHII IRAS 16424–4531 is at 3.3 kpc, though 15.5 kpc is also a possible distance for it. The H II regions G339.089–0.216 at 9.3 kpc and G339.578–0.124 at 16 kpc (though a less likely distance is 2.8 kpc) are unlikely to affect the pulsar’s DM.

Close the line of sight, at an estimated distance of about 1 kpc, is the highly obscured open star cluster Westerlund 1 (Westerlund 1961; Piatti, Bica, & Clariá 1998). Although this cluster is in front of the pulsar and its integrated spectrum contains nebular emission lines indicative of significant amounts of ionized gas, it is not clear to what extent this cluster could affect the DM of the pulsar. If the cluster is embedded entirely within higher density gas, the extent of the cluster’s H II region may be quite small. Alternately, the cluster may be on the far side of the obscuring region and producing a significant “blister” H II region.

Also close to the line of sight, though of indeterminate distances, are the supernova remnant SNR 339.2–0.4 and the H II region G339.6–0.1.

The O star HD 151018 also lies close to the line of sight to this pulsar, at an approximate distance of 1.6 kpc, and Miller & Cox (1993) predict the radius of its H II region of order 100 pc ( $= 3^{\circ}6$ ).

**PSR B1643–43** This pulsar is associated with the supernova remnant SNR 341.2+0.9 (Frail, Goss, & Whiteoak 1994; Giacani et al. 2001).

**PSR B1703–40** Our estimated distance to this pulsar ( $DM = 360 \text{ pc cm}^{-3}$ ) is 4.4 kpc. The following H II regions may lie in front of this pulsar, though because of distance ambiguities, these regions may also lie behind the pulsar: G345.450+0.209 at 1.7 kpc, though 17.7 kpc is also a possible distance; G345.645+0.010 at 1.3 kpc, though 18.1 kpc is also possible; and G346.109–0.028 at 1.5 kpc, though 17.9 kpc is also possible (Caswell & Haynes 1987). In addition the UCHII IRAS 17031–4037 is at 1.5 kpc, though 18 kpc is also a possible distance (Walsh et al. 1998). The H II regions G345.555–0.042 and G345.827+0.041 have distance estimates of approximately 18 kpc, though distances around 1 kpc are also allowed (Caswell & Haynes 1987).

Also close to the line of sight, though of indeterminate distances, are the O star GSC 07873-00112 and the supernova remnant SNR 345.7–0.2.

**J1709–4428** The H I absorption lower-distance bound of 1.8 kpc (Koribalski et al. 1995) requires a void within the Carina-Sagittarius arm; the model still overestimates the scattering by a large factor ( $\sim 70$ ).

**PSR B1715–40** Close to the line of sight to this pulsar, though of indeterminate distances, are the O stars GSC 07874-00170 and GSC 07874-01001.

**PSR B1718–36** Our estimated distance to this pulsar ( $DM = 416 \text{ pc cm}^{-3}$ ) is 4.3 kpc. Potentially in front of this pulsar is the H II region G350.813–0.019 at 1 kpc, though distance ambiguities mean that it could also be at 18.7 kpc (Caswell & Haynes 1987). Also close to the line of sight, but at indeterminate distances, are the H II region RCW 128, the O star HD 319734, and the supernova remnant SNR 351.2+0.1 (which itself has a central point source and may contain another pulsar, Becker & Helfand 1988).

**PSR B1714–34** Close to the line of sight to this pulsar, though of indeterminate distances, are the H II regions RCW 130 and Sh 2-10 and the O double star IDS 17118–3418B.

**PSR B1727–33** Our estimated distance to this pulsar ( $DM = 256.5 \text{ pc cm}^{-3}$ ) is 3.5 kpc. We have been unable to identify any ionizing source that is definitively in front of this pulsar. The H II region G354.200–0.054 is behind the pulsar, with ambiguous distance estimates of 6.5 or 13.4 kpc, as is G354.486+0.085 with a large, though uncertain distance estimate (Caswell & Haynes 1987). The UCHII IRAS 17279–3350 is close to the line of sight, but of indeterminate distance.

**PSR B1736–31** Our estimated distance to this pulsar ( $DM = 600 \text{ pc cm}^{-3}$ ) is 6.2 kpc. We have been unable to identify any ionizing source that is definitively in front of this pulsar, though, the UCHII IRAS 17352–3153 is at a distance of either 8.9 or 11.3 kpc (Walsh et al. 1997).

**PSR J1745–3040** Our estimated distance to this pulsar ( $DM = 88 \text{ pc cm}^{-3}$ ) is 1.9 kpc. The O star HD 316256 at 0.92 kpc (Kilkenny 1993) is close to the line of sight. Also close to the line of sight, though of indeterminate distances, are the H II region G358.664–0.575 and the supernova remnant SNR 359.0–0.9 (though the latter is usually taken to be in or near the Galactic center).

**PSR B1746–30** Our estimated distance to this pulsar ( $DM = 510 \text{ pc cm}^{-3}$ ) is 5.7 kpc. Along the line of sight is the O emission star HD 316341 at 1.9 kpc (Kozok 1985). Also close to the line of sight, though of indeterminate distances, are the H II regions G359.158–0.881 and G359.281–0.826 and the O star LS 4424.

#### **J1757–2421 = B1757–24 (The Duck Pulsar)**

The lower distance bound of 4.3 kpc, from H I absorption against the synchrotron nebula surrounding the pulsar (Frail et al. 1994b) requires an underdensity along this LOS in the spiral arms intersected (Carina-Sagittarius and Crux-Scutum), but with sizable fluctuation parameter ( $F \sim 10$ ) to match the scattering. Noncircular motions in the H I gas could alter this distance bound given the small Galactic longitude ( $\ell = 5.3^\circ$ ).

**J1759–2205** The DM of this pulsar is nearly identical to that of J1757–2421 while the pulse broadening time is smaller by a factor of four. The scattering requires a smaller F parameter along this line of sight through the Carina-Sagittarius spiral arm.

**PSR J1807–2715** Close to the line of sight to this pulsar, though of an indeterminate distance, is the supernova remnant SNR 004.2–3.5.

**PSR B1758–23** This pulsar has been associated with the supernova remnant W28 (Frail, Kulkarni, & Vasisht 1993; Kaspi et al. 1993). In addition the O star HD 164492B is close to the line of sight and at a distance of 1.4 kpc (Lindroos 1985). There are a few H II regions whose distances place them nominally beyond the pulsar, though the uncertainties in deriving kinematic distances toward the inner Galaxy may make these distance estimates highly uncertain: RCW 145 with an estimated distance of 2.7–13 kpc (Vilas-Boas & Abraham 2000) and G6.528+0.076, G6.6–0.1, and G6.7–0.2 all of which have distance estimates around 3.5 kpc (Wilson et al. 1970). There are also numerous H II regions with indeterminate distances close to the line of sight: Sh 30, G6.553–00.095, G6.565–00.297, G6.667–00.247, G6.979–00.250, G7.299–00.116, G7.002–0.015, G7.236+0.144, RCW 147, Ced 151, and Gum 74a, and two O stars LS 4538 and HD 313599.

**PSR B1815–14** Our estimated distance to this pulsar ( $DM = 625 \text{ pc cm}^{-3}$ ) is 6.9 kpc. Close to the line of sight is the star cluster NGC 6611, which contains a number of O and B stars, at a distance

of 1.6 kpc (Kamp 1974). Also close to the line of sight, although at an indeterminate distance, is the H II region G016.463+0.966.

**PSR 1820-14** Our estimated distance to this pulsar ( $DM = 648 \text{ pc cm}^{-3}$ ) is 4.7 kpc. Close to the line of sight is the O star LS 4971 at an estimated distance of 1.3 kpc (Kilkenny 1993). Also close to the line of sight, though of indeterminate distances, are the H II regions G16.893+0.126, G16.941-0.073, and G17.250-0.195.

**PSR B1830-08** This pulsar may be associated with the supernova remnant W41 (Clifton & Lyne 1986). Even if not associated with the SNR, there are UCHIIs that may be in front of it, modulo distance ambiguities: IRAS 18317-0845, IRAS 18317-0845, and IRAS 18324-0820 all have distance estimates between 5 and 6 kpc, though they could also be between 12 and 13 kpc distant (Walsh et al. 1997). In addition, the UCHIIs IRAS 18310-0825 and IRAS 18310-0825 have distance estimates of 6.4 kpc, placing them nominally just beyond the pulsar, though they may also be 12 kpc distant (Walsh et al. 1997). Finally, the H II regions G23.281+0.298, G22.935-0.072, G23.000+0.219, G23.162+0.023, G23.072-0.248, G23.254-0.268, G23.42-0.21, G23.538-0.041, G23.613-0.376, G23.706-0.202, and G23.817+0.224 and the supernova remnant SNR 23.6+0.3 are close to the line of sight but with indeterminate distances. Also consistent with being in front of this pulsar is the H II region G23.437-0.207 at a distance of  $6.6 \pm 0.5$  kpc (Kolpak et al. 2003).

**PSR B1832-06** While close to the SNR 24.7+0.6, this pulsar is probably not associated with it (Gaensler & Johnston 1995). In addition there are numerous H II regions, though of indeterminate distances, close to the line of sight of this pulsar: RCW 173, BBW 35201, Sh 60, G25.294+0.307, G24.91+0.57, G24.905+0.431, G25.293+0.306, and G25.161+0.069.

**PSR J1823-0154** Close to the line of sight to this pulsar is the H II region (UCHII?) IRAS 18216-0156.

**PSR B1839-04** There are a number of H II regions and supernova remnants close to this line of sight, albeit of indeterminate distances. These include G27.975+0.080, G27.997+0.317, G28.001-0.031, G28.146+0.146, G28.312-0.023, G28.400+0.478, G28.440-0.002, G28.600+0.015, G28.638+0.194, G28.658+0.030, G28.787+0.252, G28.801+0.174, and IRAS 18408-0348 (an UCHII?), which are H II regions, and G28.600-0.126 and AX J1843.8-0352, which are SNRs.

**PSR B1845-01** Our estimated distance for this pulsar ( $DM = 159 \text{ pc cm}^{-3}$ ) is 3.8 kpc. Although there are a number of objects close to its line of sight, few of the objects with estimated distances are

in front of the pulsar. One object potentially in front of the pulsar is IRAS 18452-0141 whose distance is estimated to be 1.2 kpc, though distance ambiguities mean that it might also be at 15.6 kpc (Walsh et al. 1998). Other H II regions close to the line of sight, but at indeterminate distances, are G30.9+0.1, G31.130+0.284, G31.131+0.284, G31.1-0.1, G31.2-0.1b, G31.401-0.259, G31.411+0.309, G31.602-0.227, G31.607+0.334, and the UCHIIs IRAS 18456-0129 and IRAS 18469-0132. (H II regions close to the line of sight, but nominally behind the pulsar include G31.0-0.0 at 8 kpc, G31.0+0.1 at 6.6 kpc, G31.2-0.1 at 12 kpc [Kuchar & Bania 1994], G31.28+00.06 at 8.5 kpc [Caswell & Haynes 1983], G31.3+0.1 at 7.3 kpc, G31.412+0.308 at 7.2 kpc [Kolpak et al. 2003], G31.6+0.1 at 6.5 kpc [Kuchar & Bania 1994], and the UCHIIs IRAS 18446-0150 at 7.6 or 9.1 kpc, IRAS 18449-0115 at 8.5 kpc, and IRAS 18456-0129 at 8.5 kpc [Walsh et al. 1998].)

#### **PSR B1849+00 and extragalactic source B1849+00**

Our estimated distance to this pulsar ( $DM = 680 \text{ pc cm}^{-3}$ ) is 8.4 kpc. Close to this line of sight are the H II regions G33.12-0.08 and G33.2-0.0, both at 7.1 kpc, (Kuchar & Bania 1994) and the supernova remnant SNR 33.7+0.0, which is at a distance of at least 7 kpc (Caswell et al. 1975). Also close to the line of sight, though at indeterminate distances, are the H II region G33.498+0.196, the UCHII IRAS 18504+0025, and the supernova remnant SNR 33.1-0.1 and the H II region G32.80+0.19 which has an upper distance limit of 15.6 kpc (Wink, Altenhoff, & Mezger 1982). (Also close to the line of sight, though nominally behind the pulsar, are the H II region G33.4-0.0 at 9.5 kpc [Kuchar & Bania 1994] and the supernova remnant SNR 33.6+0.1 at 10 kpc [Frail & Clifton 1989].)

The line of sight to this pulsar also provides some constraints on the size of a (single) clump. Located 13' away is the extragalactic source B1849+005, which is one of the most heavily scattered sources known (Spangler & Cordes 1988). Thus, to the extent that the enhanced dispersion and scattering along this line of sight can be modeled as due to a single clump, the clump must be at least 13' in diameter, equivalent to a linear diameter of 15 pc at 4 kpc (halfway to the pulsar).

**PSR B1859+03** The scattering requires a smaller  $F$  parameter along a substantial fraction of the LOS to this pulsar, which has a lower distance bound of 6.8 kpc. The model estimated distance to this pulsar ( $DM = 403 \text{ pc cm}^{-3}$ ) is 7.3 kpc. Within  $3^\circ$  is the H I shell GSH 036+01-21 at an estimated distance of 0.5 kpc (Heiles 1979).

**OH35.2-1.7 & PSR B1900+01** A modest constraint on the angular scale of a clump can be set from these two lines of sight. The OH maser requires

a clump along the LOS while the pulsar,  $\sim 0.6^\circ$  away, does not.

**PSR B1900+01 and OH 35.2–1.7** Our estimated distance to this pulsar ( $DM = 246 \text{ pc cm}^{-3}$ ) is 3.3 kpc. At nearly the same distance is the H II region W 48 (Radhakrishnan et al. 1972), which given distance uncertainties we regard as potentially capable of perturbing the pulsar’s DM. Also close to the line of sight, though at indeterminate distances, are the H II region G35.346–01.827 and the supernova remnant SNR 35.0–1.1. The OH maser is itself associated with an H II region (Hansen et al. 1993), but probably in front of W 48 (Caswell & Haynes 1983).

**PSR B1907+10** Close to the line of sight for this pulsar is the H II region G45.200+0.740.

**PSR B1919+21** Close to the line of sight for this pulsar is the supernova remnant SNR 55.7+3.4.

**PSR B1929+20** Close to the line of sight for this pulsar is the supernova remnant SNR 55.6+0.7.

**B1930+22** The H I-absorption distance constraints of 9.8 - 14.4 kpc are based on low signal to noise features at negative velocity. Frail et al. (1991) state that the  $-16 \text{ km s}^{-1}$  feature that corresponds to 9.8 kpc in a circular-Galactic rotation model could be a local, high-velocity cloud, in which case the pulsar could be nearer than 9.8 kpc. NE2001 places the pulsar at  $D = 7.4 \text{ kpc}$ .

**PSR B1951+32** This pulsar is associated with the supernova remnant CTB 80 (Clifton et al. 1987).

**PSR B1952+29** Close to the line of sight for this pulsar is the supernova remnant SNR 65.7+1.2.

**PSR 2053+36** Close to the line of sight for this pulsar is the H II region G78.81–5.71.

**B2127+11A-H (M15)** The DMs to pulsars in the globular cluster M15 are larger by  $\sim 13 \text{ DM}$  units than the smooth model can accommodate for  $b = -27.3^\circ$ . We have added a clump at 2 kpc distance, about that of the Cygnus superbubble, but well out of the Galactic plane.

**B2210+29** A DM excess  $\Delta DM \approx 10 \text{ pc cm}^{-3}$  persists while varying relevant model components through credible ranges. We have therefore included a clump along the line of sight at a distance of 2 kpc, about that of the Cygnus superbubble, but well out of the Galactic plane at  $b = -21.7^\circ$ .

**OH12.2–0.1** The scattering to this OH maser is overestimated by a factor of three using its attributed distance of 16.1 kpc (Hansen et al. 1993). We question the accuracy of this distance estimate.

**Objects seen through the Cygnus region** These objects include Cyg X-3 and several extragalactic sources. The Cygnus region is thought to be the

tangent to a spiral arm (Bochkarev & Sitnik 1985) and Spangler & Cordes (1998) have shown how the Cygnus OB1 association is probably responsible for a large fraction of the scattering along these lines of sight.

**Objects in the Galactic Center** The GC scattering volume described earlier adequately describes the angular broadening of Sgr A\*, the Galactic Center transient source (Zhao et al. 1991), and many of the OH masers (van Langevelde et al. 1992; Frail et al. 1994). However, the angular broadening for some of the masers is underestimated by a factor of a few. The scatter in the angular broadening predictions undoubtedly derives, in part, from their unknown true distances. We have uniformly attributed a distance of 8.5 kpc to all GC sources. The GC scattering region  $\sim 0.1 \text{ kpc}$  in radius, so changes in true distance of this order, which are expected for the population of OH/IR stars in the GC, will produce significant changes in the amount of scattering at the level seen.

By contrast, G359.87+0.18 (Lazio et al. 1999), thought to be an extragalactic source, shows much less scattering,  $\theta_d \sim 2 \text{ arc sec}$  at 1.0 GHz, compared to an expected  $\sim 300 \text{ arc sec}$ . This indicates that the GC scattering volume is either patchy or does not cover the LOS to this source. We adopt the latter interpretation and use it to attribute an offset of the scattering volume of 20 pc in the  $-z$  direction. We also use a scale height of 26 pc.

**Objects in the LMC and SMC** Five objects in our sample reside in the LMC or SMC, as is consistent with their DMs being too large to be accounted for by our final model; augmentation of the particular lines of sight with H II clumps is unwarranted because the lines of sight are well out of the Galactic plane. We estimate the DM excess attributable to their host galaxies, obtained by subtracting the Galactic contribution (with DM and  $\Delta DM$  in standard units of  $\text{pc cm}^{-3}$ ): J0045–7319,  $DM = 105, \Delta DM = 62$ ; B0456–69,  $DM = 91, \Delta DM = 41$ ; B0502–66,  $DM = 65, \Delta DM = 16$ ; B0529–66,  $DM = 100, \Delta DM = 48$ ; and B0540–69,  $DM = 146, \Delta DM = 91$ .

## 9. DISCUSSION OF THE MODEL & ITS LIMITATIONS

The NE2001 model represents a clear improvement upon the TC93 model. First, the distance estimates obtained from the model agree with available distance constraints for nearly all pulsars with such constraints (Figures 9 and 10, Paper I). Second, none of the parameters of the large-scale components are indeterminate (e.g., as was the case with the thick disk for TC93). The cost of these improvements has been an increase in the complexity of the model, particularly with respect to the number and location of clumps and voids. We believe, however, that this additional complexity is motivated both by the quantity of data and astrophysically (§8). As such our model embodies the long-known fact that a small number

of pulsars or extragalactic sources have anomalously large DMs or scattering properties or both due to intervening H II regions or supernova remnants.

The typical distance uncertainty, e.g., from unmodeled clumps, is perhaps slightly less than 20% (Figure 12 of Paper I). This is slightly better than the 25% uncertainty estimated by TC93 for their model. Nonetheless, given the available data we consider it unlikely that future models will be able to improve much upon this typical distance uncertainty, without a substantial change in the nature of the available data. The DM-independent distance constraints that we use to calibrate the model are dominated by H I absorption measurements and associations (with supernova remnants or globular clusters). The typical accuracy of these constraints is certainly no better than 10% and sometimes can be much worse. Only 10% of the distance constraints come from pulsars with parallaxes, either interferometric or timing, which can have accuracies of 5% or better. Until the number of parallaxes becomes comparable to or dominates the H I absorption measurements, substantial improvement in the distance accuracy is unlikely from NE2001 and future models.

The introduction, location, and parameters of the clumps and voids remains ad hoc to some degree. On the one hand, this would appear to limit the predictive power of the model. For instance, should a newly-discovered pulsar be considered to be affected by a clump or void in front of a known pulsar that is nearby in angle? We regard this as an opportunity to improve the model. Discovery of new pulsars will assist in constraining the location and sizes (and numbers) of clumps and voids.

Finally, in our model we have assumed that the Sun is in the Galactic plane and located at the conventional distance of 8.5 kpc from the Galactic center. In contrast, current estimates are that the Sun is approximately 20 pc above the Galactic plane (Humphreys & Larsen 1995) and is located between 7 and 8 kpc from the Galactic center (Reid 1993; Olling & Merrefield 1998). Discerning these effects in the current data may be difficult due to various selection effects in the different pulsar surveys, but we anticipate that future editions of the model will attempt to incorporate these offsets in the solar location.

Nonetheless, we can estimate crudely how these offsets would affect the model. The DM vertical to the Galactic plane is approximately  $20 \text{ pc cm}^{-3}$  (Figure 1), which is dominated by the thick disk component. Its scale height is 0.95 kpc. Thus we would expect an approximately 2% difference ( $\approx 0.4 \text{ pc cm}^{-3}$ ) in the DMs for northern and southern hemisphere pulsars. Similarly, decreasing the radial scale lengths of all of the components by 6% could

be expected to increase the nominal electron densities by a similar factor.

## 10. DISCUSSION OF FUTURE APPROACHES

While we consider NE2001 to be an improvement over TC93, we foresee a number of probable developments that will allow NE2001 to be improved further. We group these improvements into increases in the quantity of data and improvements in the modeling. Perhaps most important increase in the quantity of data will be an increase in the number of pulsar parallaxes, both from timing pulsars in the Parkes multibeam sample and from large interferometric programs. DM-independent distances provide crucial calibration information for NE2001 or any successors, and we regard it as likely that the number of pulsars with DM-independent distances will double in the next few years. We have made use of only the positions and DMs of pulsars discovered in the Parkes multibeam sample. Efforts are underway to measure the scattering along the lines of sight to many of these pulsars, which could increase the number of lines of sight with measured SMs by roughly 50% or more. The advent of the Green Bank Telescope and the refurbished Arecibo telescope suggest the possibility of conducting a northern hemisphere equivalent of the Parkes multibeam sample, which could increase the number of pulsars by at least another 50%.

Although we have provided a formalism for comparing DM and SM to EM, we have made little use of it. Future work to include observational constraints on EM, e.g., from H $\alpha$  surveys, has the potential of producing a better model at least locally.

Finally, Figure 11 of Paper I suggests that the large-scale structure of the Galaxy may be able to be determined *ab initio*, provided that a sufficient number of lines of sight exist. Rather than imposing a large-scale structure as done both here and previously, the presence and location of large-scale components, particularly the spiral arms, could be determined. Future pulsar surveys may approach the number of lines of sight required to employ this approach.

We thank Z. Arzoumanian, R. Bhat, F. Camilo, S. Chatterjee, D. Chernoff, Y. Gupta, S. Johnston, F. J. Lockman, R. N. Manchester, and B. Rickett for useful discussions. Our research is supported by NSF grants AST 9819931 and 0206036 and by the National Astronomy and Ionosphere Center, which operates the Arecibo Observatory under cooperative agreement with the NSF. Basic research in radio astronomy at the NRL is supported by the Office of Naval Research.

## REFERENCES

- Alurkar, S. K., Bobra, A. D., & Slee, O. B. 1986, *Aust. J. Phys.*, 39, 433  
 Andriasyan, R. R. & Arshakian, T. G. 2001, *Ap&SS*, 278, 175.  
 Armstrong, J. W., Rickett, B. J. & Spangler, S. R. 1995, *ApJ*, 443, 209.  
 Beck, R., Brandenburg, A., Moss, D., Shukurov, A., & Sokoloff, D. 1996, *ARA&A*, 34, 155  
 Berkhuijsen, E. M., Haslam, C. G. T., & Salter, C. J. 1971, *A&A*, 14, 252  
 Bertsch, D. L., Dame, T. M., Fichtel, C. E., Hunter, S. D.; Sreekumar, P., Stacy, J. G., & Thaddeus, P. 1993, *ApJ*, 416, 587  
 Bhat, N. D. R., Rao, A. P., & Gupta, Y. 1999, *ApJS*, 121, 483  
 Bhat, N. D. R., Gupta, Y. & Rao, A. P., 1998, *ApJ*, 500, 262  
 Blitz, L. & Spergel, D. N. 1991, *ApJ*, 379, 631.  
 Brisken, W. F., Benson, J. M., Beasley, A. J., Fomalont, E. B., Goss, W. M., & Thorsett, S. E. 2000, *ApJ*, 541, 959.  
 Brisken, W. F., Benson, J. M., Goss, W. M., & Thorsett, S. E. 2002, *ApJ*, 571, 906  
 Brisken, W. F. 2001, Thesis (PhD). PRINCETON UNIVERSITY, Source DAI-B 62/03, p. 1431, Sep 2001, 112 pages.  
 Bronfman, L., Casassus, S., May, J., & Nyman, L.-Å. 2000, *A&A*, 358, 521

- Camilo, F. & Nice, D. J. 1995, *ApJ*, 445, 756
- Caraveo, P. A., De Luca, A., Mignani, R. P., & Bignami, G. F. 2001, *ApJ*, 561, 930.
- Caswell, J. L. & Haynes, R. F. 1987, *A&A*, 171, 261
- Cha, A. N., Sahu, M. S., Moos, H. & Blaauw, A. 2000, *ApJS*, 129, 281.
- Chatterjee, S., Cordes, J. M., Lazio, T. J. W., Goss, W. M., Fomalont, E. B., & Benson, J. M. 2001, *ApJ*, 550, 287.
- Clifton, T. R., Lyne, A. G., Jones, A. W., McKenna, J., & Ashworth, M. 1992, *MNRAS*, 254, 177
- Cordes, J. M. 1986, *ApJ*, 311, 183
- Cordes, J. M. & Lazio, T. J. W. 2001, *ApJ*, 549, 997.
- Cordes, J. M. & Rickett, B. R. 1998, *ApJ*, 507, 846
- Cordes, J. M. & Lazio, T. J. W. 1991, *ApJ*, 376, 123.
- Cordes, J. M., Weisberg, J. M., Frail, D. A., Spangler, S. R., & Ryan, M. 1991, *Nature*, 354, 121
- Cordes, J. M., Weisberg, J. M., & Boriakoff, V. 1985, *ApJ*, 288, 221
- Costa, M. E., McCulloch, P. M., & Hamilton, P. A. 1991, *MNRAS*, 252, 13
- Dame, T. M., et al. 1987, *ApJ*, 322, 706
- Davies, R. D., Walsh, D., Browne, I. W. A., Edwards, M. R., & Noble, R. G. 1976, *Nature*, 261, 476
- Dennison, B., Broderick, J. J., Thomas, M., Booth, R. S., Brown, R. L., & Condon, J. J. 1984, *A&A*, 135, 199
- Dewey, R. J., Cordes, J. M., Wolszczan, A., & Weisberg, J. M. 1988, in *Radio Wave Scattering in the Interstellar Medium*, eds. J. M. Cordes, B. J. Rickett, & D. C. Backer (AIP: New York) p. 217
- Desai, K. M., et al. 1992, *ApJ*, 393, L75
- Deshpande, A. A. & Ramachandran, R. 1998, *MNRAS*, 300, 577
- Diamond, P. J., Martinson, A., Dennison, B., Booth, R. S., & Winnberg, A. 1988, in *Radio Wave Scattering in the Interstellar Medium*, eds. J. M. Cordes, B. J. Rickett, & D. C. Backer (AIP: New York) p. 195
- Duffett-Smith, P. J. & Readhead, A. C. S. 1976, *MNRAS*, 174, 7
- Fey, A. L. 1989, Ph.D. Thesis, Univ. Iowa
- Fey, A. L., Spangler, S. R., & Cordes, J. M. 1991, *ApJ*, 372, 132
- Fix, J. D., Mutel, R. L., Gaume, R. A., & Claussen, M. J. 1982, *ApJ*, 259, 657
- Foster, R. S., III 1990, Ph.D. Thesis, Univ. California, Berkeley
- Frail, D. A., Diamond, P. J., Cordes, J. M., & van Langevelde, H. J. 1994, *ApJ*, 427, L43
- Frail, D. A., Kassim, N. E., & Weiler, K. W. 1994, *AJ*, 107, 1120
- Frail, D. A., Cordes, J. M., Hankins, T. H., and Weisberg, J. M. 1992, *ApJ*, 382, 168.
- Frail, D. A. & Weisberg, J. M. 1990, *AJ*, 100, 743.
- Frisch, P. C. 1998, *Lecture Notes in Physics*, vol.506, *The Local Bubble and Beyond. Lyman-Spitzer Colloquium, Proceedings of the IAU Colloquium No. 166 held in Garching, Germany, 21-25 April, 1997, XXVII, 603pp.* Springer-Verlag Berlin Heidelberg New York (ISBN 3-540-64306-0), edited by D. Breitschwerdt, M. J. Freyberg, and J. Truemper, pp. 269-278, 506, 269
- Frisch, P. C. 1996, *Space Science Reviews*, v. 78, Issue 1/2, p. 213-222., 78, 213
- Fruchter, A. S., Taylor, J. H., Backer, D. C., Clifton, T. R., & Foster, R. S. 1988, *Nature*, 331, 53
- Geldzahler, B. J. & Shaffer, D. B. 1979, *A&A*, 76, L21
- Geldzahler, B. J., Kellermann, K. I., & Shaffer, D. B. 1979, *AJ*, 84, 186
- Georgelin, Y. M. and Georgelin, Y. P. 1976, *A&A*, 49, 57.
- Ghosh, T. & Rao, A. P. 1992, *A&A*, 264, 203
- Gothoskar, P. & Gupta, Y. 2000, *ApJ*, 531, 345
- Graham, D. et al. 1974, *A&A*, 37, 405.
- Gómez, G. C., Benjamin, R. A., & Cox, D. P. 2001, *AJ*, 122, 908 (GBC01)
- Gupta, Y. 1994, *ApJ*, 451, 717.
- Haffner, L. M., Reynolds, R. J. & Tuftes, S. L. 1998, *ApJ*, 501, L83.
- Han, J. L., Manchester, R. N., Lyne, A. G., & Qiao, G. J. 2002, *ApJ*, 570, L17
- Han, J. L., Manchester, R. N., & Qiao, G. J. 1999, *MNRAS*, 306, 371
- Hansen, J., Booth, R. S., Dennison, B., & Diamond, P. J. 1993, in *Astrophysical masers*, eds. A. W. Clegg & G. E. Nedoluha (Springer-Verlag: Berlin) p. 255
- Heiles, C. 1979, *ApJ*, 229, 533
- Heiles, C. 1998, *ApJ*, 498, 689.
- Hesser, J. E., Harris, W. E., VandenBerg, D. A., Allwright, J. W. B., Shott, P., and Stetson, D. B. 1987, *PASP*, 99, 739.
- Hoogerwerf, R., de Bruijne, J. H. J., & de Zeeuw, P. T. 2001, *A&A*, 365, 49.
- Humphreys, R. M. & Larsen, J. A. 1995, *AJ*, 110, 2183
- Johnston, S. 1990, Ph.D. Thesis, Sydney University.
- Johnston, S., Koribalski, B., Weisberg, J. M., & Wilson, W. 2001, *MNRAS*, 322, 715.
- Johnston, S., Nicastro, L., & Koribalski, B. 1998, *MNRAS*, 297, 108
- Johnston, S., Lyne, A. G., Manchester, R. N., Kniffen, D. A., D'Amico, N., Lim, J., & Ashworth, M. 1992, *MNRAS*, 255, 401
- Kent, S. R. & Mutel, R. L. 1982, *ApJ*, 263, 145
- Kolpak, M. A., Jackson, J. M., Bania, T. M., Clemens, D. P., & Dickey, J. M. 2003, *ApJ*, 582, 756
- Koribalski, B., Johnston, S., Weisberg, J. M., & Wilson, W. 1995, *ApJ*, 441, 756.
- Kulkarni, S. R. & Heiles, C. in *Galactic and Extragalactic Radio Astronomy*, eds. G. L. Vershuur & K. I. Kellermann (Springer-Verlag: Berlin) p. 95
- Kuzmin, A. 2001, *Ap&SS*, 278, 53
- Lambert, H. C. & Rickett, B. J. 1999, *ApJ*, 517, 299
- Langston, G. et al. 2000, *AJ*, 119, 2801.
- Lazio, T. J. W., Anantharamaiah, K. R., Goss, W. M., Kassim, N. E., & Cordes, J. M. 1999, *ApJ*, 515, 196
- Lazio, T. J. W. & Cordes, J. M. 1998, *ApJS*, 115, 225 (LC98a)
- Lazio, T. J. W. & Cordes, J. M. 1998, *ApJ*, 497, 238 (LC98b)
- Lazio, T. J. W. & Cordes, J. M. 1998, *ApJS*, 118, 201 (LC98c)
- Lazio, T. J. W. & Cordes, J. M. 1998, *ApJ*, 505, 715 (LC98d)
- Lo, K. Y., Backer, D. C., Ekers, R. D., Kellermann, K. I., Reid, M., and Moran, J. M. 1985, *Nature*, 315, 124.
- Lo, K. Y., Cohen, M. H., Readhead, A. S. C., & Backer, D. C. 1981, *ApJ*, 249, 504
- Lockman, F. J. 1989, *ApJS*, 71, 469
- Maíz-Apellániz, J. 2001, *ApJ*, 560, L83.
- Manchester, R. N., et al. 2001, *MNRAS*, 328, 17
- Manchester, R. N. and Taylor, J. H. 1981, *AJ*, 86, 1953.
- Manchester, R. N. and Taylor, J. H. 1977, *Pulsars*, (San Francisco: Freeman).
- Mitra, D. & Ramachandran, R. 2001, *A&A*, 370, 586
- Moran, J. M., Greene, B., Rodríguez, L. F., & Backer, D. C. 1990, *ApJ*, 348, 147
- Morris, M. & Serabyn, E. 1996, *ARA&A*, 34, 645
- Mutel, R. L. 1999, private communication
- Mutel, R. L. & Hodges, M. W. 1986, *ApJ*, 307, 472
- Narayan, R. 1992, *Phil. Trans. R. Soc. Lond. A* 341, 151.
- Nelemans, G., Hartman, J. W., Verbunt, F., Bhattacharya, D., & Wijers, R. A. M. J. 1997, *A&A*, 322, 489
- Nicastro, L., Nigro, F., D'Amico, N., Lumiella, V., & Johnston, S. 2001, *A&A*, 368, 1055
- Nordgren, T. E., Cordes, J. M., & Terzian, Y. 1992, *AJ*, 104, 1465
- Ortolani, S. 1999, *Ap&SS*, 265, 355
- Padrielli, L., Mantovani, F., Eastman, W., Spangler, S., & Gregorini, L. 1991, *A&A*, 249, 351
- Phillips, J. A. & Clegg, A. W. 1992, *Nature*, 360, 137
- Prentice, A. J. R. and ter Harr, D. 1969, *MNRAS*, 146, 423.
- Protheroe, R. J. & Biermann, P. L. 1997, *Astroparticle Phys.*, 6, 45
- Ramachandran, R., Mitra, D., Deshpande, A. A., McConnell, D. M., & Ables, J. G. 1997, *MNRAS*, 290, 260
- Rawley, L. A. 1986, Ph.D. Thesis, Princeton Univ.
- Readhead, A. C. S. & Duffett-Smith, P. J. 1975, *A&A*, 42, 151
- Reid, M. J. 1993, *ARA&A*, 31, 345
- Resch, G. M. 1974, Ph.D. Thesis, Florida State Univ.
- Reynolds, R. J. 1989, *ApJ*, 339, L29
- Reynolds, R. J. 1991, *ApJ*, 372, L17
- Rickett, B. J. 1990, *ARAA*, 28, 561
- Rickett, B. J., Coles, W. M. & Markkanen, J. 2000, *ApJ*, 533, 304
- Roberts, J. A. & Ables, J. G. 1982, *MNRAS*, 201, 1119
- Rodríguez, L. F., Canto, J., & Moran, J. M. 1982, *ApJ*, 255, 103
- Rogers, A. E. E., et al. 1994, *ApJ*, 434, L59
- Saravanan, T. P., Deshpande, A. A., Wilson, W., Davies, E., McCulloch, P. M., & McConnell, D. 1996, *MNRAS*, 280, 1027.
- Sfeir, D. M., Lallement, R., Crifo, F. & Welsh, B. Y. 1999, *A&A*, 346, 785.
- Shapirovskaia, N. Y. & Bocharov, A. 1986, *AZh*, 63, 1111.
- Shitov, Y. P. 1994, *Bulletin of the American Astronomical Society*, 26, 1443
- Snowden, S. L. 1998, *ApJ*, 493, 715.
- Sofue, Y. 1994, *ApJ*, 431, L91.
- Spangler, S. R. & Cordes, J. M. 1998, *ApJ*, 505, 766
- Spangler, S. R., Mutel, R. L., Benson, J. M., & Cordes, J. M. 1986, *ApJ*, 301, 312
- Stairs, I. H., Arzoumanian, Z., Camilo, F., Lyne, A. G., Nice, D. J., Taylor, J. H., Thorsett, S. E., & Wolszczan, A. 1998, *ApJ*, 505, 352
- Sutton, J. M. 1971, *MNRAS*, 155, 51.
- Taylor, J. H. and Cordes, J. M. 1993, *ApJ*, 411, 674.
- Taylor, J. H. and Manchester, R. N. 1977, *ApJ*, 215, 885.
- Toscano, M., Britton, M. C., Manchester, R. N., Bailes, M., Sandhu, J. S., Kulkarni, S. R., & Anderson, S. B. 1999, *ApJ*, 523, L171.
- Trotter, A. S., Moran, J. M., & Rodríguez, L. F. 1998, *ApJ*, 493, 666
- van Langevelde, H. J., Frail, D. A., Cordes, J. M., & Diamond, P. J. 1992, *ApJ*, 396, 686
- van Langevelde, H. J. & Diamond, P. J. 1991, *MNRAS*, 249, 7P
- Vallée, J. P. 2002, *ApJ*, 566, 261

- Vivekanand, M. and Narayan, R. 1982, *J. Astrophys. Astron.*, 3, 399.
- Wainscoat, R. J., Cohen, M., Volk, K., Walker, H. J., and Schwartz, D. E. 1992, *ApJS*, 83, 111.
- Weisberg, J. M., Pildis, R. A., Cordes, J. M., Spangler, S. R., & Clifton, T. R. 1990, *BAAS*, 22, 1244
- Weisberg, J. M., Siegel, M. H., Frail, D. A., & Johnston, S. 1995, *ApJ*, 447, 204
- Wilkinson, P. N., Narayan, R., & Spencer, R. E. 1994, *MNRAS*, 269, 67
- Wilkinson, P. N., Spencer, R. E., & Nelson, R. F. 1988, in *The Impact of VLBI on Astrophysics and Geophysics*, eds. M. J. Reid & J. M. Moran (Kluwer: Dordrecht) p. 305
- Yusef-Zadeh, F., Roberts, D. A., Goss, W. M., Frail, D. A., & Green, A. J. 1999, *ApJ*, 512, 230
- Zhao, J., et al. 1992, *Science*, 255, 1538

TABLE 1  
 LIKELIHOOD FITS TO DISTANCE, DM & SCATTERING DATA

Model	Components Included							Figures of Merit			
	Thick Disk	Thin Disk	LISM	Arms	GC	Clumps	Voids	$\Lambda_d$	$\Lambda_s$	$N_{\text{hits}}^d$	$N_{\text{over}}^e$
NE2001 <sup>a</sup>											
0	—	✓	✓	✓	✓	✓	✓	−3079	−3162	68	380
1	✓	—	—	—	✓	—	—	−880	−5814	59	77
2	✓	✓	—	—	✓	—	—	−824	−3512	60	70
3	✓	✓	✓	✓	✓	—	—	−971	−3327	73	30
4	✓	—	✓	✓	✓	✓	✓	−449	−1598	82	10
5	✓	✓	✓	—	✓	✓	✓	−430	−977	85	36
6	✓	✓	✓	✓	✓	✓	✓	−429	−958	88	6
TC93 <sup>b</sup>											
TC93 <sup>b</sup>	✓	✓	—	✓	—	—	—	−747	−4229	59	134
GBC01 <sup>c</sup>											
GBC01 <sup>c</sup>	✓	✓	—	—	—	—	—	−1712	—	51	183

<sup>a</sup>Fits were made while including subsets of the components included in the complete model. LISM and GC parameter values were held fixed for all fits. Results are reported for the best fit defined as a solution that maximizes the log likelihood for distance and DM data,  $\Lambda_d = \log \mathcal{L}_d$ , while also maximizing  $N_{\text{hits}}$ . The accompanying total log likelihood for scattering data,  $\Lambda_s = \log \mathcal{L}_s$  is maximized within the subset of solutions that maximizes  $\Lambda_d$ .

<sup>b</sup>TC93 = the model of Taylor & Cordes 1993, having two axisymmetric components and spiral arms. The 13 parameters were held fixed to their published values.

<sup>c</sup>GBC01 = axisymmetric model of Gómez, Benjamin & Cox 2001. The 6 parameters were held fixed to their published values. This model yields estimates only for the local mean electron density, so scattering data cannot be modeled and  $\Lambda_s$  is undefined.

<sup>d</sup> $N_{\text{hits}}$  is the number of objects for which the model provides a distance estimate within the empirical range,  $[D_L, D_U]$ . The maximum possible is 119 (c.f. Table 1 of Paper I).

<sup>e</sup> $N_{\text{over}}$  is the number of objects out of 1134 (c.f. Table 1 of Paper I) having DM estimates for which the measured DM exceeds that of the model when integrating to effectively infinite distance.

TABLE 2  
CLUMP PARAMETERS FOR PULSAR LINES OF SIGHT

LOS	$\ell$ (deg)	$b$ (deg)	$d_c$ (kpc)	$DM_c$ (pc cm <sup>-3</sup> )	$\log SM_c$ (kpc m <sup>-20/3</sup> )	$r_c$ (kpc)
0540 + 23	-175.64	-3.32	0.63	4.08	...	0.01
0611 + 22	-171.21	2.40	0.65	23.22	...	0.01
0626 + 24	-171.18	6.22	0.65	7.27	...	0.01
0820 + 02	-138.01	21.25	0.55	2.48	...	0.01
0134 - 2937	-129.78	-80.25	0.53	9.04	...	0.01
0628 - 28	-123.05	-16.76	0.91	9.39	...	0.01
GumI	-100.00	-1.00	0.50	110.51	...	0.14
GumII	-97.20	2.70	0.50	28.36	-0.59	0.03
VelaIras	-96.75	-9.00	0.25	269.41	1.54	0.04
1001 - 5507	-79.77	0.08	2.50	7.09	-0.80	0.01
1011 - 58	-76.29	-2.14	4.39	5.49	-0.32	0.01
J1019 - 5749	-76.20	-0.68	4.21	708.98	2.60	0.01
J1022 - 5813	-75.70	-0.83	4.21	354.49	2.60	0.01
1057 - 5226	-74.02	6.65	0.52	15.07	...	0.01
J1031 - 6117	-73.12	-2.88	3.00	35.45	-0.70	0.02
J1056 - 6258	-69.71	-2.97	2.20	177.25	-0.13	0.02
0401 - 7608	-69.69	-35.91	0.47	6.91	...	0.01
1112 - 60	-68.56	-0.32	6.13	9.93	0.19	0.01
J1119 - 6127	-67.85	-0.54	2.30	35.45	-0.70	0.02
J1128 - 6219	-66.51	-0.97	2.30	35.45	0.60	0.02
1131 - 62	-65.79	-1.30	6.51	10.81	0.27	0.01
1209 - 5556	-62.91	6.47	2.46	0.53	-2.35	0.01
J1201 - 6306	-62.69	-0.79	2.00	77.99	-0.02	0.02
J1216 - 6223	-61.08	0.20	2.10	106.35	0.25	0.02
1303 - 66	-55.54	-3.46	6.58	7.27	-0.08	0.01
J1305 - 6256	-55.50	-0.12	8.00	354.49	2.60	0.01
1316 - 60	-53.69	1.74	2.03	4.61	-0.47	0.01
J1324 - 6146	-53.10	0.85	8.00	354.49	2.60	0.01
1323 - 62	-52.93	0.20	1.99	4.61	-0.47	0.01
1323 - 58	-52.50	3.56	1.98	6.38	-0.19	0.01
1334 - 61	-51.63	0.30	6.50	13.47	0.46	0.01
1338 - 62	-51.27	-0.04	7.21	12.58	0.40	0.01
1257 + 12	-48.70	75.41	0.29	3.54	...	0.01
1430 - 6623	-47.35	-5.40	0.90	33.14	...	0.01
1508 - 57	-39.23	-0.11	3.00	88.62	...	0.01
1419 - 3920	-39.07	20.45	0.30	26.06	...	0.01
1518 - 58	-38.37	-1.22	1.60	7.27	-0.08	0.01
2053 - 7200	-38.13	-35.00	0.34	7.27	...	0.01
1544 - 5308	-32.73	1.32	1.50	10.63	...	0.01
1605 - 5257	-30.27	-0.48	1.20	15.95	...	0.01
1557 - 50	-29.31	1.63	3.62	5.49	-0.32	0.01
1455 - 3330	-29.28	22.56	0.30	5.32	...	0.01
1651 - 5222	-24.99	-5.17	1.48	1.24	-1.61	0.01
1556 - 4258	-24.75	7.98	1.49	1.60	-1.39	0.01
1627 - 47	-23.52	0.62	3.43	33.85	1.26	0.01
1630 - 44	-21.27	1.98	3.38	10.81	0.27	0.01
1641 - 45	-20.81	-0.20	3.40	53.17	0.25	0.02
1643 - 43	-18.89	0.97	3.34	10.81	0.27	0.01
1657 - 45	-18.64	-2.18	3.33	6.38	-0.19	0.01
1751 - 4657	-15.00	-10.18	0.27	0.18	-3.46	0.01
1703 - 40	-14.28	-0.20	1.45	15.24	0.57	0.01
1650 - 38	-14.12	3.27	1.46	6.38	-0.19	0.01
1715 - 40	-12.35	-1.53	1.46	5.49	-0.32	0.01
1732 - 4128	-12.02	-4.46	1.46	2.30	-1.07	0.01
1705 - 3422	-9.31	4.07	1.47	2.66	-0.95	0.01
1718 - 36	-9.07	-0.00	1.50	71.96	...	0.01
1714 - 34	-7.88	2.02	5.47	6.38	-0.19	0.01
1727 - 33	-5.87	0.09	1.48	21.45	0.86	0.01
1722 - 3207	-5.44	2.52	1.44	1.95	-1.22	0.01
1750 - 3506	-4.72	-4.11	1.49	3.01	-0.84	0.01
1736 - 31	-2.90	-0.22	3.31	17.02	0.66	0.01
1745 - 3040	-1.45	-0.96	1.43	0.89	-1.90	0.01
1746 - 30	-0.54	-1.24	2.00	77.28	...	0.01
0437 - 4715	-106.61	-41.96	0.10	0.97	-4.04	0.01

TABLE 2—*Continued*

LOS	$\ell$ (deg)	$b$ (deg)	$d_c$ (kpc)	$DM_c$ (pc cm <sup>-3</sup> )	$\log SM_c$ (kpc m <sup>-20/3</sup> )	$r_c$ (kpc)
0531 + 21	-175.44	-5.78	0.64	0.53	-2.50	0.01
0818 - 13	-124.11	12.60	1.00	0.18	-3.30	0.01
0823 + 26	-163.04	31.74	0.19	12.41	-3.53	0.01
1133 + 16	-118.09	69.19	0.17	0.18	-4.00	0.01
1540 - 06	0.57	36.61	0.34	9.22	...	0.01
2144 - 3939	2.66	-49.46	0.14	0.18	-3.90	0.01
1807 - 2715	3.84	-3.26	1.50	70.19	...	0.01
1706 - 16	5.77	13.66	0.29	5.32	...	0.01
1758 - 23	6.81	-0.08	6.63	17.90	0.71	0.01
1604 - 00	10.72	35.47	0.27	3.54	...	0.01
2124 - 3358	10.93	-45.44	0.14	0.71	...	0.01
1642 - 03	14.11	26.06	0.34	11.88	...	0.01
1829 - 1751	14.60	-3.42	1.74	3.72	-0.66	0.01
1949 - 2524	15.25	-23.39	0.34	6.74	...	0.01
1815 - 14	16.41	0.61	4.83	11.70	0.34	0.01
1820 - 14	17.25	-0.18	3.50	301.32	...	0.01
1541 + 09	17.81	45.77	0.46	3.54	-2.86	0.01
1807 - 0847	20.06	5.59	1.69	1.24	-1.63	0.01
1612 + 07	20.63	38.16	0.86	7.09	...	0.01
1824 - 10	21.29	0.80	1.92	15.24	0.57	0.01
1822 - 09	21.45	1.32	0.34	0.21	-3.21	0.01
1836 - 1008	22.26	-1.42	2.00	47.15	...	0.01
1830 - 08	23.39	0.06	4.40	141.80	...	0.01
1832 - 06	25.09	0.55	2.06	36.51	1.32	0.01
1818 - 04	25.46	4.73	1.50	17.72	-1.00	0.02
1834 - 04	27.17	1.13	2.17	5.49	-0.32	0.01
1823 - 0154	28.05	5.31	2.17	1.60	-1.39	0.01
1839 - 04	28.35	0.17	2.23	15.77	0.60	0.01
1903 - 0632	28.49	-5.68	2.25	1.95	-1.22	0.01
2045 - 16	30.51	-33.08	0.32	2.13	...	0.01
1911 - 04	31.31	-7.12	1.78	0.89	-1.90	0.01
1845 - 01	31.34	0.04	2.40	4.25	-0.24	0.02
1849 + 00	33.30	0.10	7.40	354.49	3.60	0.02
1905 - 0056	33.69	-3.55	2.62	1.06	-1.75	0.01
2003 - 08	34.10	-20.30	0.46	6.91	...	0.01
1821 + 05	34.99	8.86	0.44	22.51	...	0.01
1900 + 01	35.73	-1.96	2.80	141.80	0.11	0.04
1737 + 13	37.08	21.68	0.49	19.32	...	0.01
1839 + 09	40.08	6.28	0.51	8.69	...	0.01
1859 + 07	40.57	1.06	3.50	35.45	-0.70	0.02
1855 + 09	42.29	3.06	0.55	0.18	-3.90	0.01
1530 + 27	43.48	54.49	0.34	6.74	...	0.01
1907 + 10	44.83	0.99	0.60	34.56	...	0.01
1914 + 13	47.58	0.45	4.00	88.80	...	0.01
2330 - 2005	49.40	-70.19	0.20	0.18	-3.76	0.01
1933 + 15	51.88	-2.46	3.77	1.95	-1.22	0.01
1933 + 17	53.72	-1.31	4.43	2.84	-0.89	0.01
1920 + 21	55.28	2.93	1.30	1.06	-1.75	0.01
1944 + 17	55.33	-3.50	0.70	0.18	-3.90	0.01
1929 + 20	55.57	0.64	1.39	1.95	-1.22	0.01
1943 + 18	55.61	-3.00	5.12	2.84	-0.89	0.01
1919 + 21	55.78	3.50	0.56	0.18	-3.90	0.01
2044 + 15	61.11	-16.84	1.21	0.18	-3.30	0.01
1946 + 2611	62.32	0.59	2.46	4.08	-0.58	0.01
M15	65.01	-27.31	2.00	13.98	...	0.01
1952 + 29	65.92	0.77	0.36	0.18	-4.30	0.01
2016 + 28	68.10	-3.98	0.62	0.18	-3.83	0.01
1951 + 32	68.77	2.82	1.58	0.53	-2.87	0.01
2002 + 31	69.01	0.02	2.41	1.06	-1.75	0.01
1946 + 35	70.70	5.05	2.38	2.30	-1.07	0.01
1905 + 39	70.95	14.20	1.11	0.18	-3.90	0.01
2053 + 36	79.13	-5.59	2.11	1.24	-1.61	0.01
2347 - 0612	83.87	-64.08	0.46	2.13	...	0.01
2044 + 46	85.43	2.11	2.00	177.25	2.00	0.01

TABLE 2—*Continued*

LOS	$\ell$ (deg)	$b$ (deg)	$d_c$ (kpc)	$DM_c$ (pc cm <sup>-3</sup> )	$\log SM_c$ (kpc m <sup>-20/3</sup> )	$r_c$ (kpc)
1839 + 56	86.08	23.82	0.84	0.18	-3.70	0.01
B2210 + 29	86.14	-21.73	2.00	17.72	-1.30	0.02
2111 + 46	89.00	-1.27	1.59	15.07	...	0.01
2036 + 53	90.37	7.31	2.00	88.62	1.40	0.01
2154 + 40	90.49	-11.34	1.56	0.18	-3.30	0.01
1508 + 55	91.33	52.29	0.49	0.18	-3.30	0.01
2317 + 1439	91.36	-42.36	0.58	7.44	...	0.01
2315 + 21	95.83	-36.07	0.57	4.96	...	0.01
2303 + 30	97.72	-26.66	1.42	0.18	-3.30	0.01
2217 + 47	98.38	-7.60	1.17	4.08	...	0.01
2224 + 65	108.64	6.84	0.94	0.18	-3.52	0.01
0031 - 07	110.42	-69.81	0.24	2.48	...	0.01
0329 + 54	145.00	-1.22	0.54	3.37	...	0.01
0355 + 54	148.19	0.81	0.63	16.13	...	0.01

TABLE 3  
SCATTERING VALUES FOR PULSAR LINES OF SIGHT

Name		$\ell$	$b$	DM	$\hat{D}^a$	$\nu$	Observable <sup>b</sup>	log Value <sup>c</sup>	log SM <sup>d</sup>	Ref
J2000	B1950	(deg)	(deg)	(pc cm <sup>-3</sup> )	(kpc)	(GHz)		(MHz or ms)	(kpc m <sup>-20/3</sup> )	
0528 + 2200	0525 + 21	-176.14	-6.90	50.9	2.27	1.00	$\Delta\nu_d$	-0.070	-3.39	1
0543 + 2329	0540 + 23	-175.64	-3.32	77.7	3.54	1.00	$\Delta\nu_d$	-1.041	-2.74	1
0534 + 2200	0531 + 21	-175.44	-5.78	56.8	2.00	0.32	$\tau_d$	-0.638	-2.64	2
0614 + 2229	0611 + 22	-171.21	2.39	96.7	4.72	1.00	$\Delta\nu_d$	-1.022	-2.86	1
0629 + 2415	0626 + 24	-171.18	6.22	84.2	4.67	1.00	$\Delta\nu_d$	-1.092	-2.80	1
0826 + 2637	0823 + 26	-163.04	31.74	19.5	0.37	1.00	$\Delta\nu_d$	0.980	-3.60	1
0659 + 1414	0656 + 14	-158.89	8.26	14.0	0.76	1.00	$\Delta\nu_d$	0.930	-3.82	1
0452 - 1759	0450 - 18	-142.92	-34.09	39.9	3.14	1.00	$\Delta\nu_d$	-0.060	-3.51	1
0837 + 0610	0834 + 06	-140.28	26.27	12.9	0.72	1.00	$\Delta\nu_d$	1.430	-4.22	1
0823 + 0159	0820 + 02	-138.01	21.25	23.6	1.43	1.00	$\Delta\nu_d$	0.930	-4.05	1
0922 + 0638	0919 + 06	-134.58	36.39	27.3	1.24	1.00	$\Delta\nu_d$	0.310	-3.48	1
0953 + 0755	0950 + 08	-131.09	43.70	3.0	0.28	0.05	$\Delta\nu_d$	-1.495	-6.21	3
0134 - 2937		-129.78	-80.25	22.0	1.78	0.44	$\Delta\nu_d$	-0.284	-4.44	4
0820 - 1350	0818 - 13	-124.11	12.60	41.0	2.46	1.00	$\Delta\nu_d$	-0.270	-3.25	1
0630 - 2834	0628 - 28	-123.05	-16.76	34.4	2.14	1.00	$\Delta\nu_d$	1.280	-4.49	1
1136 + 1551	1133 + 16	-118.09	69.19	4.8	0.35	1.00	$\Delta\nu_d$	1.540	-4.05	1
0742 - 2822	0740 - 28	-116.23	-2.44	73.8	1.89	4.80	$\Delta\nu_d$	0.946	-1.67	4
0908 - 1739	0906 - 17	-113.88	19.85	15.9	0.63	1.00	$\Delta\nu_d$	1.080	-3.88	1
1239 + 2453	1237 + 25	-107.55	86.54	9.3	0.85	1.00	$\Delta\nu_d$	1.660	-4.47	1
0437 - 4715		-106.61	-41.96	2.6	0.14	0.44	$\Delta\nu_d$	0.558	-4.22	4
0738 - 4042	0736 - 40	-105.81	-9.19	160.8	11.03	0.33	$\tau_d$	1.881	-1.12	5
0855 - 3331	0853 - 33	-103.15	7.52	87.7	1.27	0.33	$\tau_d$	< 0.602	< -1.40	6
0846 - 3533	0844 - 35	-102.81	4.71	91.9	1.31	0.33	$\tau_d$	< 0.954	< -1.12	6
0820 - 4114	0818 - 41	-101.25	-2.73	113.4	2.38	0.33	$\tau_d$	1.477	-0.90	6
0837 - 4135	0835 - 41	-99.10	-0.34	147.6	4.30	0.16	$\tau_d$	1.380	-2.33	7
0809 - 4753	0808 - 47	-96.70	-7.96	228.3	12.72	0.33	$\tau_d$	1.898	-1.15	6
0835 - 4510	0833 - 45	-96.45	-2.79	68.2	0.25	0.40	$\tau_d$	0.531	-0.55	8
0904 - 4246	0903 - 42	-94.93	2.86	146.3	4.40	0.33	$\tau_d$	0.903	-1.60	6
0745 - 5351	0743 - 53	-93.37	-14.27	122.3	7.14	0.33	$\tau_d$	1.778	-1.05	6
0952 - 3839	0950 - 38	-91.30	12.03	167.0	8.44	0.33	$\tau_d$	< 1.146	< -1.63	6
0255 - 5304	0254 - 53	-90.14	-55.31	15.9	1.15	1.39	$\Delta\nu_d$	1.630	-4.03	4
0908 - 4913	0906 - 49	-89.73	-1.02	179.0	6.57	1.52	$\Delta\nu_d$	1.079	-4.06	4
0840 - 5332	0839 - 53	-89.23	-7.14	156.5	7.78	0.33	$\tau_d$	1.756	-1.09	6
0905 - 5127		-88.40	-2.87	196.0	8.35	0.33	$\tau_d$	< 1.041	< -1.72	6
0907 - 5157	0905 - 51	-87.85	-3.03	104.0	2.65	0.33	$\tau_d$	< 1.146	< -1.21	6
0924 - 5302	0922 - 52	-85.29	-1.93	152.9	5.61	0.33	$\tau_d$	< 0.301	< -2.19	6
0934 - 5249	0932 - 52	-84.31	-0.70	99.4	2.90	0.33	$\tau_d$	< 1.301	< -1.12	6
1003 - 4747	1001 - 47	-83.96	6.12	98.1	3.44	0.33	$\tau_d$	< 0.602	< -1.76	6
0955 - 5304	0953 - 52	-81.74	1.16	156.9	4.86	0.33	$\tau_d$	0.477	-1.99	6
0924 - 5814	0923 - 58	-81.61	-5.59	60.0	2.01	0.33	$\tau_d$	< 2.079	< -0.34	6
0942 - 5552	0940 - 55	-81.43	-2.23	180.2	6.35	0.33	$\tau_d$	0.699	-1.90	6
0711 - 6830		-80.51	-23.35	18.2	1.03	0.44	$\Delta\nu_d$	-0.432	-4.12	4
1001 - 5507	0959 - 54	-79.77	0.08	130.6	3.59	0.33	$\tau_d$	1.176	-1.30	6
1017 - 5621	1015 - 56	-77.27	0.34	439.1	11.77	0.41	$\tau_d$	< 0.778	< -1.70	7
1012 - 5857	1011 - 58	-76.29	-2.14	383.9	10.15	0.64	$\tau_d$	1.270	-0.53	9
1116 - 4122	1114 - 41	-75.55	18.07	40.5	2.68	0.16	$\tau_d$	< 0.869	< -2.59	7
1042 - 5521	1039 - 55	-74.81	3.00	306.0	6.95	0.33	$\tau_d$	< 1.230	< -1.49	6
1032 - 5910	1030 - 58	-74.09	-0.99	419.0	7.31	0.41	$\tau_d$	< 1.653	< -0.80	7
1057 - 5226	1055 - 52	-74.02	6.65	30.1	1.53	0.66	$\Delta\nu_d$	0.401	-4.30	4
1038 - 5831	1036 - 58	-73.72	-0.02	72.7	2.43	0.64	$\tau_d$	< 0.982	< -0.25	9
0536 - 7543	0538 - 75	-72.84	-30.82	18.3	1.10	0.66	$\Delta\nu_d$	0.286	-4.08	4
1048 - 5832	1046 - 58	-72.57	0.58	129.1	2.98	0.64	$\tau_d$	< 0.505	< -0.72	9

TABLE 3—*Continued*

Name		$\ell$	$b$	DM	$\hat{D}^a$	$\nu$	Observable <sup>b</sup>	log Value <sup>c</sup>	log SM <sup>d</sup>	Ref
J2000	B1950	(deg)	(deg)	(pc cm <sup>-3</sup> )	(kpc)	(GHz)		(MHz or ms)	(kpc m <sup>-20/3</sup> )	
1059 – 5742	1056 – 57	-71.66	1.95	107.9	2.74	0.33	$\tau_d$	< 0.699	< -1.60	6
1110 – 5637	1107 – 56	-70.72	3.53	262.6	9.19	0.64	$\tau_d$	< 0.982	< -0.73	9
1056 – 6258	1054 – 62	-69.71	-2.97	323.4	16.10	0.41	$\tau_d$	< 1.362	< -1.33	7
0401 – 7608	0403 – 76	-69.69	-35.91	21.7	1.52	0.66	$\Delta\nu_d$	0.470	-4.35	4
1114 – 6100	1112 – 60	-68.56	-0.32	676.8	30.00	0.64	$\tau_d$	2.176	-0.16	9
1125 – 60		-67.12	0.33	279.0	8.13	0.64	$\tau_d$	< 0.699	< -0.92	9
1133 – 6250	1131 – 62	-65.79	-1.30	567.8	30.00	0.64	$\tau_d$	2.210	-0.14	9
1157 – 6224	1154 – 62	-63.29	-0.20	325.2	6.35	0.41	$\tau_d$	< 1.431	< -0.93	7
1209 – 5556		-62.91	6.47	174.0	11.83	0.33	$\tau_d$	0.602	-2.21	5
1243 – 6423	1240 – 64	-57.95	-1.53	297.4	8.00	4.80	$\Delta\nu_d$	0.690	-1.98	4
1302 – 6350	1259 – 63	-55.82	-0.99	146.7	4.60	4.80	$\Delta\nu_d$	0.929	-1.98	4
1306 – 6617	1303 – 66	-55.54	-3.46	436.9	29.14	0.64	$\tau_d$	1.694	-0.56	9
1319 – 6056	1316 – 60	-53.69	1.74	400.9	12.63	0.64	$\tau_d$	1.017	-0.82	9
1326 – 6408	1323 – 63	-53.25	-1.53	505.0	15.94	0.41	$\tau_d$	< 1.491	< -1.21	7
1327 – 6222	1323 – 62	-52.93	0.20	318.4	8.45	0.64	$\tau_d$	0.845	-0.81	9
1326 – 5859	1323 – 58	-52.50	3.56	286.0	9.29	0.60	$\tau_d$	1.431	-0.46	10
1338 – 6204	1334 – 61	-51.63	0.31	638.0	8.14	0.64	$\tau_d$	2.301	0.41	9
1341 – 6220	1338 – 62	-51.27	-0.04	730.0	8.66	0.64	$\tau_d$	2.325	0.41	9
1359 – 6038	1356 – 60	-48.76	1.13	295.0	5.91	0.41	$\tau_d$	< 1.380	< -0.95	7
1300 + 1240	1257 + 12	-48.70	75.41	10.2	0.62	0.33	$\Delta\nu_d$	-0.337	-4.46	11
1413 – 6307	1409 – 62	-47.95	-1.72	122.0	3.68	0.64	$\tau_d$	< 1.146	< -0.26	9
1430 – 6623	1426 – 66	-47.35	-5.40	65.3	1.80	0.66	$\Delta\nu_d$	-0.553	-3.56	4
1456 – 6843	1451 – 68	-46.13	-8.54	8.6	0.45	0.44	$\Delta\nu_d$	0.146	-4.30	4
1453 – 6413	1449 – 64	-44.27	-4.43	71.1	1.84	0.66	$\Delta\nu_d$	-0.824	-3.34	4
1512 – 5759	1508 – 57	-39.23	-0.11	628.7	12.69	0.64	$\tau_d$	1.481	-0.43	9
1419 – 3920		-39.07	20.45	61.0	5.04	0.66	$\Delta\nu_d$	-0.602	-3.89	4
1522 – 5829	1518 – 58	-38.37	-1.22	199.9	4.47	0.64	$\tau_d$	1.267	-0.23	9
2053 – 7200	2048 – 72	-38.13	-35.00	18.1	1.11	0.66	$\Delta\nu_d$	0.744	-4.47	4
1539 – 5626	1535 – 56	-35.38	-0.81	176.5	4.01	0.64	$\tau_d$	< 1.384	< -0.10	9
1534 – 5334	1530 – 53	-34.28	1.94	24.8	1.13	0.64	$\tau_d$	< 1.093	< 0.12	9
2127 – 6648	2123 – 67	-33.61	-39.78	35.0	2.75	0.41	$\tau_d$	< 0.903	< -1.07	7
1544 – 5308	1541 – 52	-32.73	1.32	35.2	1.29	1.52	$\Delta\nu_d$	0.833	-3.27	4
1615 – 5537	1611 – 55	-30.96	-3.46	124.5	3.57	0.64	$\tau_d$	< 0.991	< -0.38	9
1605 – 5257	1601 – 52	-30.27	-0.48	32.0	1.24	1.52	$\Delta\nu_d$	1.305	-3.65	4
1600 – 5044	1557 – 50	-29.31	1.63	261.0	6.30	0.75	$\tau_d$	1.204	-0.16	2
1602 – 5100	1558 – 50	-29.31	1.28	169.5	6.30	0.41	$\tau_d$	< 1.318	< -1.02	7
1455 – 3330		-29.28	22.56	13.6	0.74	0.44	$\Delta\nu_d$	0.137	-4.47	4
1611 – 5209	1607 – 52	-29.08	-0.48	128.2	3.34	0.64	$\tau_d$	< 0.279	< -0.95	9
1604 – 4909	1600 – 49	-27.85	2.44	140.8	3.59	0.33	$\tau_d$	< 0.602	< -1.78	5
1614 – 5047	1610 – 50	-27.78	0.17	586.0	7.26	0.64	$\tau_d$	2.405	0.54	9
1559 – 4438	1556 – 44	-25.46	6.37	58.8	1.63	0.66	$\Delta\nu_d$	-0.796	-3.32	4
1613 – 4714	1609 – 47	-25.43	2.84	161.3	3.90	0.33	$\tau_d$	0.954	-1.51	5
1633 – 5015	1629 – 50	-25.30	-1.57	398.4	7.02	0.64	$\tau_d$	1.545	-0.16	9
1651 – 5222	1647 – 52	-24.99	-5.17	179.1	6.39	0.33	$\tau_d$	0.845	-1.78	5
1556 – 4258		-24.75	7.98	145.0	7.67	0.33	$\tau_d$	1.079	-1.65	5
1627 – 47		-23.52	0.62	510.0	8.51	0.64	$\tau_d$	3.147	1.10	9
1640 – 4715	1636 – 47	-22.29	-0.44	592.0	7.25	0.64	$\tau_d$	2.404	0.54	9
1637 – 4553	1634 – 45	-21.52	0.76	193.2	3.83	0.64	$\tau_d$	< 0.230	< -1.04	9
1639 – 4604	1635 – 45	-21.50	0.46	259.0	4.64	0.64	$\tau_d$	< 0.771	< -0.66	9
1633 – 4453	1630 – 44	-21.27	1.98	475.4	12.02	0.64	$\tau_d$	2.114	0.12	9
1623 – 4256	1620 – 42	-21.11	4.62	295.0	21.85	0.41	$\tau_d$	< 1.556	< -1.27	7
1644 – 4559	1641 – 45	-20.81	-0.19	480.0	4.60	0.75	$\tau_d$	1.602	0.29	2
1615 – 3936		-19.91	8.16	152.0	9.67	0.33	$\tau_d$	< 1.000	< -1.80	5

TABLE 3—*Continued*

Name		$\ell$ (deg)	$b$ (deg)	DM (pc cm <sup>-3</sup> )	$\hat{D}^a$ (kpc)	$\nu$ (GHz)	Observable <sup>b</sup>	log Value <sup>c</sup> (MHz or ms)	log SM <sup>d</sup> (kpc m <sup>-20/3</sup> )	Ref
J2000	B1950									
1646 – 4346	1643 – 43	-18.89	0.97	490.0	6.85	0.64	$\tau_d$	2.212	0.40	9
1701 – 4533	1657 – 45	-18.64	-2.18	526.0	17.34	0.64	$\tau_d$	1.812	-0.27	9
1705 – 44		-16.95	-2.68	75.0	1.97	0.64	$\tau_d$	< 0.415	< -0.64	9
1709 – 4428	1706 – 44	-16.90	-2.68	75.7	1.82	1.52	$\Delta\nu_d$	1.507	-3.95	4
1751 – 4657	1747 – 46	-15.00	-10.18	21.7	1.08	0.66	$\Delta\nu_d$	-0.638	-3.30	4
1707 – 4053	1703 – 40	-14.28	-0.20	360.0	5.12	0.64	$\tau_d$	2.217	0.51	9
1653 – 3838	1650 – 38	-14.12	3.27	207.2	5.12	0.64	$\tau_d$	1.164	-0.37	9
1719 – 4006	1715 – 40	-12.35	-1.53	386.6	6.29	0.64	$\tau_d$	1.576	-0.10	9
1732 – 4128	1729 – 41	-12.02	-4.46	195.0	5.93	0.33	$\tau_d$	1.447	-1.25	5
1741 – 3927	1737 – 39	-9.45	-4.75	158.5	4.75	0.41	$\tau_d$	< 1.041	< -1.15	7
1705 – 3422		-9.31	4.07	145.0	3.75	0.33	$\tau_d$	1.462	-1.08	5
1722 – 3632	1718 – 36	-9.07	0.00	416.2	5.30	0.64	$\tau_d$	1.845	0.19	9
1733 – 3716	1730 – 37	-8.42	-2.28	155.1	3.45	0.64	$\tau_d$	< 1.155	< -0.23	9
1721 – 3532	1718 – 35	-8.31	0.67	496.0	4.85	0.64	$\tau_d$	2.747	0.97	9
1717 – 3425	1714 – 34	-7.88	2.02	586.3	22.12	0.64	$\tau_d$	2.014	-0.19	9
1737 – 3555	1734 – 35	-6.83	-2.27	89.4	2.25	0.64	$\tau_d$	< 0.949	< -0.25	9
1730 – 3350	1727 – 33	-5.87	0.09	256.5	4.24	0.64	$\tau_d$	2.404	0.73	9
1722 – 3207	1718 – 32	-5.44	2.53	126.0	3.18	0.33	$\tau_d$	1.114	-1.31	5
1750 – 3506		-4.72	-4.11	195.0	5.28	0.33	$\tau_d$	1.732	-0.97	5
1739 – 3131	1736 – 31	-2.90	-0.22	600.0	7.67	0.92	$\tau_d$	2.146	0.88	12
1743 – 3150	1740 – 31	-2.70	-1.15	191.7	3.64	0.64	$\tau_d$	< 2.001	< 0.45	9
1750 – 3157	1747 – 31	-2.02	-2.52	207.5	4.45	0.64	$\tau_d$	< 1.281	< -0.22	9
1740 – 3015	1737 – 30	-1.71	0.24	153.0	3.28	0.92	$\tau_d$	< 0.477	< -0.20	12
1745 – 3040	1742 – 30	-1.45	-0.96	88.4	2.08	0.33	$\tau_d$	0.699	-1.50	5
1739 – 2903	1736 – 29	-0.79	1.06	139.0	3.20	0.92	$\tau_d$	< 0.301	< -0.34	12
1749 – 3002	1746 – 30	-0.54	-1.24	510.2	9.11	0.64	$\tau_d$	1.667	-0.16	9
1543 – 0620	1540 – 06	0.57	36.61	18.5	1.16	1.00	$\Delta\nu_d$	1.430	-4.39	1
1752 – 2806	1749 – 28	1.54	-0.96	50.9	1.53	1.00	$\Delta\nu_d$	-0.350	-3.01	1
2144 – 3939		2.66	-49.46	4.0	0.21	0.66	$\Delta\nu_d$	0.462	-3.63	4
1730 – 2304		3.14	6.03	9.6	0.51	0.44	$\Delta\nu_d$	-0.770	-3.58	4
1803 – 2712	1800 – 27	3.49	-2.53	165.0	3.62	0.64	$\tau_d$	< 1.276	< -0.15	9
1807 – 2715	1804 – 27	3.84	-3.26	313.3	9.67	0.33	$\tau_d$	1.505	-1.38	5
1753 – 2502	1750 – 24	4.26	0.50	676.0	10.24	0.92	$\tau_d$	1.903	0.58	12
1756 – 2435	1753 – 24	5.03	0.04	365.0	4.95	0.92	$\tau_d$	1.633	0.61	12
1757 – 2421	1754 – 24	5.31	0.02	178.0	3.50	0.33	$\tau_d$	1.556	-0.97	5
1709 – 1640	1706 – 16	5.77	13.66	24.9	1.27	1.00	$\Delta\nu_d$	0.740	-3.85	1
1801 – 2306	1758 – 23	6.81	-0.08	1074.0	13.51	0.64	$\tau_d$	3.306	1.07	9
1759 – 2205	1756 – 22	7.47	0.81	177.3	3.55	0.33	$\tau_d$	1.000	-1.44	5
1824 – 2452	1821 – 24	7.80	-5.58	119.8	5.50	1.00	$\Delta\nu_d$	-3.000	-1.39	13
1803 – 2137	1800 – 21	8.40	0.15	233.9	4.45	0.92	$\tau_d$	< 0.778	< -0.06	12
1808 – 2057	1805 – 20	9.45	-0.40	609.0	7.38	0.61	$\tau_d$	2.491	0.52	14
1607 – 0032	1604 – 00	10.72	35.47	10.7	0.59	1.00	$\Delta\nu_d$	1.710	-4.38	1
2124 – 3358		10.93	-45.44	4.4	0.24	0.44	$\Delta\nu_d$	0.839	-4.65	4
1824 – 1945	1821 – 19	12.28	-3.11	224.3	5.19	0.41	$\tau_d$	< 1.230	< -1.03	7
1809 – 175		13.01	0.35	720.0	11.79	0.64	$\tau_d$	2.626	0.55	9
1812 – 1718	1809 – 173	13.11	0.54	254.0	4.19	0.92	$\tau_d$	< 0.954	< 0.11	12
1820 – 1818	1817 – 18	13.20	-1.72	436.8	8.46	0.64	$\tau_d$	1.491	-0.28	9
1816 – 1729	1813 – 17	13.43	-0.42	528.0	6.51	0.92	$\tau_d$	< 1.146	< 0.11	12
1645 – 0317	1642 – 03	14.11	26.06	35.7	2.90	1.00	$\Delta\nu_d$	0.560	-4.00	1
1829 – 1751	1826 – 17	14.60	-3.42	217.8	5.52	0.33	$\tau_d$	1.982	-0.78	5
1848 – 1952	1845 – 19	14.77	-8.25	18.3	0.96	0.44	$\Delta\nu_d$	-0.638	-3.92	4
1949 – 2524	1946 – 25	15.25	-23.39	22.8	1.32	0.66	$\Delta\nu_d$	0.170	-4.05	4

TABLE 3—*Continued*

Name		$\ell$	$b$	DM	$\hat{D}^a$	$\nu$	Observable <sup>b</sup>	log Value <sup>c</sup>	log SM <sup>d</sup>	Ref
J2000	B1950	(deg)	(deg)	(pc cm <sup>-3</sup> )	(kpc)	(GHz)		(MHz or ms)	(kpc m <sup>-20/3</sup> )	
2155 – 3118	2152 – 31	15.85	–51.58	14.4	0.92	0.66	$\Delta\nu_d$	0.248	–3.98	4
1818 – 1422	1815 – 14	16.41	0.61	625.0	8.14	0.92	$\tau_d$	2.000	0.74	12
1825 – 1446	1822 – 14	16.81	–1.00	354.0	5.42	0.92	$\tau_d$	< 0.778	< –0.13	12
1741 – 0840	1738 – 08	16.95	11.30	74.9	3.50	1.00	$\Delta\nu_d$	–0.680	–3.03	1
1820 – 1346	1817 – 13	17.16	0.48	782.0	9.70	0.64	$\tau_d$	2.878	0.83	9
1822 – 1400	1820 – 14	17.25	–0.18	648.0	7.73	0.92	$\tau_d$	< 0.778	< –0.26	12
1543 + 0929	1541 + 09	17.81	45.78	35.0	2.46	1.00	$\Delta\nu_d$	–0.400	–3.14	1
1826 – 1334	1823 – 13	18.00	–0.69	231.0	4.12	0.92	$\tau_d$	< 1.079	< 0.22	12
1823 – 1115	1820 – 11	19.77	0.95	428.0	6.26	0.61	$\tau_d$	1.748	–0.04	14
1826 – 1131	1823 – 11	19.80	0.29	320.0	4.83	0.92	$\tau_d$	< 1.602	< 0.60	12
1824 – 1118	1821 – 11	19.81	0.74	582.0	7.77	0.92	$\tau_d$	1.602	0.42	12
1537 + 1155	1534 + 12	19.85	48.34	11.6	1.10	0.33	$\Delta\nu_d$	–0.137	–4.83	11
1848 – 1414		19.90	–5.82	134.0	4.36	0.33	$\tau_d$	< 1.255	< –1.30	5
1807 – 0847	1804 – 08	20.06	5.59	112.8	3.61	4.80	$\Delta\nu_d$	0.922	–1.88	4
1614 + 0737	1612 + 07	20.63	38.16	21.3	1.50	1.00	$\Delta\nu_d$	1.160	–4.26	1
1835 – 1106		21.24	–1.53	132.0	3.07	0.33	$\tau_d$	0.778	–1.57	5
1827 – 0958	1824 – 10	21.29	0.80	431.0	6.16	0.92	$\tau_d$	1.653	0.55	12
1825 – 0935	1822 – 09	21.45	1.32	19.5	1.01	1.00	$\Delta\nu_d$	0.050	–3.19	1
1832 – 1021	1829 – 10	21.59	–0.60	475.0	6.42	0.61	$\tau_d$	2.121	0.26	14
1836 – 1008	1834 – 10	22.26	–1.42	318.0	5.40	0.33	$\tau_d$	1.919	–0.83	5
1832 – 0827	1829 – 08	23.27	0.30	300.8	5.25	0.92	$\tau_d$	< 0.699	< –0.19	12
1833 – 0827	1830 – 08	23.39	0.06	411.0	4.60	0.61	$\tau_d$	1.000	–0.55	14
1835 – 0643	1832 – 06	25.09	0.55	463.0	6.34	1.41	$\tau_d$	1.672	1.24	14
1837 – 0653	1834 – 06	25.19	0.00	316.1	4.93	0.92	$\tau_d$	< 1.724	< 0.69	12
1820 – 0427	1818 – 04	25.46	4.73	84.4	1.60	1.00	$\Delta\nu_d$	–2.046	–1.61	1
1844 – 0538	1841 – 05	27.07	–0.94	411.0	6.16	0.61	$\tau_d$	1.863	0.06	14
1836 – 0436	1834 – 04	27.17	1.13	231.0	4.62	0.61	$\tau_d$	1.462	–0.17	14
1943 – 1237	1940 – 12	27.26	–17.16	29.1	1.65	0.16	$\tau_d$	< 0.643	< –2.60	7
1833 – 0338	1831 – 03	27.66	2.28	235.8	5.09	0.33	$\tau_d$	1.708	–0.98	5
1841 – 0425	1838 – 04	27.82	0.28	324.0	5.16	0.92	$\tau_d$	< 0.903	< –0.01	12
1823 – 0154		28.05	5.31	135.0	4.55	0.33	$\tau_d$	1.000	–1.53	5
1842 – 0359	1839 – 04	28.35	0.17	196.0	4.15	0.92	$\tau_d$	1.462	0.53	12
1903 – 0632	1900 – 06	28.49	–5.68	195.7	8.79	0.33	$\tau_d$	1.255	–1.56	5
1713 + 0747		28.75	25.22	16.0	1.10	0.44	$\Delta\nu_d$	0.161	–4.64	4
1847 – 0402	1844 – 04	28.88	–0.94	142.6	3.13	0.16	$\tau_d$	1.803	–1.86	7
1844 – 0244	1842 – 02	29.73	0.23	429.0	5.99	0.92	$\tau_d$	< 1.301	< 0.27	12
2048 – 1616	2045 – 16	30.51	–33.08	11.5	0.64	1.00	$\Delta\nu_d$	1.700	–4.40	1
1913 – 0440	1911 – 04	31.31	–7.12	89.4	3.22	1.00	$\Delta\nu_d$	–1.770	–2.09	1
1848 – 0123	1845 – 01	31.34	0.04	159.1	4.50	0.43	$\tau_d$	1.623	–0.57	2
1852 + 0031	1849 + 00	33.52	0.01	680.0	11.85	0.92	$\tau_d$	2.342	0.89	12
1905 – 0056	1902 – 01	33.69	–3.55	225.0	6.78	0.33	$\tau_d$	1.041	–1.64	5
2006 – 0807	2003 – 08	34.10	–20.30	32.1	1.99	1.00	$\Delta\nu_d$	0.620	–3.91	1
1904 + 0004		34.44	–2.80	234.0	6.43	0.33	$\tau_d$	1.114	–1.56	5
1823 + 0550	1821 + 05	34.99	8.86	67.2	3.03	1.00	$\Delta\nu_d$	0.010	–3.56	1
1857 + 0212	1855 + 02	35.62	–0.39	504.0	8.58	0.61	$\tau_d$	2.013	0.07	14
1903 + 0135	1900 + 01	35.73	–1.96	246.4	3.40	0.43	$\tau_d$	1.041	–0.95	2
1740 + 1311	1737 + 13	37.08	21.68	48.9	4.77	1.00	$\Delta\nu_d$	0.420	–4.06	1
1901 + 0331	1859 + 03	37.21	–0.64	401.2	10.95	0.32	$\tau_d$	2.272	–0.83	2
1909 + 0254	1907 + 02	37.60	–2.71	172.1	4.37	0.32	$\tau_d$	0.477	–2.00	2
1902 + 0556	1900 + 05	39.50	0.21	179.7	3.70	0.33	$\tau_d$	1.519	–1.02	5
1841 + 0912	1839 + 09	40.08	6.28	49.1	2.49	1.00	$\Delta\nu_d$	0.190	–3.64	1
1906 + 0641	1904 + 06	40.60	–0.30	473.0	10.25	0.92	$\tau_d$	< 0.699	< –0.43	12
1857 + 0943	1855 + 09	42.29	3.06	13.3	1.80	0.43	$\Delta\nu_d$	–1.046	–3.83	15

TABLE 3—*Continued*

Name		$\ell$	$b$	DM	$\hat{D}^a$	$\nu$	Observable <sup>b</sup>	log Value <sup>c</sup>	log SM <sup>d</sup>	Ref
J2000	B1950	(deg)	(deg)	(pc cm <sup>-3</sup> )	(kpc)	(GHz)		(MHz or ms)	(kpc m <sup>-20/3</sup> )	
2046 – 0421	2043 – 04	42.68	–27.39	35.9	3.83	1.00	$\Delta\nu_d$	0.310	–3.89	1
1532 + 2745	1530 + 27	43.48	54.49	14.6	0.97	1.00	$\Delta\nu_d$	1.580	–4.45	1
1915 + 1009	1913 + 10	44.71	–0.65	246.1	10.25	0.43	$\tau_d$	1.164	–1.25	2
1909 + 1102	1907 + 10	44.83	0.99	148.4	5.15	0.32	$\tau_d$	0.342	–2.16	2
1844 + 1454	1842 + 14	45.56	8.15	41.2	2.21	1.00	$\Delta\nu_d$	0.270	–3.66	1
1932 + 1059	1929 + 10	47.38	–3.88	3.2	0.33	1.00	$\Delta\nu_d$	2.140	–4.53	1
1916 + 1312	1914 + 13	47.58	0.45	236.9	4.85	0.32	$\tau_d$	0.740	–1.81	2
2145 – 0750		47.78	–42.08	9.0	0.50	0.44	$\Delta\nu_d$	0.170	–4.36	4
1917 + 1353	1915 + 13	48.26	0.62	94.5	5.25	1.00	$\Delta\nu_d$	–2.155	–1.93	1
2330 – 2005	2327 – 20	49.40	–70.19	8.4	0.49	0.66	$\Delta\nu_d$	0.079	–3.62	4
1915 + 1606	1913 + 16	49.97	2.12	168.8	7.13	1.40	$\Delta\nu_d$	–1.347	–2.20	15
1936 + 1536	1933 + 15	51.88	–2.46	165.0	8.40	0.43	$\tau_d$	0.763	–1.51	2
1935 + 1616	1933 + 16	52.44	–2.09	158.5	7.94	1.00	$\Delta\nu_d$	–1.796	–2.40	1
1935 + 1747	1933 + 17	53.72	–1.31	210.0	9.50	0.43	$\tau_d$	1.176	–1.21	2
1921 + 2006	1919 + 20	54.21	2.64	70.0	3.58	0.43	$\tau_d$	< 1.068	< –0.95	2
1922 + 2110	1920 + 21	55.28	2.93	217.1	12.51	0.16	$\tau_d$	1.986	–2.21	7
1946 + 1805	1944 + 17	55.33	–3.50	16.1	0.85	1.00	$\Delta\nu_d$	0.760	–3.72	1
1932 + 2020	1929 + 20	55.57	0.64	211.0	9.85	0.43	$\tau_d$	0.684	–1.64	2
1945 + 1835	1943 + 18	55.61	–3.00	215.0	12.51	0.43	$\tau_d$	1.176	–1.31	2
1921 + 2153	1919 + 21	55.78	3.50	12.4	0.66	1.00	$\Delta\nu_d$	1.380	–4.15	1
1939 + 2134	1937 + 21	57.51	–0.29	71.0	9.70	1.00	$\Delta\nu_d$	–0.590	–3.48	16
2046 + 1540	2044 + 15	61.11	–16.84	39.5	2.52	1.00	$\Delta\nu_d$	–0.330	–3.21	1
1946 + 2611		62.32	0.60	165.0	7.78	0.43	$\tau_d$	1.623	–0.77	17
2116 + 1414	2113 + 14	64.46	–23.41	56.3	4.43	1.00	$\Delta\nu_d$	–0.260	–3.47	1
1954 + 2923	1952 + 29	65.92	0.77	7.9	0.42	1.00	$\Delta\nu_d$	1.560	–4.13	1
2018 + 2839	2016 + 28	68.10	–3.98	14.2	3.20	1.00	$\Delta\nu_d$	0.800	–4.23	1
1952 + 3252	1951 + 32	68.77	2.82	45.0	2.50	1.40	$\Delta\nu_d$	0.041	–2.98	18
2022 + 2854	2020 + 28	68.86	–4.67	24.6	2.10	1.00	$\Delta\nu_d$	1.130	–4.36	1
2004 + 3137	2002 + 31	69.01	0.02	234.7	9.50	0.32	$\tau_d$	1.000	–1.84	2
2002 + 3217	2000 + 32	69.26	0.88	142.0	6.67	0.61	$\tau_d$	< 0.903	< –0.77	14
1948 + 3540	1946 + 35	70.70	5.05	129.1	7.86	0.32	$\tau_d$	1.505	–1.35	2
1907 + 4002	1905 + 39	70.95	14.20	30.1	1.71	1.00	$\Delta\nu_d$	0.470	–3.73	1
2113 + 2754	2110 + 27	74.99	–14.02	24.7	1.37	1.00	$\Delta\nu_d$	0.950	–4.05	1
2013 + 3845	2011 + 38	75.93	2.48	238.6	13.09	0.33	$\tau_d$	1.176	–1.77	5
2055 + 3630	2053 + 36	79.13	–5.59	97.5	5.56	0.32	$\tau_d$	0.875	–1.75	2
2347 – 0612		83.87	–64.08	20.0	1.95	0.66	$\Delta\nu_d$	0.086	–4.12	4
1955 + 5059	1953 + 50	84.79	11.55	31.8	1.78	1.00	$\Delta\nu_d$	0.850	–4.06	1
1840 + 5640	1839 + 56	86.08	23.82	26.5	1.69	1.00	$\Delta\nu_d$	0.370	–3.64	1
2022 + 5154	2021 + 51	87.86	8.38	22.6	1.85	1.00	$\Delta\nu_d$	1.270	–4.43	1
2113 + 4644	2111 + 46	89.00	–1.27	141.5	5.40	1.00	$\Delta\nu_d$	–1.620	–2.41	1
2157 + 4017	2154 + 40	90.49	–11.34	70.6	5.53	1.00	$\Delta\nu_d$	–0.710	–3.17	1
1509 + 5531	1508 + 55	91.33	52.29	19.6	1.93	1.00	$\Delta\nu_d$	0.370	–3.69	1
2317 + 1439		91.36	–42.36	21.9	1.89	0.44	$\Delta\nu_d$	–0.319	–4.43	4
2317 + 2149	2315 + 21	95.83	–36.07	20.5	1.40	1.00	$\Delta\nu_d$	1.230	–4.29	1
2305 + 3100	2303 + 30	97.72	–26.66	49.9	3.93	1.00	$\Delta\nu_d$	–0.660	–3.09	1
2219 + 4754	2217 + 47	98.38	–7.60	43.5	2.45	1.00	$\Delta\nu_d$	0.360	–3.77	1
2313 + 4253	2310 + 42	104.41	–16.42	17.3	0.96	0.33	$\Delta\nu_d$	–0.943	–4.11	19
2225 + 6535	2224 + 65	108.64	6.84	36.2	2.00	1.00	$\Delta\nu_d$	0.050	–3.44	1
0034 – 0721	0031 – 07	110.42	–69.82	10.9	0.68	1.00	$\Delta\nu_d$	1.640	–4.37	1
2321 + 6024	2319 + 60	112.09	–0.57	94.8	3.22	1.00	$\Delta\nu_d$	–1.523	–2.30	1
0030 + 0451		113.10	–57.60	4.3	0.17	0.44	$\Delta\nu_d$	0.748	–4.45	20
0141 + 6009	0138 + 59	129.15	–2.11	34.8	2.75	1.00	$\Delta\nu_d$	0.480	–3.91	1

TABLE 3—*Continued*

Name		$\ell$	$b$	DM	$\hat{D}^a$	$\nu$	Observable <sup>b</sup>	log Value <sup>c</sup>	log SM <sup>d</sup>	Ref
J2000	B1950	(deg)	(deg)	(pc cm <sup>-3</sup> )	(kpc)	(GHz)		(MHz or ms)	(kpc m <sup>-20/3</sup> )	
0814 + 7429	0809 + 74	140.00	31.62	5.8	0.43	1.00	$\Delta\nu_d$	1.930	-4.45	1
0332 + 5434	0329 + 54	145.00	-1.22	26.8	1.02	1.00	$\Delta\nu_d$	0.590	-3.65	1
0358 + 5413	0355 + 54	148.19	0.81	57.1	1.80	1.00	$\Delta\nu_d$	0.020	-3.38	1
0323 + 3944	0320 + 39	152.18	-14.34	25.8	1.47	1.00	$\Delta\nu_d$	0.360	-3.59	1
0454 + 5543	0450 + 55	152.62	7.55	14.6	0.79	1.00	$\Delta\nu_d$	0.980	-3.88	1
1115 + 5030	1112 + 50	154.41	60.36	9.2	0.54	1.00	$\Delta\nu_d$	1.290	-4.00	1
0304 + 1932	0301 + 19	161.14	-33.27	15.7	0.94	1.00	$\Delta\nu_d$	0.930	-3.90	1

References. — (1) Cordes (1986); (2) Cordes, Weisberg, & Boriakoff (1985); (3) Phillips & Clegg (1992); (4) Johnston, Nicastro & Koribalski (1998); (5) Ramachandran et al. (1997); (6) Mitra & Ramachandran (2001); (7) Alurkar et al. (1986); (8) Roberts & Ables (1982); (9) Johnston (1990); (10) Costa, McCulloch, & Hamilton (1991); (11) Gothoskar & Gupta (2000); (12) Weisberg et al. (1990); (13) Foster (1990); (14) Clifton et al. (1992); (15) Dewey, Cordes, & Wolszczan (1988); (16) Cordes et al. (1990); Rawley (1986); (17) Camilo & Nice (1995); (18) Fruchter et al. (1988); (19) Bhat, Rao & Gupta (1999); (20) Nicastro et al. (2001)

<sup>a</sup>Distance estimates are based on NE2001.

<sup>b</sup>Observables are the scintillation bandwidth,  $\Delta\nu_d$ , defined as the half-width-at-half maximum of the intensity correlation function of the dynamic spectrum (c.f. Cordes 1986) and the pulse broadening time,  $\tau_d$ , that is approximately the  $e^{-1}$  width of the pulse broadening function.

<sup>c</sup>Scintillation bandwidths,  $\Delta\nu_d$ , are in MHz while pulse broadening times  $\tau_d$  are in ms. Values in reference 1 are scaled to 1 GHz using a Kolmogorov scaling law,  $\Delta\nu_d \propto \nu^{-22/5}$ . Errors are not quoted because they are not reported uniformly in the different references and because scintillation bandwidths in particular can vary markedly with epoch (e.g. Bhat et al. 1999).

<sup>d</sup>Errors on log SM are not reported but would receive contributions from errors in the observables and in the distance. Typically, the error is  $\Delta \log \text{SM} \sim 0.3$ .

<sup>e</sup>Pulse broadening times reported in reference 12 are from an analysis of pulsars reported in reference 14.

TABLE 4  
SCATTERING VALUES FOR GALACTIC LINES OF SIGHT (NON-PULSARS)

Name	$\ell$ (deg)	$b$ (deg)	$\hat{D}$ (kpc)	$\nu$ (GHz)	$\theta_d$ (mas)	log SM (kpc m <sup>-20/3</sup> )	Ref
MonR2	-146.30	-12.60	0.80	1.66	3.4	-0.96	1
NGC6334H20	-8.74	0.67	1.70	22.00	< 0.5	< 1.76	2
NGC6334NOH1665(-12.6)	-8.58	0.65	1.70	1.66	18.0	0.25	3
NGC6334NOH1665(-7.3)	-8.58	0.65	1.70	1.66	19.0	0.28	3
NGC6334NOH1665(-11.5)	-8.58	0.65	1.70	1.66	31.0	0.64	3
NGC6334NOH1665(-12.2)	-8.58	0.65	1.70	1.66	15.0	0.11	3
NGC6334NOH1665(-9)	-8.58	0.65	1.70	1.66	36.0	0.75	3
NGC6334NOH1665(-12.9)	-8.58	0.65	1.70	1.66	23.0	0.42	3
NGC6334NOH1665(-7.6)	-8.58	0.65	1.70	1.66	21.0	0.36	3
NGC6334NOH1667(-10.1)	-8.58	0.65	1.70	1.67	24.0	0.46	3
NGC6334NOH1665(-8)	-8.58	0.65	1.70	1.66	25.0	0.48	3
NGC6334NOH1665(-10.8)	-8.58	0.65	1.70	1.66	33.0	0.68	3
NGC6334NOH1665(-10.5)	-8.58	0.65	1.70	1.66	26.0	0.51	3
NGC6334NOH1667(-11.9)	-8.58	0.65	1.70	1.67	20.0	0.32	3
NGC6334NOH1667(-9.4)	-8.58	0.65	1.70	1.67	34.0	0.71	3
NGC6334NOH1667(-11.2)	-8.58	0.65	1.70	1.67	26.0	0.51	3
NGC6334NOH1667(-11.5)	-8.58	0.65	1.70	1.67	21.0	0.36	3
NGC6334NOH1665(-8.7)	-8.58	0.65	1.70	1.66	27.0	0.54	3
NGC6334NOH1667(-12.2)	-8.58	0.65	1.70	1.67	22.0	0.39	3
NGC6334NOH1665(-9)	-8.58	0.65	1.70	1.66	12.0	-0.05	3
NGC6334NOH1667(-9.8)	-8.58	0.65	1.70	1.67	25.0	0.48	3
NGC6334NOH1667(-10.8)	-8.58	0.65	1.70	1.67	20.0	0.32	3
NGC6334NOH1665(-9.4)	-8.58	0.65	1.70	1.66	13.0	0.01	3
OH351.78 - 0.54	-8.22	-0.53	6.50	1.67	40.0	0.82	4
OH353.298 - 1.537	-6.70	-1.54	8.50	1.61	360.0	2.36	5
OH355.641 - 1.742	-4.36	-1.74	8.50	1.61	329.0	2.30	5
OH355.897 - 1.754	-4.10	-1.75	8.50	1.61	348.0	2.34	5
OH357.849 + 9.744	-2.15	9.74	8.50	1.61	157.0	1.76	5
OH359.140 + 1.137	-0.86	1.14	8.50	1.61	269.0	2.15	5
OH359.517 + 0.001	-0.48	0.00	8.50	1.61	820.0	2.96	6
OH359.564 + 1.287	-0.44	1.29	8.50	1.61	81.0	1.28	5
OH359.581 - 0.240	-0.42	-0.24	8.50	1.61	640.0	2.78	6
OH359.762 + 0.120	-0.24	0.12	8.50	1.61	531.0	2.64	5
OH359.880 - 0.087	-0.12	-0.09	8.50	1.61	1060.0	3.14	6
SgrAOH1720 : H(49)	-0.07	-0.06	8.50	1.72	< 1780.0	< 3.62	7
SgrAOH1720 : I(58)	-0.07	-0.06	8.50	1.72	< 1780.0	< 3.62	7
A1742 - 28	-0.07	-0.03	8.50	1.60	530.0	2.63	8
SgrAOH1720 : G1(54)	-0.07	-0.06	8.50	1.72	1310.0	3.40	7
SgrAOH1720 : D(53)	-0.07	-0.07	8.50	1.72	857.0	3.09	7
SgrAOH1720 : G2(56)	-0.07	-0.06	8.50	1.72	< 1780.0	< 3.62	7
GCT	-0.06	-0.05	8.50	1.00	1280.0	2.52	9
SgrAOH1720 : F(62)	-0.06	-0.07	8.50	1.72	< 1780.0	< 3.62	7
SgrAOH1720 : A(66)	-0.06	-0.07	8.50	1.72	638.0	2.88	7
SgrAOH1720 : E(56)	-0.06	-0.07	8.50	1.72	810.0	3.05	7
SgrA*	-0.06	-0.05	8.50	1.00	1350.0	2.56	10
OH359.938 - 0.077	-0.06	-0.08	8.50	1.61	571.0	2.69	11
SgrAOH1720 : C(43)	-0.05	-0.04	8.50	1.72	< 1780.0	< 3.62	7
OH359.954 - 0.041	-0.05	-0.04	8.50	1.61	591.0	2.72	11
SgrAOH1720 : B2(134)	-0.04	-0.04	8.50	1.72	526.0	2.74	7
SgrAOH1720 : B4(132)	-0.04	-0.04	8.50	1.72	580.0	2.81	7
SgrAOH1720 : B1(132)	-0.04	-0.04	8.50	1.72	541.0	2.76	7
SgrAOH1720 : B3(136)	-0.04	-0.04	8.50	1.72	< 1150.0	< 3.31	7
OH359.986 - 0.061	-0.01	-0.06	8.50	1.61	950.0	3.06	6
OH000.125 + 5.111	0.12	5.11	8.50	1.61	35.0	0.67	5

TABLE 4—*Continued*

Name	$\ell$ (deg)	$b$ (deg)	$\hat{D}$ (kpc)	$\nu$ (GHz)	$\theta_d$ (mas)	log SM (kpc m <sup>-20/3</sup> )	Ref
OH000.190 + 0.036	0.19	0.04	8.50	1.61	103.0	1.46	11
OH000.319 - 0.040	0.32	-0.04	8.50	1.61	1200.0	3.23	6
OH000.334 - 0.181	0.33	-0.18	8.50	1.61	1220.0	3.24	6
SGRB2	0.70	0.01	8.50	1.67	90.0	1.41	3
OH000.892 + 1.342	0.89	1.34	8.50	1.61	57.0	1.03	5
OH12.2 - 0.1	12.22	-0.13	16.10	1.66	25.6	0.50	1
W33A(39.6)	12.92	-0.25	4.40	1.66	3.8	-0.88	1
W33A(37.4)	12.92	-0.25	4.40	1.66	3.5	-0.94	1
OH20.1 - 0.1(45.3)	20.07	-0.09	4.10	1.66	40.7	0.83	1
OH20.1 - 0.1(46.5)	20.07	-0.09	4.10	1.66	41.1	0.84	1
OH25.1 - 0.4(154.8)	25.06	-0.35	9.10	1.61	< 61.0	< 1.08	1
OH25.1 - 0.4(129.7)	25.06	-0.35	9.10	1.61	< 74.2	< 1.22	1
OH28.5 - 0.0(120.6)	28.53	-0.01	8.80	1.61	< 38.6	< 0.75	1
OH28.5 - 0.0(93.5)	28.53	-0.01	8.80	1.61	< 43.2	< 0.83	1
OH32.8 - 0.3(45)	32.83	-0.32	5.00	1.61	< 36.3	< 0.70	1
OH32.8 - 0.3(74)	32.83	-0.32	5.00	1.61	< 31.9	< 0.61	1
OH35.2 - 1.7(43.5)	35.20	-1.73	2.90	1.66	0.8	-2.01	1
OH35.2 - 1.7(41.7)	35.20	-1.73	2.90	1.66	2.4	-1.21	1
OH39.7 + 1.5(34.8)	39.71	1.50	1.50	1.61	< 25.4	< 0.44	1
OH39.7 + 1.5(2.9)	39.71	1.50	1.50	1.61	< 30.1	< 0.56	1
OH40.6 - 0.2	40.62	-0.14	2.30	1.66	21.0	0.36	1
W49NOH1667(1.5)	43.16	0.01	14.00	1.67	62.0	1.14	3
W49NOH1667(19.0)	43.16	0.01	14.00	1.67	67.0	1.20	3
W49NOH1667(8.1)	43.16	0.01	14.00	1.67	71.0	1.24	3
W49NOH1667(1.8)	43.16	0.01	14.00	1.67	70.0	1.23	3
W49NOH1667(4.3)	43.16	0.01	14.00	1.67	67.0	1.20	3
W49NOH1667(18.7)	43.16	0.01	14.00	1.67	70.0	1.23	3
W49NOH1665(5)	43.16	0.01	14.00	1.66	63.0	1.15	3
W49NOH1665(11.6)	43.16	0.01	14.00	1.66	57.0	1.08	3
W49NOH1665(18.0)	43.16	0.01	14.00	1.66	54.0	1.04	3
W49NOH1667(4.3)	43.16	0.01	14.00	1.67	70.0	1.23	3
W49NOH1665(4.6)	43.16	0.01	14.00	1.66	59.0	1.10	3
W49NOH1665(12)	43.16	0.01	14.00	1.66	57.0	1.08	3
W49NOH1667(5)	43.16	0.01	14.00	1.67	73.0	1.26	3
W49NOH1665(20.4)	43.16	0.01	14.00	1.66	42.0	0.86	3
W49NOH1665(16.9)	43.16	0.01	14.00	1.66	50.0	0.98	3
W49NOH1665(16.6)	43.16	0.01	14.00	1.66	46.0	0.92	3
W49NOH1665(16.2)	43.16	0.01	14.00	1.66	57.0	1.08	3
W49NOH1665(18.3)	43.16	0.01	14.00	1.66	61.0	1.13	3
W49NOH1665(15.2)	43.16	0.01	14.00	1.66	63.0	1.15	3
W49NOH1665(20.8)	43.16	0.01	14.00	1.66	39.0	0.80	3
W49NOH1665(16.2)	43.16	0.01	14.00	1.66	77.0	1.30	3
W49NOH1665(14.8)	43.16	0.01	14.00	1.66	73.0	1.26	3
W49NOH1665(18)	43.16	0.01	14.00	1.66	52.0	1.01	3
W49NOH1665(17.6)	43.16	0.01	14.00	1.66	47.0	0.94	3
W49NOH1665(16.9)	43.16	0.01	14.00	1.66	47.0	0.94	3
W49NOH1665(16.6)	43.16	0.01	14.00	1.66	44.0	0.89	3
W49NOH1665(21.1)	43.16	0.01	14.00	1.66	43.0	0.88	3
W49NOH1665(15.5)	43.16	0.01	14.00	1.66	58.0	1.09	3
W49NOH1665(7.4)	43.16	0.01	14.00	1.66	60.0	1.12	3
W49NOH1665(7.8)	43.16	0.01	14.00	1.66	67.0	1.20	3
W49NOH1665(15.5)	43.16	0.01	14.00	1.66	55.0	1.05	3
OH43.80 - 0.13	43.78	-0.14	2.70	1.66	8.0	-0.34	1
OH44.8 - 2.3	44.78	-2.31	6.00	1.61	< 36.6	< 0.71	1

TABLE 4—*Continued*

Name	$\ell$ (deg)	$b$ (deg)	$\hat{D}$ (kpc)	$\nu$ (GHz)	$\theta_d$ (mas)	log SM (kpc m <sup>-20/3</sup> )	Ref
OH45.5 + 0.0	45.41	0.14	9.70	1.66	3.0	-1.05	1
CygX - 3	79.85	0.70	10.00	0.41	2800.0	1.67	12
W75S	81.80	0.64	2.50	1.66	4.0	-0.84	1
CepA	109.87	2.10	0.73	1.66	3.0	-1.05	1
NGC7538	111.54	0.77	3.50	1.66	3.7	-0.90	1
OH127.8 - 0.0	127.81	-0.02	2.90	1.61	< 9.7	< -0.25	1
W3(OH)[-44.3]	133.95	1.06	2.20	1.66	3.5	-0.94	1
W3(OH)[-46.4]	133.95	1.06	2.20	1.66	4.4	-0.77	1
OH138.0 + 7.3(-47.4)	137.97	7.26	2.40	1.61	< 7.9	< -0.40	1
OH138.0 + 7.3(-28.9)	137.97	7.26	2.40	1.61	< 8.4	< -0.36	1

References. — (1) Hansen et al. (1993); (2) Trotter et al. (1998); (3) Kent and Mutel (1982); (4) Fix, Mutel, Gaume & Claussen (1982); (5) van Langevelde et al. (1992); (6) Frail et al. (1994); (7) Yusef-Zadeh et al. (1999); (8) Davies et al. (1976); (9) Zhao et al. (1991); (10) Lo et al. (1981); (11) van Langevelde & Diamond (1991); (12) Wilkinson, Spencer & Nelson (1988)

TABLE 5  
SCATTERING VALUES FOR EXTRAGALACTIC LINES OF SIGHT

Name	$\ell$ (deg)	$b$ (deg)	$\nu$ (GHz)	$\theta_d$ (mas)	log SM (kpc m <sup>-20/3</sup> )	Ref
87GB0600 + 2957	-178.86	3.95	1.00	1.5	-3.22	1
87GB0558 + 2325	-173.40	0.32	1.00	3.7	-2.57	1
0611 + 131	-163.00	-2.20	0.41	< 40.0	< -2.26	2
0622 + 147	-163.00	1.10	0.41	< 160.0	< -1.26	2
87GB0621 + 1219	-161.14	-0.41	1.00	2.8	-2.77	1
87GB0622 + 1153	-160.57	-0.33	1.00	< 18.0	< -1.42	1
0629 + 109	-158.50	0.50	1.00	25.0	-1.18	2
0758 + 143	-152.40	21.90	0.07	210.0	-3.88	3
0700 - 007	-145.00	2.30	0.41	< 60.0	< -1.97	2
0605 - 085	-144.25	-13.52	0.61	< 20.0	< -2.13	4
0650 - 063	-141.20	-2.60	0.41	< 50.0	< -2.10	2
0650 - 072	-140.30	-2.90	0.41	< 70.0	< -1.86	2
0607 - 157	-137.39	-16.18	0.61	< 40.0	< -1.63	4
0705 - 142	-132.40	-2.90	0.41	130.0	-1.41	2
3C237	-127.90	46.60	0.07	220.0	-3.84	3
1117 + 146	-120.55	65.26	0.61	< 69.0	< -1.23	4
1055 + 018	-108.49	52.77	0.61	< 20.0	< -2.13	4
1226 + 023	-70.10	64.40	0.07	370.0	-3.47	3
NGC6334B	-9.00	0.70	1.42	3000.0	2.84	5
1416 + 067	-7.90	61.00	0.07	320.0	-3.57	3
B1741 - 312	-2.14	-1.00	5.00	18.2	1.15	6
B1739 - 298	-1.08	0.07	5.00	27.9	1.46	6
sourceJ	-0.13	0.18	1.00	< 2000.0	< 1.99	7
IPS	0.00	90.00	0.08	160.0	-3.86	8
1745 - 283	0.04	0.26	1.00	< 1900.0	< 1.95	1
1743 - 2736	0.06	1.17	1.00	< 540.0	< 1.04	1
1328 + 307	22.50	81.00	0.07	190.0	-3.95	3
1832 - 078	24.12	0.13	1.00	< 4660.0	< 2.60	9
1835 - 065	25.60	-0.04	1.00	< 1950.0	< 1.97	10
1835 - 060	26.03	0.22	1.00	< 3340.0	< 2.36	10
1836 - 060	26.24	-0.08	1.00	< 3820.0	< 2.46	10
1849 + 005	33.30	0.20	1.00	4600.0	2.59	11
1845 + 018	34.20	1.70	0.41	< 40.0	< -2.26	2
1851 + 012	34.43	-0.02	1.00	< 3430.0	< 2.38	10
1852 + 021	35.31	0.14	1.00	< 307.0	< 0.63	10
1904 + 013	36.00	-2.80	0.41	230.0	-1.00	2
1854 + 02B	36.00	-0.03	1.00	< 2340.0	< 2.10	10
1854 + 026	36.01	-0.06	1.00	< 1110.0	< 1.56	10
1855 + 031	36.55	0.00	1.00	191.0	0.29	12
1858 + 05B	38.59	0.23	1.00	< 368.0	< 0.76	10
1901 + 058	39.57	-0.04	1.00	< 143.0	< 0.08	10
1902 + 067	40.63	0.05	1.00	< 143.0	< 0.08	10
1905 + 079	41.91	0.09	1.00	< 680.0	< 1.21	10
1906 + 083	42.36	0.08	1.00	< 2290.0	< 2.09	10
1908 + 087	42.99	-0.15	1.00	< 514.0	< 1.01	10
1909 - 161	49.70	2.90	0.41	< 40.0	< -2.26	2
1922 + 155	50.62	-0.03	1.00	< 20.7	< -1.32	10
1932 + 174	53.60	-1.30	0.41	< 70.0	< -1.86	2
1923 + 210	55.60	2.30	1.00	< 16.3	< -1.49	12
1932 + 204	56.08	0.10	1.00	< 14.0	< -1.60	10
1328 + 254	56.50	80.70	0.07	190.0	-3.95	3
1934 + 207	56.55	-0.07	1.00	< 9.6	< -1.88	10
1633 + 382	61.09	42.34	0.61	< 34.0	< -1.75	4
1901 + 319	63.03	11.76	0.61	< 15.0	< -2.34	4

TABLE 5—*Continued*

Name	$\ell$ (deg)	$b$ (deg)	$\nu$ (GHz)	$\theta_d$ (mas)	log SM (kpc m <sup>-20/3</sup> )	Ref
1641 + 399	63.44	40.95	0.61	< 40.0	< -1.63	4
1954 + 282	65.31	-0.21	1.00	< 8.3	< -1.98	10
1954 + 282	65.31	-0.21	1.00	8.5	-1.96	12
2001 + 304	67.97	-0.29	1.00	< 13.6	< -1.62	10
2008 + 33D	71.16	-0.09	1.00	130.0	0.01	12
2021 + 317	71.40	-3.10	1.00	25.7	-1.16	12
2023 + 336	73.10	-2.40	1.00	67.6	-0.46	12
2014 + 358	74.04	0.36	1.00	67.0	-0.47	13
2020 + 351	74.14	-1.01	1.00	206.0	0.34	13
2005 + 372	74.18	2.61	1.00	174.0	0.22	13
2048 + 313	74.60	-8.04	1.00	64.7	-0.49	12
2013 + 370	74.90	1.20	1.00	39.0	-0.86	13
2012 + 383	75.78	2.19	1.00	74.0	-0.40	13
2113 + 293	76.60	-13.30	1.00	< 1.2	< -3.38	12
2018 + 386	76.77	1.39	1.00	< 194.0	< 0.30	13
2005 + 403	76.80	4.30	1.00	79.5	-0.34	12
2027 + 383	77.50	-0.17	1.00	< 189.0	< 0.28	10
G77.7 + 1.1	77.70	1.10	8.40	< 3.0	< 0.67	14
G78.5 + 2.5	78.50	2.50	8.40	< 8.1	< 1.39	14
2050 + 364	78.90	-5.10	0.61	25.0	-1.97	15
G79.1 + 0.0	79.10	0.00	8.40	< 6.8	< 1.26	14
G80.0 + 0.1	80.00	0.10	8.40	< 11.6	< 1.65	14
G81.2 + 3.3	81.20	3.30	8.40	< 5.1	< 1.06	14
G83.4 - 0.2	83.40	-0.20	8.40	< 8.6	< 1.43	14
1954 + 513	85.30	11.80	1.00	< 4.3	< -2.46	12
3C418	88.80	6.00	1.00	< 8.0	< -2.01	11
2022 + 542	90.10	9.70	1.00	< 1.4	< -3.27	12
2255 + 415	101.23	-16.11	0.61	< 50.0	< -1.47	4
1358 + 624	109.59	53.13	0.61	< 46.0	< -1.53	4
0016 + 731	120.60	10.70	1.00	< 8.0	< -2.01	11
0224 + 671	132.12	6.23	0.61	< 7.0	< -2.89	4
0134 + 329	134.00	-28.70	0.07	290.0	-3.64	3
0241 + 622	135.70	2.40	5.00	2.0	-0.45	16
87GB0433 + 4706	157.35	-0.04	1.00	< 48.0	< -0.71	1
0503 + 467	161.00	3.70	1.00	< 4.0	< -2.51	11
87GB0451 + 4309	162.53	-0.10	1.00	< 5.1	< -2.33	1
CTA21	166.70	-33.60	0.07	200.0	-3.91	3
87GB0537 + 3059	177.97	0.20	1.00	< 3.7	< -2.57	1
87GB0547 + 3044	178.95	1.80	1.00	< 6.1	< -2.20	1
87GB0512 + 2455	179.68	-7.71	1.00	6.8	-2.12	1

References. — (1) LC98a; (2) Dennison et al. (1984); (3) Resch (1974); (4) Rodriguez, Canto & Moran (1982); (5) Trotter et al. (1998); (6) LC98c; (7) Lazio et al. (1999); (8) Readhead & Duffet-Smith (1975); (9) Frail et al. (1994); (10) Fey et al. (1991); (11) Spangler, Mutel, Benson & Cordes (1986); (12) Fey (1989); (13) Spangler & Cordes (1998); (14) Mutel (1999) private communication; (15) Mutel & Hodges (1985); (16) Geldzahler & Shaffer (1979)

## APPENDIX

## SCATTERING MEASURE DEFINITION AND ESTIMATION

Here we derive our expressions for the scattering measure and its relationship to observable quantities. To have a consistent estimate of scattering from angular broadening, temporal broadening, and scintillation measurements, we account for the fundamental differences in the kinds of measurements. VLBI of extragalactic sources requires consideration of plane waves impinging on a Galactic scattering medium while spherical waves must be considered for pulsars that are embedded in the medium. We define a scattering measure as the integral over path length  $D$ ,

$$SM = \int_0^D ds C_n^2(s), \quad (\text{A1})$$

where  $C_n^2$  is the coefficient in the wavenumber spectrum.

$$P_{\delta n_e}(q) = C_n^2 q^{-\beta} \exp[-(q\ell_1/2)^2], \quad q_0 \leq q < \infty. \quad (\text{A2})$$

The spectrum is a power law with index  $\beta = 11/3$  for a Kolmogorov spectrum and incorporates an ‘inner scale’,  $\ell_1$  and a lower wavenumber cutoff  $q_0 = 2\pi/\ell_0$ , where  $\ell_0$  is the ‘outer scale’. Here we derive estimators for  $SM$  in terms of observable quantities.

## A1. Angular Broadening

Consider the phase structure functions implied by eqn (A2). For a plane wave impinging on a medium with scattering measure  $SM$  we have (Coles *et al.* 1987) for  $2 < \beta < 4$  and assuming  $q_0 b \ll 1$  for all  $b$  of interest

$$D_p(b) = 8\pi^2 r_e^2 \lambda^2 SM \times \begin{cases} g(\beta) b^2 \ell_1^{\beta-4} & b \ll \ell_1 \\ f(\beta) b^{\beta-2} & \ell_1 \ll b \ll \ell_0 \\ (\beta-2)^{-1} q_0^{2-\beta} & b \gg \ell_0 \end{cases} \quad (\text{A3})$$

where we have considered the three limiting regimes  $b \ll \ell_1$ ,  $b \gg \ell_1$ , and  $b \gg \ell_0$ , and where

$$g(\beta) = \frac{\Gamma(2 - \beta/2)}{2^{\beta-1}} \quad (\text{A4})$$

$$f(\beta) = \frac{\Gamma(2 - \beta/2) \Gamma(\beta/2 - 1)}{[\Gamma(\beta/2)]^2 2^{\beta-1}}. \quad (\text{A5})$$

In this Appendix we are interested in using diffraction phenomena to estimate the scattering measure. Observations suggest that the relevant spectrum for the interstellar medium has an outer scale  $\ell_0 \equiv 2\pi/q_0$  that is larger than any diffraction scale or baseline that we consider.

For spherical waves from a source embedded in the scattering medium we have

$$D_s(b) = \int_0^D ds \left[ \frac{\partial D_p(b/D)}{\partial s} \right]_{b=sb/D} \quad (\text{A6})$$

which implies, for a medium with  $C_n^2 = \text{constant}$ , that

$$D_s(b) = D_p(b) \times \begin{cases} 3^{-1} & b \ll \ell_1 \\ (\beta-1)^{-1} & b \gg \ell_1. \end{cases} \quad (\text{A7})$$

If  $b_e$  is the  $1/e$  point of the visibility function

$$\Gamma(b) = \exp[-D_{p,s}(b)/2], \quad (\text{A8})$$

then the scattering diameter (FWHM) is

$$\theta_d = \frac{2\sqrt{\ln 2}}{\pi} \left( \frac{c}{\nu b_e} \right) \quad (\text{A9})$$

from which it follows that the scattering measure for the plane wave case is

$$SM_p = \begin{cases} C_\beta \nu^\beta \theta_d^{\beta-2} & \theta_d \lesssim \theta_{\text{cross}} \\ D_\beta \nu^4 \theta_d^2 \ell_1^{4-\beta} & \theta_d \gtrsim \theta_{\text{cross}} \end{cases} \quad (\text{A10})$$

where

$$C_\beta = \left( \frac{\pi}{2\sqrt{\ln 2}} \right)^{\beta-2} [4\pi^2 r_e^2 c^\beta f(\beta)]^{-1}$$

$$D_\beta = \left( \frac{\pi}{2\sqrt{\ln 2}} \right)^2 [4\pi^2 r_e^2 c^4 g(\beta)]^{-1}.$$

The angle  $\theta_{\text{cross}}$  is the boundary between the two regimes and is

$$\theta_{\text{cross}} = \left[ \frac{g(\beta)}{f(\beta)} \right]^{1/(4-\beta)} \theta_1 \quad (\text{A11})$$

where

$$\theta_1 \equiv \frac{2\sqrt{\ln 2}}{\pi} \left( \frac{c}{\nu \ell_1} \right) \quad (\text{A12})$$

is the scattering diameter if the  $1/e$  half width of the visibility function happens to be equal to the inner scale  $\ell_1$  (cf. Eqn. A9).

For spherical waves the estimators for the structure function become

$$SM_s = \begin{cases} (\beta - 1) C_\beta \nu^\beta \theta_d^{\beta-2}, & \theta \lesssim \theta_{\text{cross}} \\ 3 D_\beta \nu^4 \theta_d^2 \ell_1^{4-\beta}, & \theta \gtrsim \theta_{\text{cross}}. \end{cases} \quad (\text{A13})$$

### A2. Temporal Broadening

Williamson (1972, 1975) has argued that temporal broadening of an impulse may be treated with stochastic ray tracing through extended random media even though broadening is really a diffraction phenomenon. Williamson demonstrated the equivalence of ray tracing and a proper treatment of diffraction for a statistically homogeneous medium having a Gaussian wavenumber spectrum for the irregularities. We assume the equivalence also holds for media with power law wavenumber spectra. Lambert & Rickett (1999) have demonstrated this equivalence using numerical integrations of Kolmogorov media. Therefore, we relate the mean square scattering angle to the temporal broadening time and consider the (nontrivial) relationship of the mean square angle to the measureable angular diameter of the scattered brightness distribution.

Following the discussion in CL91, Cordes & Rickett (1998, hereafter CR98), and Lambert & Rickett (1999), we write the scintillation bandwidth  $\Delta\nu_d$  as

$$\Delta\nu_d = \frac{C_1}{2\pi\langle\tau(D)\rangle} \quad (\text{A14})$$

with  $C_1 = 1.16$  for a Kolmogorov wavenumber spectrum with  $\beta = 5/3$  and for a medium that uniformly fills the line of sight.

The observable angular diameter corresponding to  $\tau_d$  is

$$\theta_d = \left( \frac{16 \ln 2 c \tau_d}{D} \right)^{1/2} = 2.14 \text{ arc sec} \left( \frac{\tau_d}{D_{\text{kpc}}} \right)^{1/2} \quad (\text{A15})$$

which may be substituted into eqn (A14) to obtain the scattering measure. For measurements of the scintillation bandwidth,  $\Delta\nu_d$ , eqn's (A21) and (A26) may be used to solve for the scattering diameter,

$$\theta_d = \left( \frac{8 \ln 2 c C_1}{\pi \Delta\nu_d D} \right)^{1/2} = 0.919 \text{ mas} (\Delta\nu_{\text{dMHz}} D_{\text{kpc}})^{-1/2}. \quad (\text{A16})$$

We now restrict ourselves to  $\beta = 11/3$  for an inner scale  $\ell_1 = 100\ell_{100\text{km}}$ , for which  $f(\beta) = 1.118$  and  $g(\beta) = 0.877$ .

The scattering measure estimators become for plane waves (extragalactic sources)

$$SM_p = \begin{cases} \left( \frac{\theta_d}{0.128 \text{ arc sec}} \right)^{5/3} \nu_{\text{GHz}}^{11/3} & \theta_d \lesssim \theta_{\text{cross}} \\ \left( \frac{\theta_d}{0.133 \text{ arc sec}} \right)^2 \nu_{\text{GHz}}^4 \ell_{100}^{1/3} & \theta_d \gtrsim \theta_{\text{cross}} \end{cases} \quad (\text{A17})$$

while for spherical waves (Galactic sources)

$$SM_s = \begin{cases} \left( \frac{\theta_d}{0.071 \text{ arc sec}} \right)^{5/3} \nu_{\text{GHz}}^{11/3} & \theta_d \lesssim \theta_{\text{cross}} \\ \left( \frac{\theta_d}{0.076 \text{ arc sec}} \right)^2 \nu_{\text{GHz}}^4 \ell_{100}^{1/3} & \theta_d \gtrsim \theta_{\text{cross}} \end{cases}. \quad (\text{A18})$$

The cross-over angle is

$$\theta_{\text{cross}} = 0.16 \text{ arc sec } (\nu_{\text{GHz}} \ell_{100})^{-1}, \quad (\text{A19})$$

corresponding to a temporal broadening time

$$\tau_{\text{cross}} = 5.46 \text{ ms } D_{\text{kpc}} (\nu_{\text{GHz}} \ell_{100})^{-2} \quad (\text{A20})$$

and to a scintillation bandwidth

$$\Delta\nu_{\text{cross}} = 33.6 \text{ Hz } D_{\text{kpc}}^{-1} (\nu_{\text{GHz}} \ell_{100})^2. \quad (\text{A21})$$